AUS DEM INSTITUT FÜR SCHLAGANFALL- UND DEMENZFORSCHUNG
DER LUDWIG-MAXIMILIANS-UNIVERSITÄT MÜNCHEN
DIREKTOR: PROF. DR. MED. MARTIN DICHGANS

The choroid plexus in post-stroke neuroinflammation

DISSERTATION

ZUM ERWERB DES DOKTORGRADES DER
NATURWISSENSCHAFTEN
AN DER MEDIZINISCHEN FAKULTÄT DER
LUDWIG-MAXIMILIANS-UNIVERSITÄT ZU MÜNCHEN

VORGELEGT VON

Gemma Llovera Garcia
aus Terrassa (Barcelona)
2018

Gedruckt mit Genehmigung der Medizinischen Fakultät der

Ludwig-Maximilians-Universität München

Betreuer: Priv. Doz. Dr. Christof Haffner

Zweitgutachter: Priv. Doz. Dr. Reinhard Obst

Dekan: Prof. Dr. med. Dent. Reinhard Hickel

Tag der mündlichen Prüfung: 26.03.2019

Per tu Laia, gràcies per ser-hi sempre

Affidavit

I hereby confirm that my thesis entitled “The choroid plexus in post-stroke neuroinflammation” is the result of my own work. I did not receive any help or support from commercial consultants. All sources and / or materials applied are listed and specified in the thesis.

Furthermore, I confirm that this thesis has not yet been submitted as part of another examination process neither in identical nor in similar form.

München, date Munich, 02.04.2019 Signature Gemma Llovera

Table of contents

Abbreviations 6

Publication list 8

1. Introduction 11

1.1 Stroke and stroke treatments 11

1.2 Inflammation after stroke 12

1.3 Immune cell migration routes into the brain after stroke 15

1.3.1 Blood-Brain Barrier 15

1.3.2 Blood-Cerebrospinal Fluid Barrier 16

1.4 Obstacles in translational research 19

1.5 Research project and conclusions 22

2. Summary 25

3. Zusammenfassung 27

4. Publication I 29

The choroid plexus is a key cerebral invasion route for T cells after stroke

5. Publication II 57

Results of a preclinical randomized controlled multicenter trial (pRCT):

Anti-CD49d treatment for acute brain ischemia

References 86

Acknowledgments 95

Curriculum vitae 96

Abbreviations

AD	Alzheimer´s disease
BB	Blocking buffer
BBB	Blood-brain barrier
BCSFB	Blood-cerebrospinal fluid barrier
BEC	Brain endothelial cells
BLMB	Blood leptomeningeal barrier
CC	Corpus callosum
CCL12	Chemokine ligand 12
CCL2	Chemokine ligand 2
CCL7	Chemokine ligand 7
CCR2	Chemokine receptor 2
ChP	Choroid plexus
cMCAO	Permanent distal middle cerebral artery occlusion
CNS	Central nervous system
CSF	Cerebrospinal fluid
CV	Cresyl violet
DAPI	4′,6-Diamidine-2′-phenylindole dihydrochloride
EAE	Experimental autoimmune encephalitis
fMCAO	Transient proximal middle cerebral artery occlusion
HE	Hematoxylin-eosin
ICAM-1	Intercellular adhesion molecule-1
IFN	Interferon

IgG	Imunoglobulin G
LFA	Lymphocyte function-associated antigen 1
PBS	Phosphate buffered saline
PFA	Paraformaldehyde
pRCT	Preclinical randomized controlled multicenter trials
PSGL-1	P-selectin glycoprotein ligand 1
PT	Phototrombosis
TBI	Traumatic brain injury
TCR	T cell receptor
Th1/2	Type 1/2 T helper cell
tMCAo	Transient proximal middle cerebral artery occlusion
rtPA	Recombinant tissue plasminogen activator
Treg	Regulatory T cell
TUNEL	Terminal deoxynucleotidyltransferase-mediated dUTP nick-end
VCAM-1	Vascular cell adhesion molecule-1
VLA-4	Leukocyte very late antigen-4

Publication list

Benakis C, Llovera G, Liesz A. "The meningeal and choroidal infiltration routes for leukocytes in stroke". Therapeutic Advances in Neurological Disorders (in press).

Heindl S, Gesierich B, Benakis C, Llovera G, Duering M, Liesz A. "Automated Morphological Analysis of Microglia After Stroke". Front Cell Neurosci. 2018 Apr 19; 12:106.

Simats A, García-Berrocoso T, Penalba A, Giralt D, Llovera G, Jiang Y, Ramiro L, Bustamante A, Martinez-Saez E, Canals F, Wang X, Liesz A, Rosell A, Montaner J."CCL23: A new CC chemokine involved in human brain damage". J Intern Med. 2018 May; 283(5):461-475.

Singh V, Sadler R, Heindl S, Llovera G, Roth S, Benakis C, Liesz A. "The gut microbiome primes a cerebroprotective immune response after stroke". J Cereb Blood Flow Metab. 2018 Jan 1:271678X18780130.

Llovera G, Benakis C, Enzmann G, Cai R, Arzberger T, Ghasemigharagoz A, Mao X, Malik R, Lazarevic I, Liebscher S, Ertürk A, Meissner L, Vivien D, Haffner C, Plesnila N, Montaner J, Engelhardt B, Liesz A. "The choroid plexus is a key cerebral invasion route for T cells after stroke". Acta Neuropathol. 2017 Dec;134(6):851-868C.

Daria A, Colombo A, Llovera G, Hampel H, Willem M, Liesz A, Haass C, Tahirovic S. "Young microglia restores amyloid plaque clearance capacity of aged microglia". EMBO J.2017 Mar 1;36(5):583-603.

Erturk A, Mentz S, Stout E, Hedehus M, Dominguez SL, Neumaier L, Krammer F, Llovera G, Srinivasan K, Hansen D, Liesz A, Scearce-Levie K, Sheng M. "Interfering with the chronic immune response rescues chronic degeneration after traumatic brain injury". J Neurosci. 2016 Sep 21;36(38):9962-75.

Singh V, Roth S, Llovera G, Sadler R, Garzetti D, Stecher B, Dichgans M, Liesz A. "Microbiota Dysbiosis Controls the Neuroinflammatory Response after Stroke". J Neurosci. 2016 Jul 13;36(28):7428-40.

Llovera G, Liesz A. "The next step in translational research: Lessons learned from the first preclinical RCT". Journal of Neurochemistry. 2016 Oct;139 Suppl 2:271-279.

Llovera G, Hofmann K, Roth S, Salas-Pérdomo A, Ferrer-Ferrer M, Perego C, Zanier ER, Mamrak U, Rex A, Party H, Agin V, Fauchon C, Orset C, Haelewyn B, De Simoni MG, Dirnagl U, Grittner U, Planas AM, Plesnila N, Vivien D, Liesz A. "Results of a preclinical randomized controlled multicenter trial (pRCT): Anti-CD49d treatment for acute brain ischemia". Science Translational Medicine. 2015 Aug 5;7(299):299ra121.

Llovera G, Roth S, Plesnila N, Veltkamp V, Liesz A. "Modeling stroke in mice: permanent coagulation of the distal middle cerebral artery". Journal of visualized experiments. 2014 Jul 31;(89):e51729.

Shrivastava K, Llovera G, Recasens M, Chertoff M, Giménez-Llort L, Gonzalez B and Acarin L. "Temporal expression of cytokines and stat3 activation after hypoxia/ischemia in mice". Developmental Neuroscience. 2013;35(2-3):212-25.

Shrivastava K, Chertoff M, Llovera G, Recasens M and Acarin L. "Short and long-term analysis and comparison of neurodegeneration and inflammatory cell response in the ipsilateral and contralateral hemisphere of the neonatal mouse brain after hypoxia/ischemia". Neurology Research International. 2012;2012:781512.

1. Introduction

1.1 Stroke and stroke treatments

Stroke is one of the most common causes of death and is a major cause of disability worldwide. Although strokes can be either ischemic or hemorrhagic, 80%–85% of all stroke cases are ischemic (Donnan et al., 2008). Ischemic strokes occur in cases in which a brain blood vessel is occluded, triggering an irreversible brain injury followed by neurological deficits. Stroke symptoms include sudden confusion and numbness of the face, arm or leg, often on one side of the body. Also, trouble walking, dizziness, loss of balance or coordination, trouble seeing in one or both eyes and difficulty speaking or understanding speech can occur. Although stroke patients are a tremendous medical and economic burden, there are few approved treatment options for stroke patients.

The most common drug treatment for ischemic stroke patients involves intravenous thrombolysis with alteplase (recombinant tissue plasminogen activator [rtPA]). rtPA selectively hydrolyzes plasminogen to plasmin, and this, in turn, leads to the degradation of the fibrin clot. Although rtPA has been used for 20 years, this treatment has two significant limitations: 1.) It has to be administered within a short time window (3–4.5 h) after the ischemic insults occur, and 2.) It has crucial contraindications, including hemorrhage or oral anticoagulation (Hacke et al., 2008; Jauch et al., 2013). Furthermore, rtPA has been reported to have low effectiveness in re-stabilizing blood flow in large vessel (such as the cerebral or distal carotid artery) occlusions (Bhatia et al., 2010). For these reasons, rtPA is only administered to a small percentage of stroke patients. Mechanical thrombectomy is another approved therapy for stroke patients. Recently, some randomized trials of new mechanical thrombectomy devices (coil retrievers, aspiration devises, and stent retrievers) demonstrated a probable better outcome for stroke patients compared to that of thrombolysis treatment (Dargazanli et al., 2017; Hamidi et al., 2010; Wisloff et al., 2010).

However, only a minority of patients are eligible to receive these specific treatment options due to the narrow therapeutic time window and multiple exclusion criteria. For the last two decades, translational stroke research focused on neuroprotective approaches in the acute phase after stroke, but all compounds reaching the clinical trials did not show any improvement in the patient (O'Collins et al., 2006). Therefore, novel treatment strategies for delayed pathophysiological events (such as inflammation) need to be further explored.

1.2 Inflammation after stroke

Within the early period after cerebral blood flow impairment, oxygen and glucose levels are reduced in the affected brain region. As a result of the energy depletion, membrane potential is lost and neurons and glial cells depolarize triggering a complex pathogenic cascade of biochemical events inducing excitotoxicity, peri-infarct depolarizations, inflammation, and apoptosis (Fig.1) (Dirnagl et al., 1999).

In the core of the lesion, cerebral blood flow is reduced 20% and cells are instantly killed. While, on the one hand, the core tissue is irreversibly lost, the perilesional tissue at risk (located around the surrounding core tissue) is of particular interest as this tissue could be rescued from subsequent deterioration with appropriate therapy (Dirnagl et al., 1999). Excitotoxicity not only induces acute cell death (necrosis), it can also lead to a more delayed cell death (apoptosis). Although in the core of the region, cells depolarized and never repolarized again, in the perilesional tissue cells can repolarize investing a high amount of energy. Different peri-infarct depolarizations can occur after the lesion, increasing the initial infarct size (Strong et al., 2007).

This necrotic tissue from the lesion core prompts a robust inflammatory response with the release of damage-associated molecular patterns (Iadecola and Anrather, 2011a), which, in turn, can activate astrocytes and the local immune cells like microglia. Moreover, proinflammatory

mediators such as cytokines and chemokines released from tissue-resident cells as well as the induction of transcription factors, prompt the expression of adhesion molecules on the endothelial cell surface and participate in the recruitment of peripheral leukocytes to the injury site (Gelderblom et al., 2009). In fact, in the last decades several experimental stroke studies focused on inflammatory mechanisms after stroke due to their contribution to secondary brain damage (Dirnagl, 2004; Liesz et al., 2009) and a possible focus for a therapeutic intervention (Dirnagl et al., 1999; Gelderblom et al., 2009).

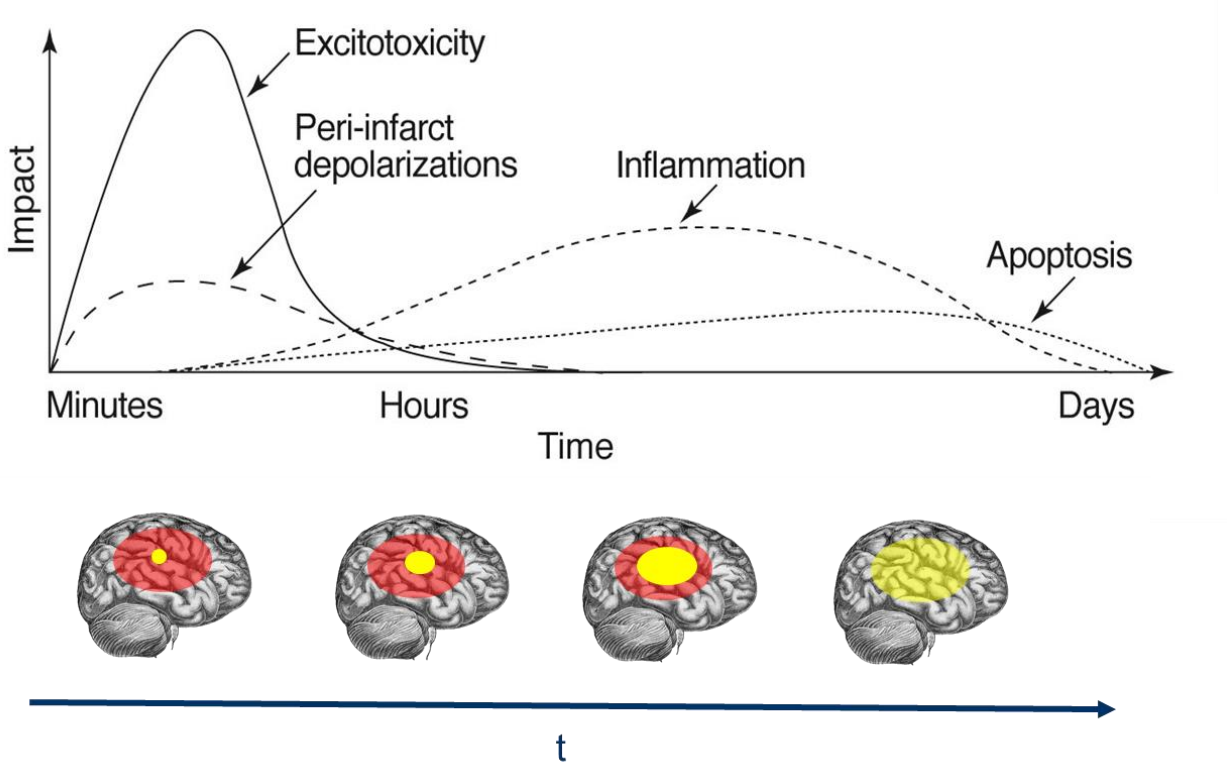

Figure 1. Cascade of damaging events in focal cerebral ischemia. The x-axis reflects the evolution of cascades over time, the y-axis shows the impact of each element of the cascade on final outcome. Schematic picture of the brain shows the extent of core (yellow) and penumbra (red) as it would be seen histologically or on imaging studies. Figure adapted from Dirnagl U et al., 1999.

In several experimental stroke studies, circulating leukocyte recruitment to the injured brain has been associated with an expansion of the infarct lesion. Indeed, leukocyte invasion after a stroke is a critical component of the neuroinflammatory response leading to secondary expansion of the brain damage (Chamorro et al., 2012; Wang et al., 2007). Consequently, some studies sought to block the migration of leukocytes into the ischemic brain and showed a reduction of the infarct volume in different stroke models (Liesz et al., 2011; Llovera et al., 2015). Although new contributions to the understanding of the role of immune cells after stroke have been done, the mechanisms of leukocyte migration of the injured brain are still incompletely understood.

1.3 Immune cell migration routes into the brain after stroke

The central nervous system (CNS) has an immune-privileged environment; it is tightly protected from the fluctuating milieu of the bloodstream by the blood-brain barrier (BBB), which is formed by brain endothelial cells (BECs) and the blood-cerebrospinal fluid barrier (BCSFB) composed of the choroid plexus (ChP) epithelial cells (Redzic, 2011). There are two essential roles of these barriers: 1.) Prevention of free diffusion between brain fluids and blood and 2.) Maintenance of brain homeostasis via transport of crucial nutrients, ions, and waste products (Ransohoff et al., 2003; Takeshita and Ransohoff, 2012).

1.3.1 Blood-Brain Barrier

The blood-brain barrier (BBB) is formed by microvascular endothelial cells, which are surrounded by basement membranes, pericytes, and astrocytes. Astrocytic endfeet processes form the glia limitans, which, along with its basement membrane and the endothelial basement membrane, forms the perivascular space (Man et al., 2007). Moreover, tight junction proteins connect the endothelial cell layer and its basement membrane, forming a tight seal to avoid diffusion of solutes into the brain (Abbott et al., 2010). Therefore, under physiological conditions, the vascular system acts as a barrier that prevents the access of molecules into the brain and limits leukocyte access to the CNS. Acute brain injuries and other CNS pathologies lead to the common pathophysiological mechanisms of secondary neuroinflammation and dysfunctional BBB integrity (Choi and Kim, 2008; Stamatovic et al., 2008). After an ischemic stroke, several groups of molecules initiate leukocyte recruitment across the vascular endothelial barrier into the central nervous system (CNS). Once leukocytic P-selectin glycoprotein ligand 1 (PSGL-1) and very late antigen-4 (VLA-4) bind to the endothelial P-selectin and vascular cell adhesion molecule-1 (VCAM-1), it allows leukocytes to adhere to endothelial cells. Leukocytes

can then migrate to the brain parenchyma across the endothelial cell via the paracellular or transcellular pathway (Engelhardt and Ransohoff, 2005; Engelhardt and Sorokin, 2009; Laschinger and Engelhardt, 2000; Takeshita and Ransohoff, 2012).

Natalizumab, an effective therapy for multiple sclerosis patients, has been shown to reduce lymphocyte invasion into the brain by blocking the α-chain of VLA-4 (anti-CD49d antibodies)(Polman et al., 2006; Rice et al., 2005; Steinman, 2005; Yednock et al., 1992). Consequently, anti-CD49 antibodies have been investigated in the stroke field to reduce leukocyte infiltration into the brain after stroke. Inhibition of the cerebral lymphocyte infiltration resulted in a reduction of the infarct volume and improved the behavior outcome after ischemic stroke (Liesz et al., 2009; Liesz et al., 2011). Despite this promising new approach, more research is needed to be able to translate these findings into a clinical setting.

1.3.2 Blood-Cerebrospinal Fluid Barrier

The blood-cerebrospinal fluid barrier (BCSFB) is formed by the epithelial cells of the choroid plexus (ChP) interconnected by tight junctions. The ChP is localized in the brain ventricles, which is filled with cerebrospinal fluid (CSF). Apart from CSF production, BCSFB's primary function is to restrict immune cell and molecule entrance into the brain. Moreover, the ChP is responsible for brain homeostasis and plays a critical role as a filtration system via removal of metabolic waste from the brain (Bennett et al., 2003; Mortazavi et al., 2014; Wilson et al., 2010).
The ChP is formed by a cuboidal epithelium surrounding the capillaries and loose connective tissue. While the epithelial layer has tight junctions that prevent substances from crossing into the CSF, ChP capillaries are fenestrated and are permeable to molecules and immune cells (Deczkowska et al., 2016; Shechter et al., 2013a; Ueno et al., 2016). The ChP stroma is home to a

diverse number of immune cells, including $CD4^+$ T cells, macrophages, and dendritic cells, thus serving as a possible port for these immune cells to first enter the brain parenchyma (Kunis et al., 2013; Meeker et al., 2012; Ransohoff and Engelhardt, 2012). After a CNS injury, the ChP rapidly responds to pro-inflammatory mediators released from injured brain parenchyma or invading inflammatory cells via the upregulation of adhesion molecules and chemokine expression that are essential for lymphocyte trafficking (Ghersi-Egea et al., 2018; Shechter et al., 2013b; Szmydynger-Chodobska et al., 2012) (Fig.2). Therefore, ChP epithelial cells play a substantial role in controlling the leukocyte entrance into the brain.

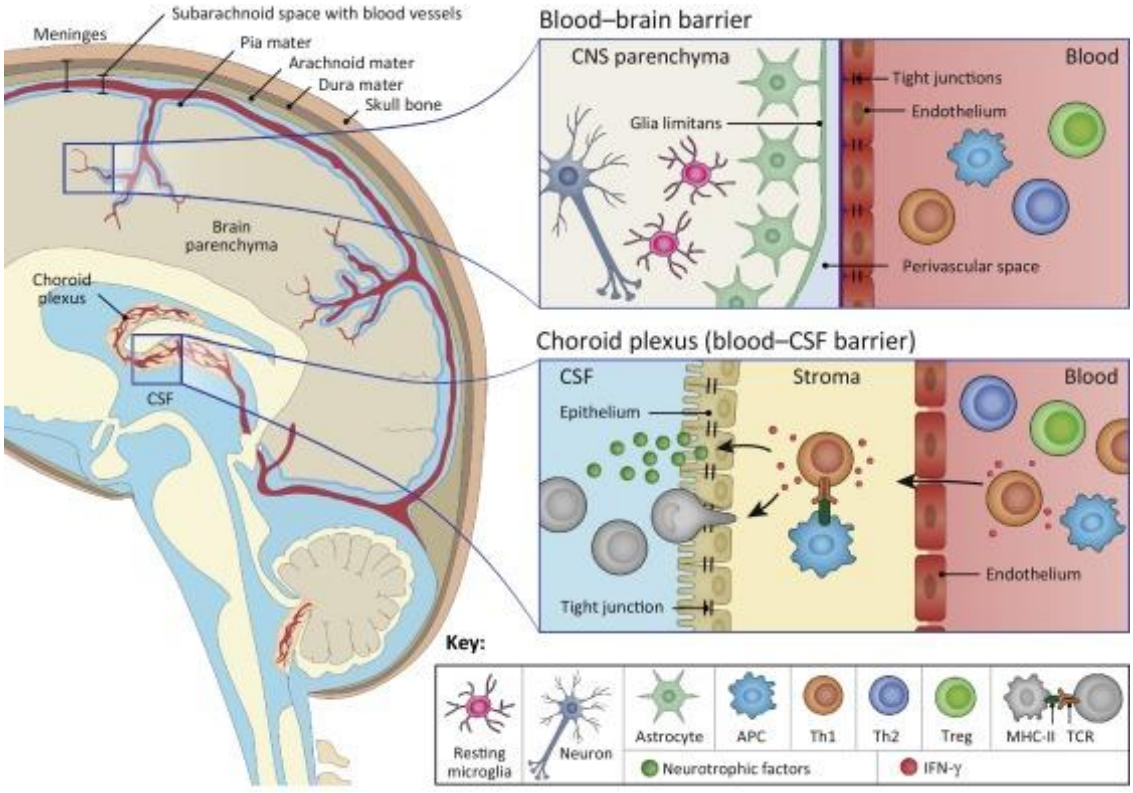

Figure 2.The Central Nervous System (CNS) barriers. The blood–brain barrier (BBB) consists of a layer of endothelial cells (interconnected by tight junctions) and glia limitans (a surface made of astrocyte endfeet processes). The blood–CSF barrier (BCSFB) at the choroid plexus (ChP) is a structure located in brain ventricles and comprises an endothelial wall of fenestrated blood capillaries and a monolayer of tight junction-connected epithelial cells. Figure adapted from Deczkowska et al., 2016.

Current research studies investigating immune-targeted therapies against post-stroke cellular neuroinflammation assume that the BBB is the main leukocyte infiltration route after a stroke (Enzmann et al., 2013; Lopes Pinheiro et al., 2016; Zhou et al., 2013). However, recent studies in primary neuroinflammatory diseases, such as experimental autoimmune encephalitis (EAE), have reported that leukocytes can migrate into the brain through alternative pathways, such as the BCSFB (Bennett et al., 2003; Kunis et al., 2015; Mony et al., 2014; Wilson et al., 2010). This alternative leukocyte invasion route is yet to be analyzed in post-stroke neuroinflammation.

1.4 Obstacles in translational research

Recently, new experimental studies have been increased to test alternative therapies to improve ischemic stroke outcomes such as postischemia, excitotoxic neural damage, depolarization spread, and apoptosis or inflammation (Iadecola and Anrather, 2011b; O'Collins et al., 2006). Unfortunately, at this time, none of the drugs that showed promise in stroke animal models have been translated into clinical use for patients (Moskowitz, 2010; Zivin et al., 1985).

The availability of reliable preclinical data is essential for selecting drug candidates with high clinical potential and consequently for designing the most effective clinical studies. Academic and industrial researchers agree on the existence of a "reproducibility crisis": the results of preclinical studies in many research fields (including stroke) lack robustness, and only a small fraction of these studies can be replicated (McNutt, 2014). Therefore, international consortia, the EU-funded Multi-PART consortium for stroke research and the NIH consortium for preclinical assessment of cardioprotective therapies (CAESAR), have attempted to establish guidelines to overcome the limitations and low reproducibility of clinical trials of promising preclinical treatments to the clinic. Moreover, multicenter preclinical randomized controlled trials (pRCTs) were proposed as a promising tool to overcome the current limitations of preclinical *in vivo* studies (Bath et al., 2009; Dirnagl et al., 2013; Lefer and Bolli, 2011).

Replicating an experiment from one laboratory to another one should be relatively easy when using the same protocol and materials, however, Phil Bourne and colleagues (Garijo et al., 2013) could conclude that an inexperienced researcher would need an average of 280h to reproduce a published method. If then, we also add how complex and sensitive can be surgical protocols, probably this time would be even higher. Therefore, one could question the reliability of the already published preclinical studies (McNutt 2014). For sure not all failures are due to the lack of reproducibility (Tymianski, 2015), preclinical trials also cover other complex steps and each of

them provides an opportunity to fail (Editorial, 2013). We could agree that the reproducibility of preclinical trials will improve the translation from bench to bedside, but also study design has to be important. Some groups reported difficulties associated with translational studies (Bath et al., 2009; Dirnagl and Fisher, 2012; Ioannidis, 2005; Ioannidis et al., 2014), such as insufficient power in most of the studies or missing cross-validation of data by independent study centers (Crossley et al., 2008; Dirnagl and Fisher, 2012; Dirnagl et al., 2013; Howells et al., 2014; O'Collins et al., 2006).

Therefore, to solve the current crisis in translational research and contribute to bridge the gap between preclinical and clinical research, diverse issues must be undertaken. Single-center studies have weaknesses such as low validity, inadequate sample size or low confidence and multicenter pRCTs are designed to overcome these issues. In order to improve the validity of preclinical research, pRCTs control several elements that clinical RCTs utilize, including a randomization, blinded study design or analysis of data by an independent study center. Importantly, in contrast to most preclinical single-center trials, pRCT is a confirmatory study (Kimmelman et al., 2014).

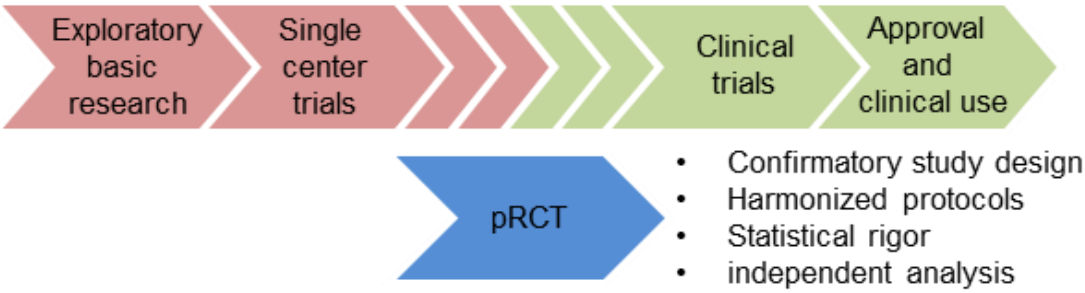

Figure 3. Preclinical randomized controlled trials (pRCTs) can serve as a link in the translational research. Preclinical research is mainly exploratory from basic research to single-center drug efficacy trials. In contrast, clinical trials are confirmatory studies with the goal of drug approval and establishing clinical use. A pRCT adopts elements from preclinical and clinical study design and might be able to better predict clinical drug efficacy. Figure adapted from Llovera et al., 2016.

To sum up, pRCT studies can provide a large number of samples, a single standardized protocol and it is performed by different research centers, thus pRCT studies must be capable helping to fill the gap in between preclinical single center research trial studies and human Phase I studies clinical trials (Fig. 3). pRCTs may not be the definitive solution, even though they address diverse key aspects that have been identified as hidden in the reproduction crisis in preclinical research. Therefore, in response to the growing reproducibility crisis in translational medicine, pRCT has been developed as a novel research tool.

Consequently, the first clinical trials have been initiated to test three drugs that are currently approved for multiple sclerosis: 1) Fingolimod (FTY720), 2) Enlimomab (anti-ICAM-1 antibody), and 3) Natalizumab (humanized anti-α4-integrin IgG4). Although Fingolimod studies showed promising results with a reduction of infarct volume (Fu et al., 2014; Zhu et al., 2015), Natalizumab and Enlimomab studies failed to improve the clinical outcome in stroke patients (Elkins, 2016; Investigators, 2001).

1.5 Research project and conclusions

As described above, pRCTs may shed some light on how to build a bridge to connect preclinical research and clinical trials. Therefore, the first aim of this thesis was to demonstrate the feasibility and usefulness of preclinical multicenter trials and to test the efficacy of an anti-inflammatory therapeutic intervention (blocking leukocyte migration with anti-CD49d antibodies) in two experimental stroke models. As described previously, most immune-targeted stroke therapies are focused on the endothelium and BBB, but it is still unclear how exactly leukocytes migrate to the brain. For this reason, the second aim of this thesis was to investigate the BCSFB as an alternative leukocyte cerebral invasion route, which has an essential role in primary inflammatory brain diseases (such as EAE), but to date, BCSFB's role has not been investigated after stroke.

To investigate the first aim of the thesis, we used antibodies (anti-CD49) against the α chain of the integrin, very late antigen-4 (VLA-4), to block leukocyte transendothelial migration to the brain. Anti-CD49d antibodies demonstrated high efficacy in different models of autoimmune diseases, and the humanized antibody Natalizumab is one of the most effective therapies for multiple sclerosis patients. Moreover, pRCT studies were proposed to increase the robustness of novel therapeutic approaches for clinical translation. For this study, we used two different stroke models and a total of 315 male C57BL/6J mice from six independent European research centers. Among all of the results, we found differences between the results from two ischemic stroke models concerning cerebral leukocyte invasion and the efficacy of anti-CD49d treatment. Anti-CD49d treatment could reduce only 30% of the leukocyte infiltration into the brain parenchyma in the permanent distal middle artery occlusion (cMCAO) model, conferring a neuroprotective benefit. Besides, different stroke models have different infiltration patterns. Whereas the cMCAO

model has an increase of leukocyte infiltration localized in the peri-infarct cortex, the transient middle cerebral artery occlusion (fMCAO) model has a lower leukocyte infiltration number without a defined localization in the injured hemisphere.

Apart from the feasibility and usefulness of preclinical multicenter trials, we can describe several points of potential improvement for future pRCTs. An obvious limitation of our analysis strategy was the constraint to a per-protocol analysis and the lack of an additional intention-to-treat analysis.

For the second aim of this thesis, we attempted to comprehend how leukocytes migrate into the brain after an ischemic stroke as this mechanism is still unclear. We could observe that T cells were predominantly clustered in the peri-infarct cortex and were the most abundant population in the ChP five days after the stroke. A series of experiments revealed that T cells were able to invade the brain parenchyma from the ChP stroma, thus avoiding entry into the CSF via the tight BCSFB. T cells were localized along the proposed invasion route from the ChP stroma to the medial-lateral ventricle wall, to the apical corpus callosum (CC), and along the CC to the peri-ischemic infarct. Furthermore, we could identify that about two-thirds of the infiltrated T cells used the ChP of the ipsilateral ventricle while only one-third used other pathways. Moreover, CSF pathway blockage caused by matrigel injection into the ipsilateral ventricle after cortical stroke did not alter T cell counts in the peri-ischemic region. Altogether, these findings indicate ChP is not only an alternative invasion route but also a key invasion route for T cells into the brain parenchyma after a stroke. Furthermore, previous reports have demonstrated that larger infarcts (fMCAO) induce lower T cell infiltration into the brain parenchyma compared to the cortical infarcts (cMCAO). In fact, we could show that in the fMCAO model, the ChP function is affected, resulting in a reduction of T cell invasion. Moreover, we could detect a significant

decrease in the total cerebral T cells in mice that received a localized photothrombotic (PT) lesion of the ipsilateral ChP. These approaches targeting the ChP function validated the crucial role of the ChP in the ischemic brain's T cell migration.

Altogether, in our first pRCT study, anti-CD49d antibodies could block only 30% of the leukocyte infiltration through the BBB endothelium. Moreover, in our second study, we detected that two-thirds of the T cells migrate to the peri-ischemic region through the ipsilateral ChP. While BBB expresses anti-CD49d in their endothelial cells, BCSFB expresses anti-CD49 in their epithelial cells (Steffen et al., 1996). Therefore, CD49d plays a minor role at the ChP, which means that stromal lymphocytes in the ChP could not be blocked by anti-CD49d, which is able to infiltrate the peri-infarct lesion. Consequently, these data serve as an explanation for the discrepant post-stroke T cell infiltration findings.

In conclusion, we identified ChP as a principal alternative leukocyte migration route into the brain after ischemic stroke. Moreover, the first preclinical randomized controlled multicenter trial (pRCT) was successfully performed, and we could define several points of potential improvement for future pRCTs. Therefore, ChP has to be considered in future translational and clinical studies that investigate therapies targeted at post-stroke leukocyte infiltration.

2. Summary

Ischemic stroke affects a large number of people all over the world. The current treatment for ischemic stroke, recombinant tissue plasminogen activator (rtPA), is not eligible for all ischemic stroke patients due to its short administration time window and contraindications such as hemorrhage or oral anticoagulation. Although new and different treatments approaches have been reported to provide positive outcomes in experimental stroke models, all failed in clinical trials. To overcome the translational research limitations of most biomedical fields, international consortia have attempted to establish guidelines for study design and reporting the resultant data. Moreover, multicenter preclinical randomized controlled trials (pRCTs) have been proposed as tools for "bridging the gap" between experimental research and clinical trials. On the other hand, it is known that after a stroke, proinflammatory mediators are released from the peri-infarcted tissue, and this leads to the recruitment of leukocytes to the lesion and increases the infarct size. Therefore, some studies aimed to block leukocyte migration into the ischemic brain.

The first aim of the thesis was to confirm some preclinical results and test the viability of performing a pRCT. To achieve this, six independent European research centers were involved in a project to test the efficacy of anti-CD49d antibodies, which inhibit the migration of leukocytes into the brain, in two distinct mouse models of stroke. Pooled results from all centers showed a significant reduction of both leukocyte brain infiltration and infarct volume only after the permanent distal occlusion of the middle cerebral artery, which causes small cortical lesions. This study confirmed that blocking brain leukocyte invasion is an important therapeutic option. Moreover, this study supports the feasibility of performing pRCTs.

Although we had successful results in our previous study, it is still not clear how leukocytes infiltrate the brain after stroke. Previous research studies have been focused on the BBB vasculature as the main leukocyte invasion of the brain after stroke. On the other hand, alternative

leukocyte brain migration routes, such as the blood-leptomeningeal barrier (BLMB) or the blood-cerebrospinal fluid barrier (BCSFB), were described in other neuroinflammatory diseases, but not after stroke.

Therefore, the second aim of the thesis was to investigate the role of the choroid plexus (ChP) as a possible infiltration route of leukocytes after an ischemic stroke. Indeed, we reported an accumulation of T cells in the peri-infarcted region, as well as the presence of T cells in the ipsilateral ChP in mice and humans after stroke. In vivo cell tracking of photoactivated T cells confirmed the migration of T cells from the ChP to the peri-infarcted cortex. The photothrombotic lesion of the ipsilateral ChP induces a reduction of T cell invasion into the ischemic brain. Moreover, a CCR2-ligand gradient was detected as a potential driving force for the T cell intracerebral migration. To sum up, our study showed that ChP is a key invasion route for post-stroke cerebral T cell invasion.

Taken altogether, future stroke therapy studies may consider planning a proper pRCT study before performing a clinical trial. Moreover, the ChP has to be under consideration as a potential relevant pathway for future therapies for inhibiting leukocyte invasion after stroke.

3. Zusammenfassung

Ischämischer Schlaganfall betrifft eine große Anzahl von Menschen auf der ganzen Welt. Die derzeitige Behandlung des ischämischen Schlaganfalls mit rekombinantem gewebespezifischem Plasminogenaktivator (rtPA) ist nur für einen geringen Teil der Schlaganfallpatienten geeignet, da die Anwendung durch zahlreiche Kontraindikationen einschränkt wird. Obwohl verschiedene neue Behandlungsansätze ein positives Ergebnis in experimentellen Schlaganfallmodellen zeigen, scheiterten diese bisher alle in klinischen Studien. Um die Grenzen der translationalen Forschung im biomedizinischen Bereichen zu überwinden, haben internationale Konsortien versucht, Richtlinien für das Studiendesign und für die Berichterstattung der daraus resultierenden Daten zu erstellen. Darüber hinaus wurden multizentrische, präklinische, randomisierte kontrollierte Studien (pRCTs) als geeignetes Instrument vorgeschlagen, um zwischen experimenteller Forschung und klinischen Studien eine Brücke zu schlagen.

Auf der anderen Seite ist bekannt, dass nach einem Schlaganfall entzündungsfördernde Mediatoren aus dem Peri-Infarktgewebe freigesetzt werden. Dies führt zur Rekrutierung von Leukozyten in das geschädigte Gehirn und zu einer sekundären Infarktexpansion. Daher zielen mehrere aktuelle Studien darauf ab, die Einwanderung von Leukozyten in das ischämische Gehirn zu blockieren.

Das erste Ziel dieser Arbeit bestand darin, präklinische Ergebnisse zu bestätigen und die Realisierbarkeit einer pRCT zu testen. Um dies zu erreichen, waren sechs unabhängige europäische Forschungszentren involviert, um die Wirksamkeit von CD49d-spezifischen Antikörpern, welche die Migration von Leukozyten in das Gehirn hemmen, in zwei verschiedenen Maus-Schlaganfallmodellen zu testen. Die zusammengefassten Ergebnisse aus den Zentren zeigten eine signifikante Verringerung sowohl der ins Hirn einwandernden Leukozyten als auch des Infarktvolumens. Diese Studie bestätigte, dass das Blockieren der Invasion von

Leukozyten eine mögliche therapeutische Option für Schlaganfall-Patienten darstellen könnte. Darüber hinaus zeigte diese Studie die Machbarkeit solcher pRCTs als neuartiges Studiendesign auf.

Trotz unserer vielversprechenden Ergebnisse in unserer früheren Studie ist es noch nicht klar, wie Leukozyten nach Schlaganfall ins Gehirn infiltrieren. Frühere Forschungsstudien konzentrierten sich auf zerebrale Kapillaren als Hauptinvasionsroute für Leukozyten in das Gehirn nach einem Schlaganfall. Auf der anderen Seite wurden alternative Invasionsrouten, wie die leptomeningeale Blut-Hirn-Schranke oder die Blut-Liquor-Schranke bei neuroinflammatorischen Erkrankungen beschrieben, jedoch nicht nach einem Schlaganfall.

Der zweite Teil der Arbeit beschäftigte sich daher mit der Rolle des Choroid plexus (ChP) als mögliche Einwanderungsroute von Leukozyten nach ischämischen Schlaganfall. Wir konnten in diesem Teil der Arbeit tatsächlich eine Akkumulation von T-Zellen in der Peri-Infarktregion sowie das Vorhandensein von T-Zellen im ipsilateralen ChP bei Mäusen und Menschen nach einem Schlaganfall feststellen. Die Analyse von in vivo photoaktivierten T-Zellen im Seitenventrikel bestätigte die Migration von T-Zellen vom ChP in den schlaganfallnahen Cortex. Eine photothrombotische Läsion des ipsilateralen ChP induzierte eine Reduktion der T-Zell-Invasion in das ischämische Gehirn. Darüber hinaus wurde ein CCL2-Gradient als potentieller Mechanismus für die intrazerebrale, gerichtete Migration von T-Zellen nachgewiesen. Zusammenfassend zeigte unsere Studie, dass der ChP eine Hauptinvasionsroute für die zerebrale T-Zellinvasion nach Schlaganfall ist.

Abschließend betrachtet sollten zukünftige Schlaganfall-Therapiestudien die Planung einer geeigneten pRCT-Studie erwägen, bevor eine klinische Studie durchgeführt wird. Darüber hinaus muss der ChP als ein relevanter Weg für zukünftige Therapien zur Hemmung der Invasion der Leukozyten nach Schlaganfall berücksichtigt werden.

4. Publication I

The choroid plexus is a key cerebral invasion route for T cells after stroke.

Authors: Gemma Llovera[1,2], Corinne Benakis[1], Gaby Enzmann[3], Ruiyao Cai[1,2], Thomas Arzberger[4,5], Alireza Ghasemigharagoz[1], Xiang Mao[1], Rainer Malik[1], Ivana Lazarevic[3], Sabine Liebscher[2,6], Ali Ertürk[1,2], Lilja Meissner[1], Denis Vivien[7], Christof Haffner[1], Nikolaus Plesnila[1,2], Joan Montaner[8], Britta Engelhardt[3], Arthur Liesz[1,2]*

Affiliations:

[1]Institute for Stroke and Dementia Research, Klinikum der Universität München, Feodor-Lynen-Str. 17, 81377 Munich, Germany.

[2]Munich Cluster for Systems Neurology (SyNergy), Munich, Germany.

[3]Theodor Kocher Institute, University of Bern, Freiestrasse 1, 3012 Bern, Switzerland.

[4]Center for Neuropathology and Prion Research, Ludwig-Maximilians-Universität, Feodor-Lynen-Str. 23, 81377 Munich, Germany.

[5]Department of Psychiatry and Psychotherapy, Ludwig-Maximilians-Universität, Nussbaumstraße 7, 80336 München

[6]Institute of Clinical Neuroimmunology, Klinikum der Universität München, Ludwig-Maximilians-University, Grosshaderner Str. 9, 82152 Munich, Germany

[7]INSERM, UMR-S U919, Institut National de la Santé Et de la Recherche Médicale (INSERM), University Caen Basse-Normandie, team Serine Proteases and Pathophysiology of the neurovascular Unit, GIP CYCERON, F-14074 Caen Cedex, France

[8]Neurovascular Research Laboratory, Vall d'Hebron Research Institute (VHIR), Universitat Autònoma de Barcelona, Barcelona, Spain

Author contributions:

G.L., C.B., X.M., G.E., R.C., T.A., I.L., S.L., and L.M. performed experiments; G.L., C.B., A.G., T.A., R.M., A.E., N.P., B.E. and A.L. analyzed data; J.M. provided critical material and analyzed data; D.V., C.H., N.P., B.E. and G.L. contributed critical input to the manuscript; A.L. initiated the study, designed experiments and wrote the manuscript.

Acta Neuropathol
DOI 10.1007/s00401-017-1758-y

ORIGINAL PAPER

The choroid plexus is a key cerebral invasion route for T cells after stroke

Gemma Llovera[1,2] · Corinne Benakis[1] · Gaby Enzmann[3] · Ruiyao Cai[1,2] · Thomas Arzberger[4,5] · Alireza Ghasemigharagoz[1] · Xiang Mao[1] · Rainer Malik[1] · Ivana Lazarevic[3] · Sabine Liebscher[2,6] · Ali Ertürk[1,2] · Lilja Meissner[1] · Denis Vivien[7] · Christof Haffner[1] · Nikolaus Plesnila[1,2] · Joan Montaner[8] · Britta Engelhardt[3] · Arthur Liesz[1,2]

Received: 22 February 2017 / Revised: 27 July 2017 / Accepted: 27 July 2017
© Springer-Verlag GmbH Germany 2017

Abstract Neuroinflammation contributes substantially to stroke pathophysiology. Cerebral invasion of peripheral leukocytes—particularly T cells—has been shown to be a key event promoting inflammatory tissue damage after stroke. While previous research has focused on the vascular invasion of T cells into the ischemic brain, the choroid plexus (ChP) as an alternative cerebral T-cell invasion route after stroke has not been investigated. We here report specific accumulation of T cells in the peri-infarct cortex and detection of T cells as the predominant population in the ipsilateral ChP in mice as well as in human post-stroke autopsy samples. T-cell migration from the ChP to the peri-infarct cortex was confirmed by in vivo cell tracking of photoactivated T cells. In turn, significantly less T cells invaded the ischemic brain after photothrombotic lesion of the ipsilateral ChP and in a stroke model encompassing ChP ischemia. We detected a gradient of CCR2 ligands as the potential driving force and characterized the neuroanatomical pathway for the intracerebral migration. In summary, our study demonstrates that the ChP is a key invasion route for post-stroke cerebral T-cell invasion and describes a CCR2-ligand gradient between cortex and ChP as the potential driving mechanism for this invasion route.

Introduction

Ischemic stroke remains one of the main causes of death and disability in the world with only very limited therapeutic options [10]. Over the past decade, post-ischemic neuroinflammation in secondary neuronal loss and repair after stroke has come into the focus of preclinical stroke research [14, 25]. Invasion of circulating, pro-inflammatory lymphocytes has been described as the key mechanism of the post-ischemic neuroinflammatory response, which aggravates the

Electronic supplementary material The online version of this article (doi:10.1007/s00401-017-1758-y) contains supplementary material, which is available to authorized users.

✉ Arthur Liesz
Arthur.Liesz@med.uni-muenchen.de

1 Institute for Stroke and Dementia Research, Klinikum der Universität München, Feodor-Lynen-Str. 17, 81377 Munich, Germany

2 Munich Cluster for Systems Neurology (SyNergy), Munich, Germany

3 Theodor Kocher Institute, University of Bern, Freiestrasse 1, 3012 Bern, Switzerland

4 Center for Neuropathology and Prion Research, Ludwig-Maximilians-Universität, Feodor-Lynen-Str. 23, 81377 Munich, Germany

5 Department of Psychiatry and Psychotherapy, Ludwig-Maximilians-Universität, Nussbaumstraße 7, 80336 Munich, Germany

6 Institute of Clinical Neuroimmunology, Klinikum der Universität München, Ludwig-Maximilians-University, Grosshaderner Str. 9, 82152 Munich, Germany

7 INSERM, UMR-S U919, Institut National de la Santé Et de la Recherche Médicale (INSERM), Team Serine Proteases and Pathophysiology of the Neurovascular Unit, GIP CYCERON, University Caen Basse-Normandie, 14074 Caen Cedex, France

8 Neurovascular Research Laboratory, Vall d'Hebron Research Institute (VHIR), Universitat Autònoma de Barcelona, Barcelona, Spain

Published online: 31 July 2017

initial infarct volume and exacerbates stroke outcome [4, 24]. Recent experimental studies demonstrated that amelioration of cerebral lymphocyte invasion by reducing the number of circulating lymphocytes in different experimental stroke models improved functional outcome [1, 18, 26, 31]. In parallel, first clinical trials have been initiated which tested this treatment approach in stroke patients using two drugs currently approved for multiple sclerosis, fingolimod (FTY720) and natalizumab (humanized anti-α4-integrin IgG4). Even though the early translation of immune-targeted therapies in stroke and the first positive results are very promising, these attempts have also been criticized as premature in face of several unsolved key questions in the field of stroke immunology [9, 39]. One of these main unresolved questions in the field is the exact mechanism of lymphocyte migration into the ischemic brain. In stroke research, the vascular migration route across the (damaged) blood–brain barrier (BBB) has been assumed as the main invasion route for circulating lymphocytes into the ischemic brain [41]. Although other infiltration routes such as meningeal blood vessels or the choroid plexus (ChP) have previously been characterized as important entry sites of lymphocytes in primary inflammatory brain disorders such as experimental autoimmune encephalitis (EAE) [30, 45], these alternative invasion sites have not been analyzed in post-stroke neuroinflammation.

Therefore, in the present study, we aimed to investigate the role of the ChP as a potential infiltration route for lymphocytes—particularly pro-inflammatory T cells—into the post-ischemic brain. We particularly focused on the ChP as an infiltration route for T cell due to the key pathophysiological role of T cells in post-stroke neuroinflammation and a specific invasion pattern observed for T cells in contrast to myeloid cells. We observed that a large proportion of brain-invading T cells migrate through the ChP after stroke. Moreover, we could identify the CCR2-dependent pathway as a key chemoattractant signal for T cells along the choroidal infiltration route.

Materials and methods

Mice

All experiments were conducted in accordance with national guidelines for the use of experimental animals, and all protocols were approved by the German governmental committees (Regierung von Oberbayern, Munich, Germany). 83 wild-type male C57BL6/J mice were obtained from Charles River. 17 *Rag1*$^{-/-}$ (B6.129S7-Rag1$^{tm1Mom/J}$), 10 *CAG-EGFP* (C57BL/6-Tg (CAG-EGFP)131$^{osb/LeySopJ}$), 22 heterozygous *PA-UBC-GFP* (B6.Cg-Ptprc Tg (UBC-PA-GFP)1$^{Mnz/J}$), 5 *CCL2-RFP* (B6.Cg-*Ccl2tm1.1*$^{Pame/J}$) and 5 *CCL2*$^{-/-}$ (B6.129S4-*Ccl2tm1*$^{Rol/J}$) male mice were obtained from Jackson Laboratories (USA). Eight female *LysM-eGFP* (Lyz2tm1.1^{Graf}) mice were kindly donated by M.Sperandio (Walter BrendlCenter for Experimental Research, Munich, Germany). CCR2$^{RFP/RFP}$CX3CR1$^{GFP/+}$ and CCR2$^{RFP/+}$CX3CR1$^{GFP/+}$ mice were originally generated by Israel Charo and Richard Ransohoff [32] and bred at the Theodor Kocher Institute, University of Bern, Switzerland. All other animals were housed at the core animal facility of the Institute for Stroke and Dementia Research, Munich, under controlled temperature (22 ± 2 °C), with a 12-h light–dark cycle period and had access to pelleted food and water ad libitum. All animals used for this study were at 8–12 weeks of age, expect for the aged mice which were 8 months old. Number of excluded animals from each experiment is shown in Suppl. Table 1.

Human samples

Both lateral ventricles with surrounding brain tissue from five stroke and six control human patients were obtained from the Human Brain and Spinal Fluid Resource Center (HBSFRC) Los Angeles, USA. Patient characteristics are described in Suppl. Table 2. Samples were sent frozen to our facility where they were kept at −80 °C until used. Samples were slowly defrosted at 4 °C for 3 h and then fixed in 4% paraformaldehyde (PFA) (pH 7.4) for 1 h at 4 °C and afterwards at room temperature (RT) for 48 h in the dark. After parafinization, 5 µm thick sections were cut for histology and immunohistochemistry. For conventional histological investigations, hematoxylin–eosin (H&E) stains were performed. Immunohistochemistry for CD3 (rabbit polyclonal, A0452/DAKO, diluted 1:50) or CD68 (mouse clone KP1, M0814/DAKO, diluted 1:50) was done in a Ventana Benchmark GX using the i-View detection system and diaminobenzidine as chromogen following the instructions of the manufacturer. Counterstaining was done with hematoxylin. ChP samples were analyzed under a microscope (Axio ImagerM2, Zeiss) and each CD3- and CD68-positive cell was counted. Total cell count per staining and per sample was normalized to the ChP area which was manually determined on H&E-stained sections.

Human RNA samples from six patients were obtained from the Hospital de la Vall d´Hebron, Barcelona. Patient characteristics are described in Suppl. Table 3. RNA from the ipsilateral and contralateral cortex of each patient was isolated using the Speed tools total RNA extraction kit (21.211, Biotools). 20 µl of total RNA was hybridized with reporter and capture probes in human nCounter gene expression code sets GX Human Immunology Kit V2 (XT-SC-HIM2-12) according to manufacturer's instruction (NanoString Technologies). Data were analyzed using nSolver Analysis software. Additional analysis was performed using "NanoStringNorm" in R (version 3.3.1) [43].

The geometric mean was used to summarize the CodeCount (positive) and SampleContent (housekeeping genes) controls, thus minimizing the impact of outliers. Stringent background correction was applied (mean + 2 standard deviations) to minimize false positives and therefore increasing specificity. As an additional QC step, housekeeping genes with high variability (SD >2) were removed before normalizing the data.

Permanent middle cerebral artery occlusion (pMCAo) model

As previously described [21], animals were anesthetized with volatile anesthesia (isoflurane in 30%O_2/70%N_2O) and placed in lateral position. After a skin incision between eye and ear, the temporal muscle was removed and the MCA identified. Then, a burr hole was drilled over the MCA and the dura mater was removed. The MCA was permanently occluded using bipolar electrocoagulation forceps. Permanent occlusion of the MCA was visually verified before suturing the wound. During the surgery, body temperature was maintained using a feedback-controlled heating pad. Mice that developed a subarachnoid hemorrhage during surgery were excluded from the analysis.

Transient middle cerebral artery occlusion (fMCAo) model

Animals were anesthetized (isoflurane in 30%O_2/70%N_2O, local lidocaine) and received an incision between ear and eye to expose the temporal skull. A laser Doppler probe was placed over on the skull above the MCA territory. Animals were then placed in supine position. After a midline neck incision, the common carotid artery and left external carotid artery were isolated and ligated, a 5 mm silicon-coated filament (Doccol, #7019PK5Re) was inserted into the internal carotid artery and MCA occlusion checked by a corresponding laser Doppler flow reduction. After 90-min MCAo, animals were anesthetized again and the filament was removed. For the survival period, animals were kept in their home cage with facilitated access to water and food. Mice without a reduction in blood flow to <20% of the baseline, controlled by a laser Doppler flow, were excluded from the analysis.

Photothrombosis (cortical and choroid plexus lesion)

Animals were placed in a stereotactic device under anesthesia (isoflurane in 30%O_2/70%N_2O).

For ChP lesions, a midline incision was performed to expose the skull and both bregma and Lambda points were identified. A burr hole was drilled at 3 mm anterior from bregma, 1 mm left from midline. Animals then received 10 µl/g body weight (BW) of 1% Rose Bengal in phosphate buffer saline (PBS) intraperitoneally (i.p). and after 5 min an optical fiber with an inner diameter of 200 µm and a NA of 0.22 was inserted at 4 mm depth from the brain surface to reach the left ventricle with an inclination angle of 30°. Photothrombosis of the ChP was achieved by 15 min illumination via the fiber probe at 532 nm wavelength (Luxivision, Germany). Control animals received the same treatment with saline injection instead of the Rose Bengal administration, including illumination of the lateral ventricle.

For cortical lesions, after midline incision and skull exposure, a laser (Cobolt HS-03, Solna, Sweden) was centered at 4 mm lateral to bregma on the left side. A fiber optic bundle of 1.5 mm diameter at the tip was used to obtain a stroke lesion similar to that induced by the pMCAo model. Animals then received 10 µl/g body weight of 1% Rose Bengal in PBS i.p. and after 5 min the brain was illuminated through the intact skull for 15 min at constant 561 nm wavelength.

Traumatic brain injury

Traumatic brain injury (TBI) was induced as previously described [34]. Briefly, mice were anesthetized with a gas mixture containing 2% isoflurane, 65% N_2O, and 33% O_2. A craniotomy window was drilled over the right parietal cortex under continuous cooling with saline. A cortical contusion was produced using a controlled cortical impact device optimized for use in mice (cylinder diameter 3.0 mm; velocity 6.0 m/s; penetration depth 0.5 mm; contact time 150 ms). Immediately following the impact, the bone flap was reimplanted and fixed using histoacrylic glue. The animals were then allowed to wake in a recovery chamber (33 °C and 50% humidity) and killed 5 days post-injury.

Assessment of infarct volume

Mice were deeply anesthetized 5 days after stroke induction and transcardially perfused with 10 ml saline. Brains were removed, frozen immediately on powdered dry ice and stored at −20 °C. For infarct volumetry, brains were serially sectioned (400 µm intervals, 20 µm thick) and stained for cresyl violet (CV) as previously described [21]. CV-stained sections were scanned at 600 dpi on a flatbed scanner (Canon). For the pMCAo and PT model, direct infarct measurement was used after validating the absence of edema at the investigated time point (5 days after pMCAo or PT). The total infarct volume was measured with ImageJ and determined by integrating measured areas and distances between sections.

Intraventricular matrigel injection

Immediately after pMCAo, animals were prepared as described above for the photothrombosis procedure.

Specifically, a 10 µl Hamilton syringe with a 10 mm length needle (Hamilton, #7804-03) was introduced into the lateral ventricle at an inclination angle of 30°. For the CSF blockage, 6 µl of matrigel (BD Matrigel™ Matrix, BD Biosciences, #354230) was injected over 5 min. Matrigel was kept at 12 °C in a cooling block until the time of injection, in order to prevent its polymerization. 5 days after pMCAo and matrigel injection, mice were transcardially perfused with 10 ml saline and 10 ml 4% PFA. For the visualization of the matrigel into the ventricle, 5 µl of matrigel + 1 µl of Evans Blue was injected in 5 min, 24 h after the injection mice were killed, brain was cut and immediately visualized under a microscope.

Immunohistology

Mice were transcardially perfused at the indicated time points with 10 ml saline and 10 ml 4% PFA (pH 7.4), then post-fixed in 4% PFA for 4 or 24 h for *PA-UBC-GFP* animals at 4 °C and immersed with 30% sucrose in PBS, then brains were frozen in −20 °C isopentane. 12 µm thick coronal sections were obtained at the level of anterior commissure for immunohistochemical analysis. Sections were mounted on SuperfrostPlus Slides (Thermo Scientific) and stored at −80 °C. Then sections were dried at room temperature for 1 h. After washing with PBS, slides were fixed with acetone at −20 °C for 5 min, this was followed by washing with PBS and PBS containing 0.1% Triton and incubation in blocking buffer containing 0.1% Triton, 0.05% Tween20, 1% bovine serum albumin, 0.1% cold fish skin gelatine and 2% goat serum in PBS at RT for 1 h before overnight incubation at 4 °C with the primary rabbit anti-CD3 antibody (1:50, abcam #16669), rat anti-CD4 antibody (clone GK1.5, 1:200, Abcam), chicken anti-laminin (1:200, Abcam) or mouse anti-CD45 (1:100, clone 104-2, Abcam) and labeled for 1 h with the secondary antibody AF594 goat anti-rabbit (1:200, Invitrogen), Cy3 goat anti-rat IgG + IgM (H + L) (1:200, Jackson Immunoresearch), FITC anti-chicken Ig H& <l (1:200, Abcam) or AF488 goat anti-mouse IgG (H + L) (1:100, Invitrogen). Finally, sections were stained with DAPI and mounted with fluoromount medium (Sigma). Samples were analyzed on an epifluorescence microscope (Zeiss Axiovert 200 M) or a confocal microscope (Zeiss 880). CD3+ cells were counted on one 12 µm section per brain at bregma or on three consecutive 12 µm sections at bregma ±60 µm for *PA-UBC-GFP* animals. The infarct core was delimitated on consecutive CV-stained sections for each individual animal. Only cells at the outer border of this area (peri-infarct region) were included for quantification analysis. The localization of each single $CD3^+$ and $CD45^+$ was marked on a topographic map according to the mouse brain atlas to achieve cumulative localization maps.

For the ChP cell death analysis: 24 h after pMCAo and fMCAo, mice were perfused with 10 ml saline and brains were removed, placed in cold PBS and the ChP from both lateral ventricles were isolated. Apoptotic cell death was detected by terminal deoxy-nucleotidyl-transferase-mediated dUTP nick-end labeling (TUNEL) according to the manufacturer's instructions (Millipore). 20-µm thick coronal sections were stained with the TUNEL kit to verify cell death in the brain.

Flow cytometry

After perfusion with saline, the ChP was removed under a stereomicroscope (Leica) and collected in 200 µl Dulbecco's Modified Eagle Medium (DMEM) + 10% fetal calf serum (FCS). ChP cells were isolated by incubating the samples in 2 ml of digestion mix [DMEM + 10% FCS + 0.4% DNASEI (#11284932001, Roche) + 3% CollagenaseD (#11088866001, Roche)], 10 min at 37 °C, and then mechanically dissociated. Brain homogenates of both hemispheres were prepared by the same dissociation/digestion protocol. Cerebral mononuclear cells were subsequently isolated using a 70 and 40% discontinuous Ficoll gradient. The following mouse antigen-specific antibodies were purchased from eBioscience: CD45 eF450 (30-F11), CD11b PE-Cy7 (M1/70), CD3 V510 or FITC (17A2), CD19 APC-Cy7 (eBisID3), CD8 PE (53-6.7), CD4 PerCP5.5 (45-0042-82), Ly6C APC (HK1.4), Ly6G PE Cy7 (RB6-8C5) and Ly6G PE (1A8). To quantify the various cell populations, cells were stained with specific antibodies in accordance with the manufacturer's protocols, acquired in a FACSVerse flow cytometer and analyzed with FlowJo software (version 10, Tree Star).

Adoptive T-cell transfer

Spleen and mesenteric lymph nodes from *CAG-eGFP* mice were isolated under sterile conditions and kept in MACS buffer (PBS + 0.5% BSA + 2 mM EDTA). After preparing a single cell suspension, T cells were isolated using a mouse T-cell enrichment kit (eBioscience). $Rag1^{-/-}$mice received 10^6 T cells in 500 µl PBS i.p. Stroke induction was performed 7 days after the T-cell transfer to allow expansion of T cells in the recipient mice.

Clearing and light-sheet microscopy

For visualization of the T-cell invasion pattern, mice were perfused transcardially with 10 ml saline and 10 ml 4% PFA (pH 7.4) 5 days after pMCAo induction in $Rag1^{-/-}$ mice receiving adoptive (eGFP+) T-cell transfer. For the study of the neuroanatomical structure of the ChP of lateral ventricles, mice were perfused with lectin-FITC in normal saline. Then mice were perfused

transcardially with 10 ml saline and 10 ml 4% PFA (pH 7.4). Whole brains were cleared using uDISCO protocol [28]: first, they were serially incubated in *tert*-butanol in 12 h until overnight incubation in 100% *tert*-butanol. The next day, samples were incubated for 1 h and 30 min in dichloromethane and finally incubated in refractive index matching solution BABB-D15, prepared by mixing BABB (benzyl alcohol + benzyl benzoate 1:2) with diphenyl ether (DPE) at a ratio of 15:1 and adding 0.4% vol DL-alpha-tocopherol (Vitamin E), for at least 4 h until the samples became transparent. Next, samples were imaged by a light-sheet microscope (LaVision BioTec). Images were acquired with a z-step of 4–8 µm, using 50 ms as exposure time and tiling scans to cover the entire specimen. Images obtained by light-sheet microscopy were analyzed by Amira software (version 6) for segmentation and 3D reconstruction. Due to uneven light penetration through the sample, we equalized raw image stacks using the pseudo flat-field correction method with the BioVoxxel plugin in Fiji software. The infarct core was segmented manually for exclusion from further analyses. T cells were segmented as individual cells for illustration using a 1.7-fold ratio of the transcellular fluorescence intensity profile peak over the neighboring tissue background fluorescence. This threshold was determined using manual identification of cells based on size, shape and peak signal intensity. No additional autofluorescence correction or background subtraction was performed.

In vivo photoactivation

Animals were prepared as described above for the photothrombosis procedure including insertion of an optical fiber into the lateral ventricle at an inclination angle of 30°. For the in vivo "pulse-chase experiment": photoactivation was performed for 5 min with a laser source of 405 nm wavelength (Luxivision, Germany) with an effective output power at the tip of the fiber of 5 mW. For 24-h photoactivation in freely behaving mice: immediately after pMCAo a burr hole was drilled under isoflurane anesthesia 3 mm anterior from bregma, 1 mm left from midline. Then a mono fiberoptic cannula with an inner diameter of 200 µm, a NA of 0.22 and 4 mm length was inserted into the left lateral ventricle with an inclination angle of 30° and fixed with dental cement (Cyano Veneer, Hager Werken). In another set of experiments, photoactivation was performed 4 days after pMCAo for 24 h at constant 405 nm illumination. Mice were then transcardially perfused with 10 ml saline and 10 ml 4% PFA. PA-GFP^{+} and PA-GFP^{-} cells were quantified on coronal sections. Percentage of infiltrated T cells shown in Fig. 2h was calculated as follows: [(T cells at 5 days − T cells at 4 days)/total T cells at 5 days] × 100].

RT-PCR array

Four 100 µm thick brain cryosections from naïve animals and 24 h pMCAo animals were collected into a MembraneSlides 1.0 Pen (Zeiss). Microbeam laser microdissection (Zeiss) was used to cut the ChP and peri-infarct cortex (880 µm × 620 µm) of the sections. Microdissectioned tissue was carefully placed with sterile forceps into a 0.5 ml sterile sample tube. Arcturus-PicoPure RNA Isolation Kit (Applied Biosystems) was used for RNA extraction and RT^{2}PreAMPcDNA syntesis Kit (Qiagen) was used for the cDNA synthesis. Finally, a RT2 Profiler PCR Array for chemokines and chemokine receptors (PAMM-022Z, Qiagen) was run on a Roche LightCycler 480 following the manufacturer's instructions. Data were analyzed with RT^2 Profiler PCR Array Data analysis software (version3.5) from SABiosciences.

Histological CCL2 gradient analysis

24 h after pMCAo induction in *CCL2-RFP* reporter mice, animals were prepared as described above for immunohistological analyses. A mosaic picture from a 12 µm coronal section at bregma level was obtained with a confocal microscope (Zeiss 880) (40× magnification), producing 346 regions of interest (ROI). Mean RFP signal per individual ROI from each individual z-stack was analyzed by the thresholding technique using ImageJ software. Following this, RFP values were rasterized from each ROI, and normalized to the range between 1.0 and 10.0, representing 1.0 the lowest and 10.0 the highest RFP expression. Each ipsilateral ROI was subsequently normalized to the anatomically homotypical ROI of the contralateral hemisphere to normalize for unspecific background fluorescence.

Statistical analysis

Data were analyzed using GraphPad Prism (version 6.0). Summary data are expressed as the mean ± standard deviation (SD) or mean ± standard error of the mean (SEM). All data sets were tested for normality using the Shapiro–Wilk normality test. The groups containing normally distributed data were tested using a two-way Student's *t* test (for 2 groups) or ANOVA (for >2 groups). The remaining data were analyzed using the Mann–Whitney *U* test. Differences with a p value <0.05 (or <0.1 for the PCR array) were considered to be statistically significant.

Results

The invasion patterns of myeloid and T cells differ after stroke

We investigated the regional distribution pattern of myeloid and T cells in a focal, cortical ischemia model in mice by

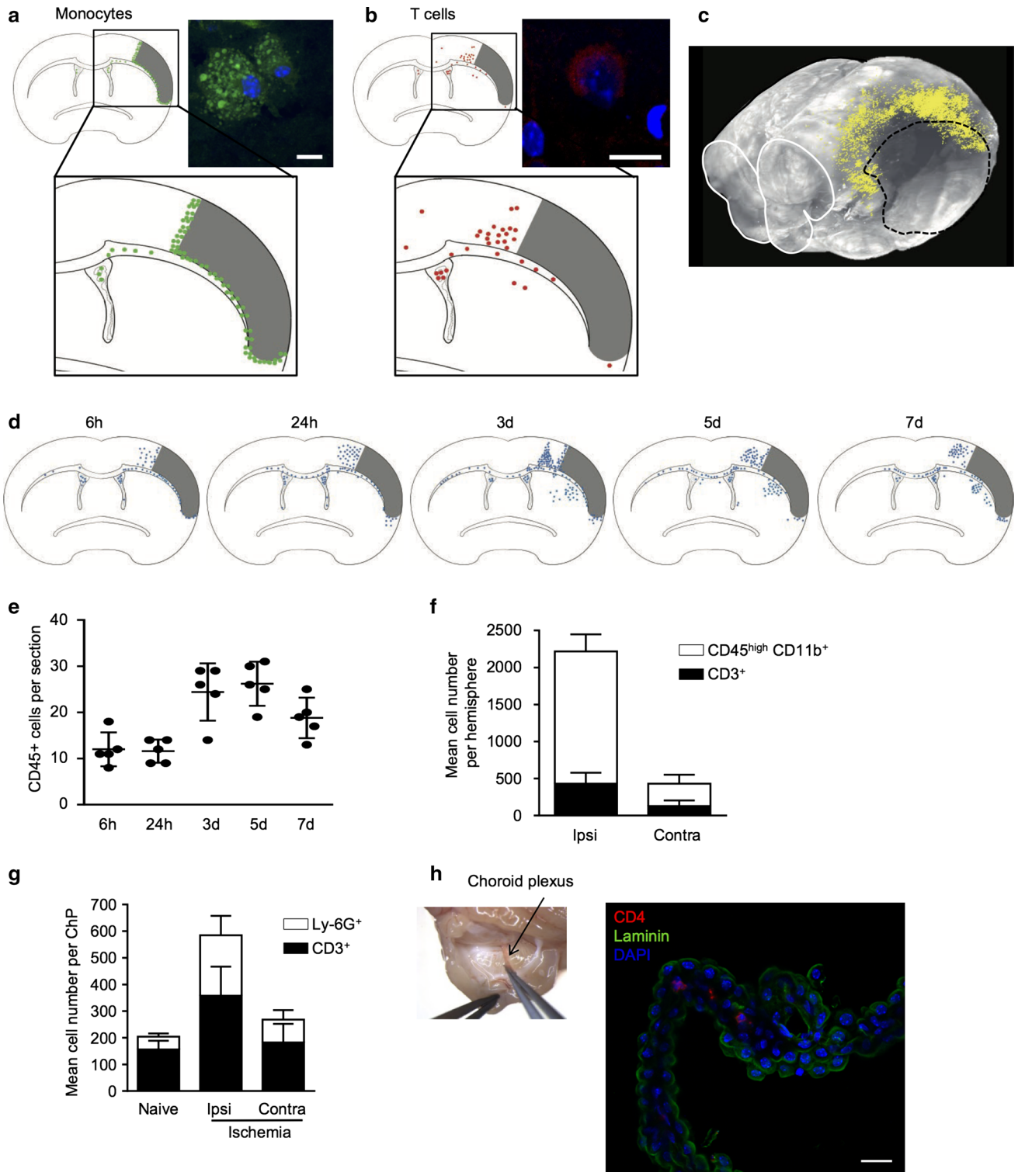

permanent occlusion of the distal middle cerebral artery (pMCAo). Cerebral T cells where visualized by immunohistological staining and myeloid cells by *LysM-eGFP* reporter mice. The ischemic core itself was excluded from this and any subsequent analyses, as we focused on the role of invading leukocytes to secondary mechanisms in the surrounding tissue at risk rather than the already necrotic infarct tissue, which undergoes later liquefaction. 5 days after stroke induction—which was the time point of maximum cerebral leukocyte invasion in this model (Fig. 1d, e)—we observed LysM-eGFP-positive myeloid cells to uniformly surround the ischemic core (Fig. 1a). In contrast, analysis of regional

◂**Fig. 1** Lymphocytes display a distinct cerebral invasion pattern. Accumulative topographic representation of each single **a** myeloid cell (*inset*: *green* LysM-eGFP$^+$ myeloid cells, *blue* nuclear DAPI stain) and **b** CD3$^+$ T cell (*inset*: *red* CD3$^+$ T cell, *blue* nuclear DAPI stain) 5 days after permanent MCA occlusion (pMCAo). Cells were accumulated from one section at bregma level of five animals each. The infarct is depicted in *gray*. *Scale bar* 10 µm. **c** T-cell segmentation and 3D reconstruction after brain clearing of 5 days post-lesion of transferred eGFP + T cells to lymphocyte-deficient *Rag1*$^{-/-}$ mice revealed specific T-cell distribution (*yellow dots*) in the peri-infarct cortex between the ipsilateral ventricle and the lesion 5 days after pMCAo. The *dashed line* demarcates the infarct core. **d** Corresponding cumulative topographic maps of CD45+ leukocytes at the indicated time points after stroke. Cells were accumulated from one section at bregma level of five animals each. Each cell is represented as a *single dot*. The infarct is depicted in *gray*. **e** Quantification of total leukocytes at the indicated time points after pMCAo, indicating the peak of the infiltrated cells at 5 days after pMCAo. Comparative analysis are represented as mean ± SD. **f** Flow cytometric analysis showing the absolute number of myeloid cells (CD45+CD11b+) and T cells (CD3+) in the ipsilateral ischemic (Ipsi) and contralateral (Contra) brain hemispheres 5 days after pMCAO. **g** Myeloid cells (CD45^{high} CD11b$^+$) cells and T cell (CD3$^+$) ratios in ChP 5 days after pMCAO were substantially different between the ipsi- and contralateral ChP after stroke as well as an increased cellularity of the ipsilateral ChP was observed after stroke compared to a naïve ChP (n = 10–18, 3 individual experiments). Data are presented as mean ± SEM **h** *left*, photograph showing the ChP located in the lateral ventricle 5 days after stroke. *Right* representative image demonstrating T-cell (CD4+) accumulation in ChP 5 days after stroke. *Scale bar* 20 µm

T-cell distribution revealed a completely different invasion pattern with T cells predominantly clustering in the peri-infarct cortex between the lateral ventricle and the lesion site (Fig. 1b). To better visualize this serendipitous observation of a specific T-cell distribution pattern, we performed 3D light-sheet microscopy of uDISCO solvent-cleared brains [28]. For this analysis, we adoptively transferred eGFP + T cells to lymphocyte-deficient *Rag1*$^{-/-}$ mice. Seven days later, we induced the stroke lesion and at 5 days post-lesion performed clearing and imaging of whole brains by light-sheet microscopy. Thereby, we were able to confirm 3-dimensional T-cell invasion clustering as a "wave front" in the peri-infarct cortex between the lateral ventricle and cortical infarct core (Fig. 1c). This obvious difference in the invasion pattern between T cells and myeloid cells prompted us to further investigate potential differences in cerebral migratory pathways between leukocyte subsets. We performed a quantification of myeloid cells and T-cell counts in the brain parenchyma and ChP by flow cytometry. As expected, both populations, myeloid cells (CD45^{high}CD11b$^+$) and T cells (CD3$^+$), were increased in the ipsilateral compared to the contralateral hemisphere after stroke. The total cell number of myeloid cells was substantially higher than of T cells in the parenchyma (Fig. 1f). In contrast to the brain parenchyma, cellular distribution of leukocyte subpopulations differed in the ChP isolated from both lateral ventricles. Flow cytometric analysis revealed a surprisingly high absolute cell numbers of T cells in the ChP (Fig. 1g), which we were able to confirm by histological staining demonstrating accumulation of T cells in the ChP stroma (Fig. 1h). To test whether the specific clustering of T cells in the peri-infarct cortex is merely a model-dependent effect after pMCAo surgeries or a distinct feature attributable to specific mechanisms of post-stroke T-cell invasion, we analyzed regional T-cell distribution in an independent cortical infarct model. We induced photothrombosis (PT) of the cortex through the intact skull without any surgical manipulation at the skull or intracerebral structures, resulting in ischemic lesions of similar shape and location as pMCAo (Suppl. Figure 1). Although the infarct volume was smaller in the PT model, we detected a comparable cerebral T-cell invasion pattern with peri-infarct cortical T-cell clustering and with similar absolute cell counts per histological section as in the pMCAo model. Additionally, we could confirm a similar T-cell invasion pattern also in a third independent model of cortical injury: mild TBI and finally, also after pMCAo in aged animals (Suppl. Figure 1). These results confirmed a previously unrecognized and specific invasion pattern of T cells after cortical infarction in the different acute brain injury models tested. Considering the differences in regional invasion patterns and relative abundance in the ChP between monocytes and T cells, these results indicated a potentially specific role of the ChP for cerebral invasion of T cells after stroke.

The choroid plexus is a primary entry site for T cells into the ischemic brain

Based on these descriptive results, we next aimed to investigate specifically the intracerebral migration of T cells from the ChP to the peri-ischemic cortex after stroke. To this end, we used transgenic *UBC-PA-GFP* mice expressing photoactivatable (PA)-GFP in T cells, in which illumination at 405 nm results in a stable shift in the peak excitation wavelength with a half-life of approximately 30 h [42]. This model enabled us to perform an in vivo "pulse-chase experiment" with labeling of T cells within one lateral ventricle with high anatomical precision. Four days after pMCAo, a 40 µm thin laser fiber was introduced into the ipsilateral ventricle and illuminated at a wavelength of 405 nm for 5 min (Fig. 2a), then animals were killed at different time points after the illumination and histologically analyzed for the localization of GFP-positive/-negative T cells stained for CD3+ (Fig. 2b). This validation of T-cell-specific photoactivation was necessary due to the potential expression of PA-GFP also in other hematopoietic cell populations, which was, however, not observed in this model. We detected photoactivated T cells (CD3$^+$ PA-GFP$^+$) in the peri-infarct cortex as early

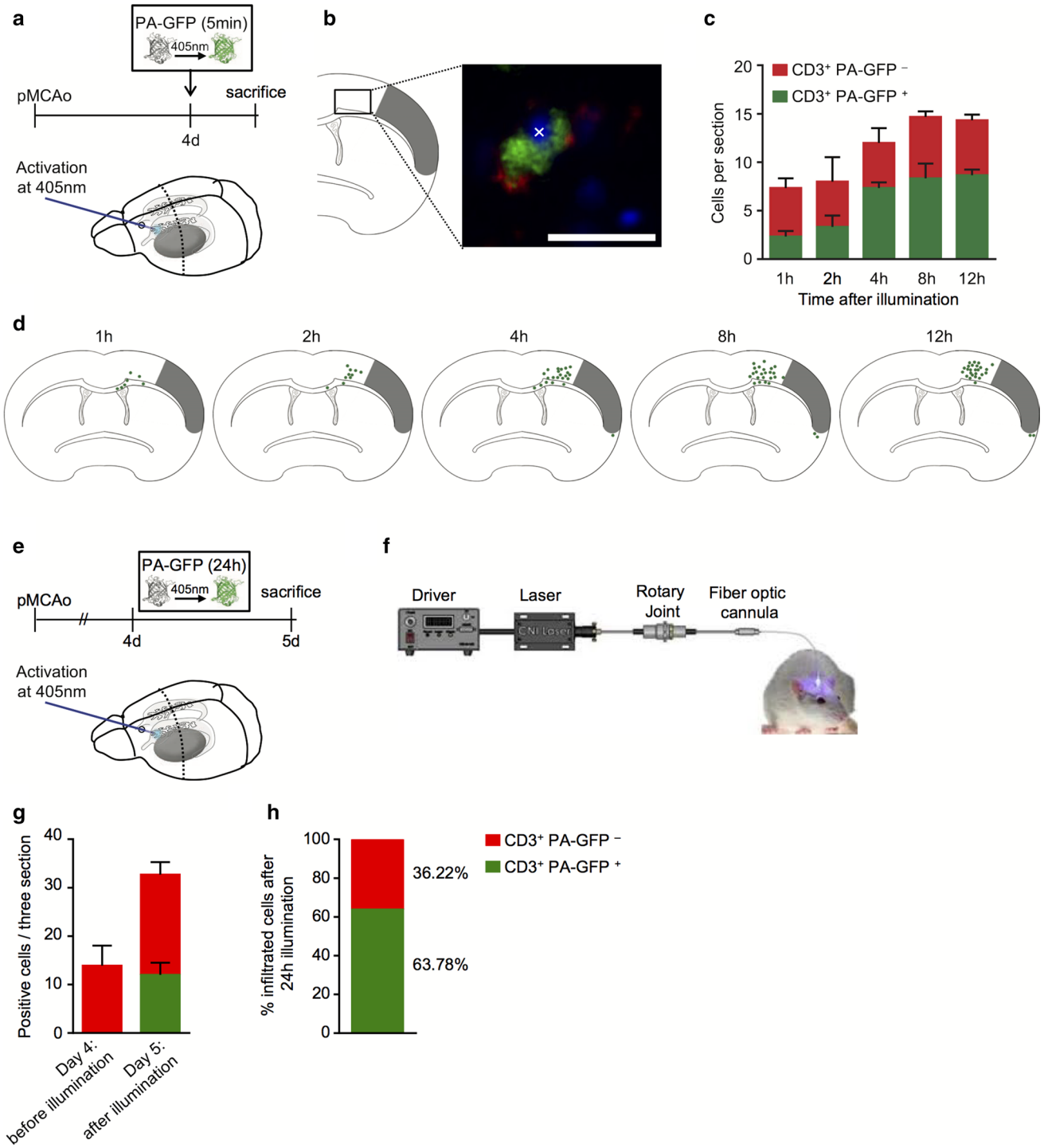

as 1 h after illumination and the number of photoactivated T cells peaked and reached a plateau at 8 h after intraventricular illumination (Fig. 2c, d). These results demonstrate a directed intracerebral migration of T cells from the ChP of the ipsilateral ventricle to the peri-infarct cortex after stroke. Importantly, as a control experiment, we did not observe photoconverted cells in the brain parenchyma at the proximity of the ventricle 24 h after inducing illumination in the ventricle (Suppl. Figure 3). Interestingly, at early time points after intraventricular illumination photoactivated T cells were located in the corpus callosum while at later time points, GFP-positive T cells were mainly detected in the cortex (Fig. 2c, d). This shift in the photoactivated T-cell localization suggests an

◂**Fig. 2** T cells migrate from the ChP to the peri-infarct cortex. **a** Schematic illustration of the experimental design to perform intraventricular/ChP optical labeling of T cells for an "in vivo pulse-chase" experiment of intracerebral T-cell migration. **b** Representative picture of photoactivated PA-GFP$^+$(*green*) and immunostained CD3$^+$ T (*red*) cells of ventricular origin in the peri-infarct cortex (marked by a *cross*). The nucleus is stained with DAPI (*blue*). *Scale bar* 10 µm. **c** Quantification of three independent animals per time point for PA-GFP-negative (*red*) and PA-GFP-positive (*green*) T cells, 4 days after pMCAo and indicated time points after illumination per one coronal section at the bregma level in the ipsilateral hemisphere. **d** Corresponding accumulative topographic maps of PA-GFP$^+$CD3$^+$ photoactivated T cells at the indicated time points after stroke from three individual animals. **e** Experimental design for estimating cerebral T-cell counts entering via the ChP over a 24 h time period at the peak infiltration period after stroke (d4–d5). **f** Schematic illustration of the optogenetic setup for intraventricular photoactivation of PA-GFP T cells. **g** Quantification of PA-GFP-negative (*red*) and PA-GFP-positive (*green*) T cells, 4 days after pMCAo without illumination ($n = 10$) or with 24 h of constant illumination ($n = 7$) per one coronal section at the bregma level in the ipsilateral hemisphere and **h** calculation of the percentage of ventricularly photoconverted PA-GFP$^+$ and PA-GFP$^-$CD3+ T cells in the ipsilateral hemisphere after subtraction of baseline T-cell counts before 24-h illumination at 4 days after pMCAo. All comparative analyses are illustrated as mean ± SD

intraparenchymal migration from the lateral ventricle to the cortex along the corpus callosum.

Notably, a single 5 min pulse for PA-GFP activation in the lateral ventricle resulted in optical labeling of more than 50% of T cells detected in the peri-infarct cortex analyzed at the late time points after photoactivation (8 and 12 h, Fig. 2c, d). Yet, this experiment was not able to precisely estimate the proportion of cerebral T cells entering via the ChP. Therefore, we performed a similar intraventricular photoactivation experiment starting 4 days after stroke induction, however, with prolonged illumination over 24 h of freely behaving mice using an optogenetic illumination setup and killing the animals directly at the end of the illumination period in awake, freely moving mice (Fig. 2e, f). We aimed to determine a rough estimate for the ratio of invading T cells via the ipsilateral ChP in the lateral ventricle or by other invasion routes over this 24-h period from 4 to 5 days after stroke by subtracting the number of T cells detected at 4 days post-lesion (i.e., before intraventricular photoactivation, Fig. 2g), which was determined in a second set of control-operated animals without intraventricular illumination. Importantly, long-term photoactivation of the lateral ventricle itself did not induce an inflammatory reaction compared to mice that underwent the same procedure without illumination (Suppl. Figure 4). Hereby, we detected by this approximation that about two-thirds of the T cells infiltrated via the ChP of the ipsilateral ventricle while one-third of T cells infiltrated along other pathways (Fig. 2g, h), confirming that the ChP of the lateral ventricle is the predominant invasion route for T cells after cortical infarction.

Choroidal T cells invade the brain parenchyma

The above-shown results obtained in the UBC-PA-GFP mouse model suggested infiltration of T cells through the ChP and migration to the peri-infarct cortex along the corpus callosum. Surprisingly, the neuroanatomical structure of the ChP of lateral ventricles in adult mice as well as the exact migration pathway of T cells from the ChP stroma to the brain parenchyma have previously not been well described. Therefore, we performed light-sheet microscopy of lectin-perfused and cleared brains enabling 3-dimensional visualization of choroidal vascularization and its anatomical junction to the ventricle wall. In accordance with previous studies on ChP development during embryogenesis [23], we detected attachment of the ChP to the medial wall of the lateral ventricle (Fig. 3a, b) clearly visible by vasculature penetrating from the brain parenchyma into the ChP (Suppl. video). 3-dimensional reconstruction of segmented ChP, lateral ventricle and the corpus callosum revealed the close proximity of these anatomical structures (Fig. 3c, d). Therefore, we hypothesized that T cells shall be able to directly invade the brain parenchyma from the ChP stroma, avoiding first the entry into the CSF via the tight BCSFB and passage through the CSF. This hypothesis was further supported by detecting eGFP-positive T cells localized along the proposed invasion route from the ChP stroma, the medio-basal ventricle wall, the apical corpus callosum (CC) and along the CC to the peri-ischemic infarct in lymphocyte-deficient *Rag1*$^{-/-}$ mice reconstituted with eGFP + T cells (Fig. 3e, f). Finally, to test the potential alternative migration route of T cells from the ChP to the cortex via the CSF, we blocked this migration pathway by matrigel injection into the ipsilateral ventricle (Fig. 3f). Matrigel—a non-toxic agent polymerizing at body temperature—was confined to the ipsilateral ventricle and did not diffuse to lower compartments (Fig. 3g). Moreover, this technique of blocking CSF flow and intraventricular leukocyte migration was previously shown to not induce neuroinflammation or affect ChP integrity [36]. Blocking of CSF flow by matrigel injection did not significantly alter T-cell counts at the peri-ischemic infiltration site compared to control-operated mice (needle introduction and PBS injection), indicating that intraventricular lymphocytes as well as migration via the ventricular CSF space might not play a significant role for cerebral T-cell invasion after stroke (Fig. 3h).

Choroid plexus infarction reduces post-stroke T-cell invasion

Several previous reports demonstrated that experimental brain ischemia by transient, proximal occlusion of the

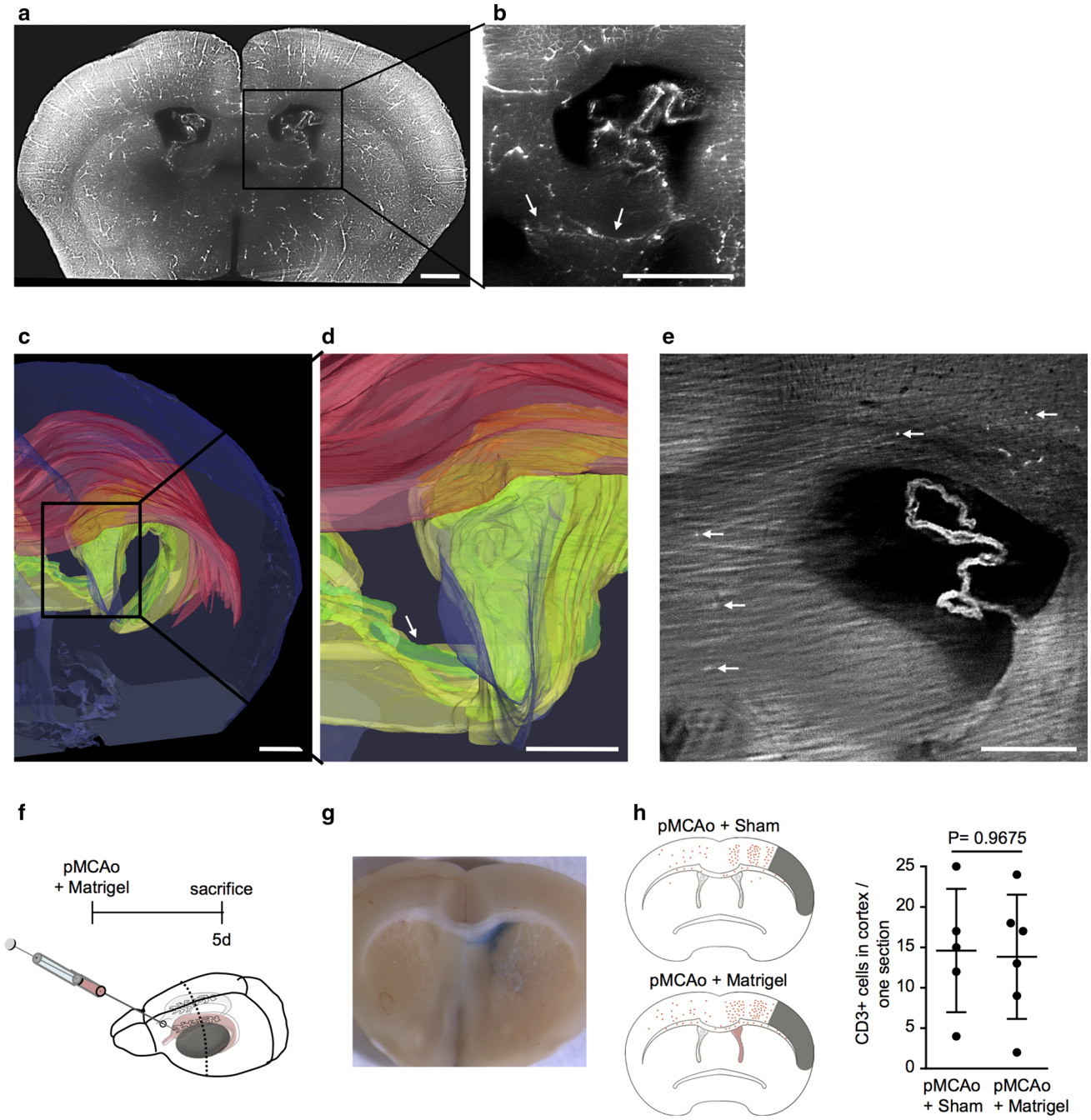

Fig. 3 Choroidal T cells directly invade the brain parenchyma. **a**, **b** Coronal image from a lectin-perfused, cleared brain. *Arrows* highlight penetrating cerebral vessels to the ChP, indicating the ChP–brain parenchyma junction. *Scale bar* 0.5 mm. **c–d** Lectin-perfused solvent-cleared brains have been imaged by light-sheet microscopy and segmented for brain parenchyma (*blue*), the ChP (*green*), ventricle (*yellow*) and the corpus callosum (*red*) in order to illustrate the anatomical relation of these structures presumably involved in intraparenchymal T-cell migration. Arrows indicate the junction of the ChP stroma with the brain parenchyma at the mediobasal ventricle wall. *Scale bar* 0.5 mm. **e** Source image used for the 3D reconstruction shown in Fig. 1c. *Arrows* indicate eGFP + T cells which have been transferred to lymphocyte-deficient *Rag1*$^{-/-}$ mice for T-cell-specific identification in solvent-cleared brains, *scale bar* 250 µm. **f** Experimental design to block intraventricular cell migration by injection of matrigel into the ipsilateral ventricle. **g** Representative image illustrating polymerized matrigel inside the left lateral ventricle. Matrigel was supplemented with *Evans blue* for a better visualization of the matrigel in this image. **h** Accumulative topographic maps and **i** quantification of CD3^{+} T cells per one ipsilateral coronal brain section at bregma location 5 days after pMCAo + Sham or pMCAo + matrigel treatment (n = 6 per group, three independent experiments). Comparative analyses are represented as mean ± SD

MCA (tMCAo model) resulted in substantially lower T-cell infiltration despite much larger infarcts than after permanent, distal occlusion of the MCA (pMCAo model) [20, 47]. Following the previous results revealing the ChP as a key invasion route for cerebral T-cell invasion after stroke, we tested the hypothesis that proximal MCA occlusion might affect ChP function thereby resulting in reduced T-cell invasion. Hence, we analyzed T-cell infiltration 3 days after pMCAo or tMCAo (Fig. 4a). In accordance with our previous studies, large ischemic lesions in the tMCAo model resulted in significantly lower T-cell infiltration compared to cortical lesions in the pMCAo model (Fig. 4b). Impaired post-ischemic T-cell infiltration in the tMCAo model was associated with a more than twofold increase in TUNEL+ cells of the ipsilateral ChP stroma, while distal MCA occlusion in the pMCAo model did not induce choroidal cell death compared to the contralateral control ChP (Fig. 4c, d). Ischemic lesion after proximal occlusion of the MCA is fully compatible with the transient occlusion of the anterior choroidal artery, which supplies predominantly the ChP and originates from the proximal MCA [3, 11]. To further corroborate the critical role of the ChP in post-stroke T-cell invasion, we induced a localized photothrombotic (PT) lesion of the ipsilateral ChP directly after pMCAo by a laser probe introduced into the ipsilateral ventricle (Fig. 4e, f). 5 days after surgery, cell death was observed specifically in the ChP after PT (Fig. 4f) and we detected a significant reduction in total cerebral T-cell counts in mice undergoing choroidal photothrombosis (pMCAo + PT) in comparison to sham-operated (pMCAo + Sham) mice (Fig. 4g, h). More specifically, choroidal infarction massively reduced cortical T-cell invasion while some T cells were detected in the caudal ventricle region most likely as a reaction to the photothrombotic lesion itself (Fig. 4f, g). Notably, we did not detect a significantly difference in the infarct volume in mice with choroidal photothrombosis (pMCAo + PT) in comparison to sham-operated animals (pMCAo + Sham) (Fig. 4i) despite the substantial reduction in T-cell infiltration. These

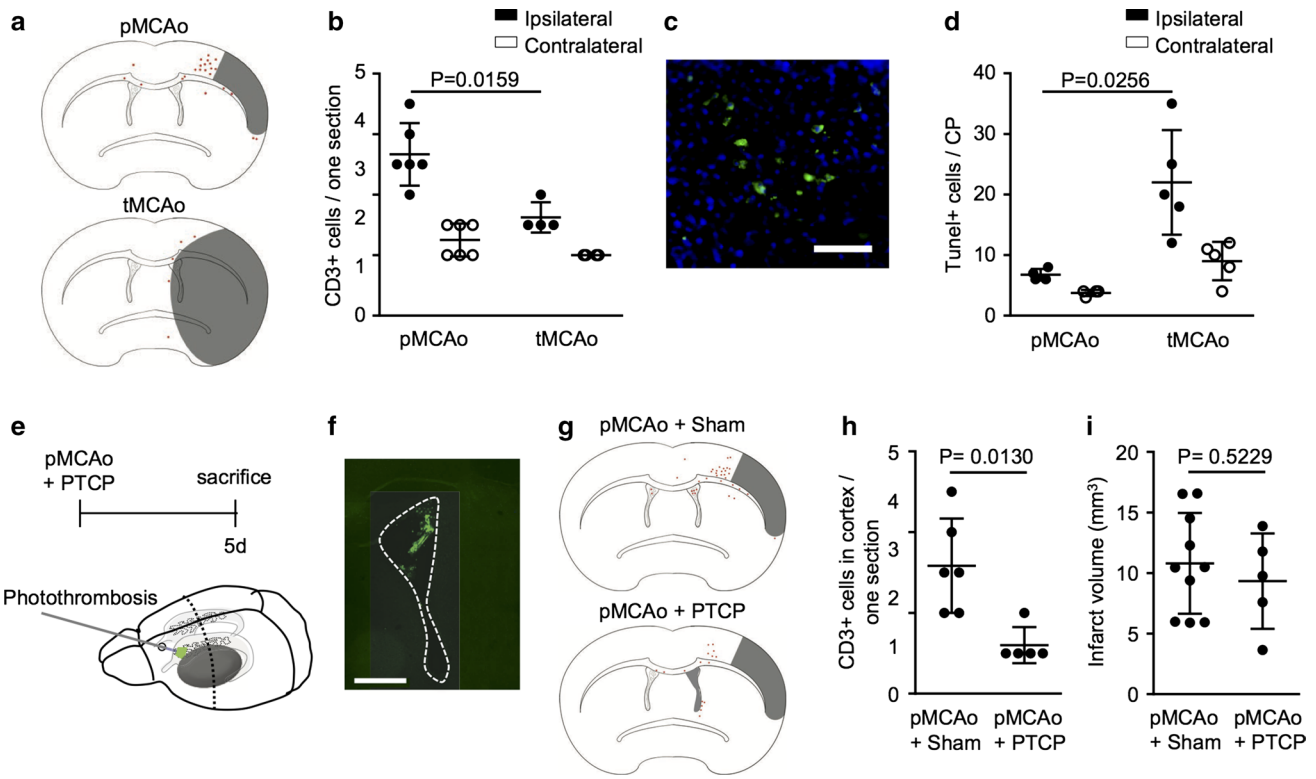

Fig. 4 Choroid plexus infarction reduces T-cell invasion after cortical ischemia. **a** Cumulative topographic maps of one coronal section from six mice (*each dot* represents one cell, infarct area shown in *gray*) and **b** quantitative analysis of T cells per one ipsilateral and contralateral hemisphere section at bregma level 3 days after pMCAo or tMCAo ($n = 6$ per group). **c** Representative image of TUNEL+ (*green*) stained apoptotic cells within the ChP of the ipsilateral ventricle 24 h after tMCAo; nuclear stain with DAPI (*blue*). *Scale bar* 50 µm. **d** Quantitative analysis of TUNEL-positive cells per one ipsilateral and contralateral ChP 24 h after pMCAo or tMCAo ($n = 4$–5). **e** Experimental design to test the role of the ChP in post-stroke T-cell infiltration by an isolated photothrombotic ChP lesion (PT-ChP). **f** Representative image of TUNEL+ (*green*) stained apoptotic cells within the ChP of the ipsilateral ventricle 5 days after pMCAo + PT-ChP. *Scale bar* 500 µm. **g** Cumulative topographic maps of T cells from one section at bregma level from five mice per group, 5 days after pMCAo + Sham or pMCAo + PT-ChP surgery. **h** Quantification of cortical T cells in both groups per one coronal section in the ipsilateral hemisphere and **i** infarct volume of both treatment groups ($n = 5$ per group)

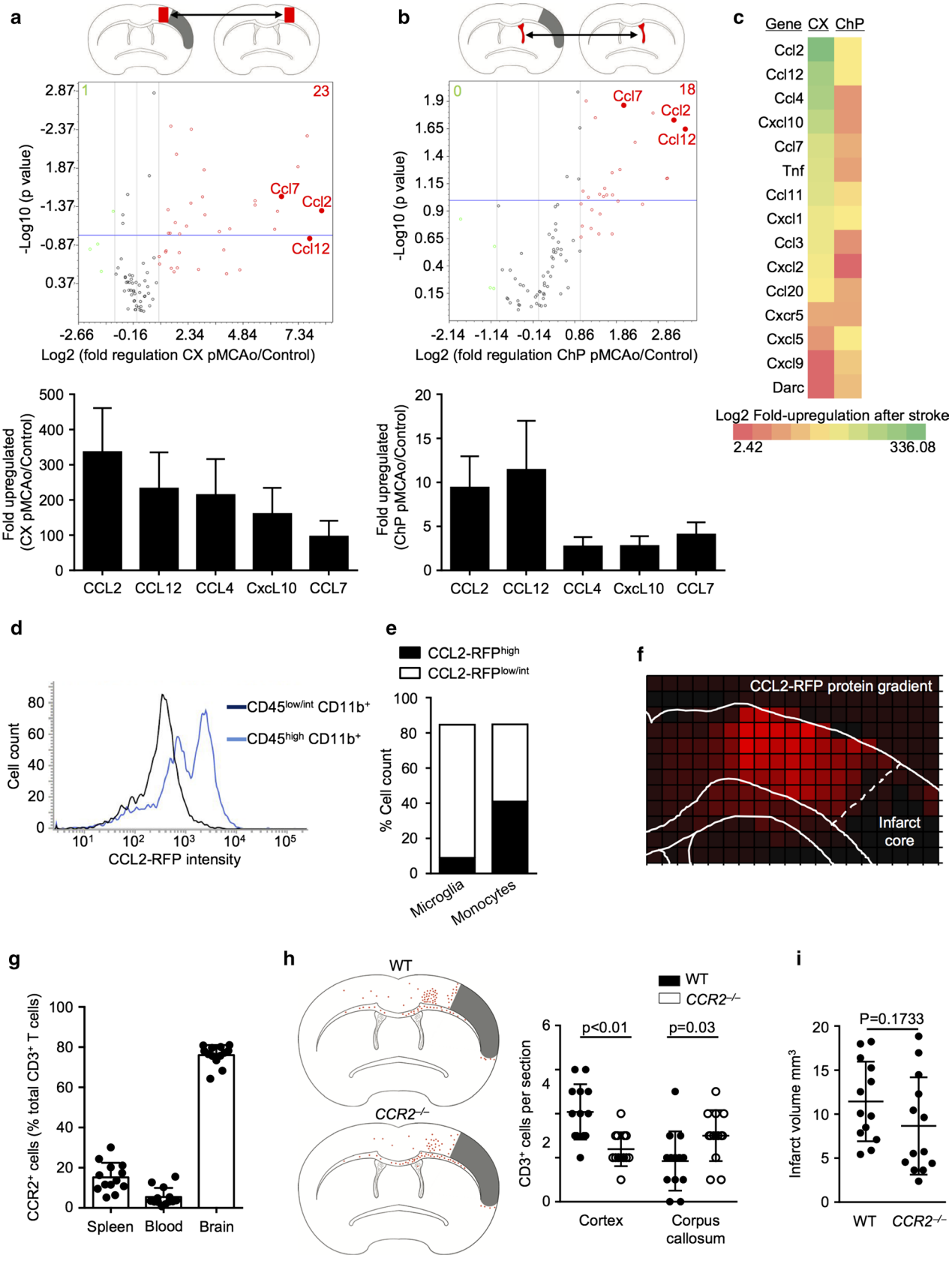
a
b
c
Gene CX ChP
Ccl2
Ccl12
Ccl4
Cxcl10
Ccl7
Tnf
Ccl11
Cxcl1
Ccl3
Cxcl2
Ccl20
Cxcr5
Cxcl5
Cxcl9
Darc
Log2 Fold-upregulation after stroke
2.42
336.08
-Log10 (p value)
Log2 (fold regulation CX pMCAo/Control)
Log2 (fold regulation ChP pMCAo/Control)
Ccl7
Ccl2
Ccl12
Fold upregulated (CX pMCAo/Control)
Fold upregulated (ChP pMCAo/Control)
CCL2
CCL12
CCL4
CxcL10
CCL7
d
e
f
Cell count
CD45low/int CD11b+
CD45high CD11b+
CCL2-RFP intensity
CCL2-RFPhigh
CCL2-RFPlow/int
% Cell count
Microglia
Monocytes
CCL2-RFP protein gradient
Infarct core
g
h
i
CCR2+ cells (% total CD3+ T cells)
Spleen
Blood
Brain
WT
CCR2-/-
CD3+ cells per section
p<0.01
p=0.03
Cortex
Corpus callosum
Infarct volume mm3
P=0.1733

◂**Fig. 5** Intraparenchymal T-cell migration follows a CCR2-ligands gradient between peri-infarct cortex and choroid plexus. **a**, **b** Volcano plot illustration of the regulation of gene expression of 84 chemokines and chemokine receptors (*upper panels*) and bar graphs for top 5 regulated genes (*lower panels*) in **a** the cortex (CX) and **b** the ChP between 24 h after pMCAo or Sham surgery ($n = 6$ per group, 3 individual experiments per analysis). **c** Heat map of the top 10 upregulated genes in the cortex and ChP24h after pMCAo compared to Sham surgery, indicating substantial differences in the magnitude of regulation of the same genes in the CX and ChP after pMCAo. **d** Representative histogram of the expression intensity of CCL2-RFP in the $CD45^{low/int}CD11b^{+}$microglial population and $CD45^{high}CD11b^{+}$ monocytes 24 h after pMCAo. **e** Quantification of "high" and "low/intermediate" CCL2-RFP expression cells within the microglial and monocyte cell populations corresponding to the cell populations shown in panel D. **f** Illustration of rasterized, relative CCL2-RFP expression intensity normalized to the homotypic contralateral hemisphere (see "Materials and methods" section for details) 24 h after pMCAo in the ipsilateral hemisphere revealing a CCL2 focus in the peri-infarct cortex. *Dashed line* indicates the border to the infarct core. **g** Frequency of CCR2-positive cells among total T cells (CD3) was analyzed by flow cytometry 5 days after stroke in spleen, blood and the ipsilateral brain hemisphere. **h** Cumulative topographic maps (*left*; 13 mice per group) and quantification (*right*) of T-cell counts 5 days after pMCAo in WT and $CCR2^{-/-}$mice per one coronal section in ipsilateral cortex and corpus callosum and **i** infarct volume of both groups ($n = 13$ per group, 2 individual experiments)

results clearly demonstrate the importance of the ChP for post-stroke T-cell infiltration, however, without affecting stroke severity in contrast to previous studies linking cerebral T-cell infiltration to stroke outcome.

CCL2 chemokine gradient between the peri-infarcted cortex and choroid plexus

We next aimed at investigating the molecular basis for the directed intracerebral migration of T cells from the ChP to the peri-infarct cortex and hypothesized an underlying chemokine gradient between cortex and the ChP to be responsible for this fast intraparenchymal T-cell migration. Therefore, we performed a PCR array for 84 chemokines and chemokine receptors from microdissected samples of ChP and the peri-infarct cortex 24 h after pMCAO and control animals. We detected 23 up-regulated genes in the peri-infarct compared to control cortex (Fig. 5a; Suppl. Table 4) and 18 up-regulated genes in the post-stroke ChP compared to control ChP (Fig. 5b; Suppl. Table 5), using twofold regulation and $p < 0.1$ as significant thresholds. Interestingly, the two most abundantly upregulated chemokines in the cortex after stroke—CCL2 and CCL12—were also most highly upregulated in the post-ischemic ChP. However, overall chemokine upregulation was manifold higher in the peri-infarct cortex compared to the ipsilateral ChP with, e.g., more than 300-fold upregulation of CCL2 in the cortex compared to a tenfold upregulation in the ChP after stroke (Fig. 5a–c), suggesting a biologically relevant gradient for these chemokines between cortex and ChP. Notably, three out of the five most abundantly upregulated chemokines in the cortex as well as in the ChP are ligands of the CC chemokine receptor 2 (CCR2), namely CCL2, CCL12 and CCL7 [17, 19, 27]. This indicated a potentially relevant involvement of the CCR2 chemokine axis in post-ischemic T-cell attraction from the ChP to the peri-infarct cortex. To reveal the cellular source of cortical CCL2 expression after stroke, we performed a flow cytometric analysis of *CCL2-RFP* reporter mice 24 h after stroke induction. Here, we detected $CD45^{low/int}CD11b^{+}$ (presumably microglia) and $CD45^{high}CD11b^{+}$ (presumably monocyte/macrophages) as the main RFP positive cells, however, with differences in CCL2-RFP expression levels between these two populations (Fig. 5d). While microglial cells displayed homogenous low-intermediate CCL2-RFP expression levels, we detected two distinct subpopulations of $CD45^{high}$monocytic cells with low/intermediate and high CCL2-RFP expression, respectively (Fig. 5d, e). Next, we analyzed histologically coronal brain sections of *CCL2-RFP* reporter mice to test for the cellular source of the regional chemokine gradient suggested by the results of the PCR array. Indeed, after rasterizing the fluorescence intensity images and generating density maps, we detected a marked gradient of RFP expression with its center at the same anatomical area of predominant T-cell invasion in the peri-infarct cortex (Fig. 5f). Notably, this CCL2 gradient focusing in the peri-infarct cortex was observed already at early time points after stroke (24 h post-lesion) preceding cerebral T-cell invasion and can, therefore, be assumed rather as a cause than a consequence of cortical T-cell clustering. Taken together, our chemokine screening analysis identified CCR2 ligands being substantially upregulated after stroke and we were able to confirm a relevant CCL2 gradient also at the protein level, mainly secreted by innate immune cells in the peri-infarct cortex. Consequently, we hypothesized that CCR2 might be involved in attraction of T cells from the ChP along the CCL2 gradient to the peri-infarct cortex. Analyzing the organ-specific frequency of $CCR2^{+}$ T cells in the peripheral immune compartment (spleen, blood) and the post-ischemic brain, we observed a substantial enrichment of $CCR2^{+}$ T cells in the ischemic hemisphere supporting a potential role of CCR2 in cerebral T cells migration (Fig. 5g). We next aimed to block the CCR2 chemokine axis using $CCR2^{-/-}$ mice to probe its impact on post-stroke T-cell migration. CCR2-deficiency indeed significantly reduced T-cell migration to the peri-infarct cortex. Interestingly, lack of CCR2 resulted in slightly increased T-cell counts in the corpus callosum (Fig. 5h). Notably, we did not detect a significant difference in infarct volume between groups, indicating a stroke severity-independent effect of CCR2 expression in T-cell migration (Fig. 5i). This finding suggests that chemotaxis driven by CCR2 ligands might be important for intracerebral

migration along a chemokine gradient to the peri-infarct region but might not be involved for initial entry of T cells through the ChP.

The role of choroid plexus after stroke in humans

Next, we aimed to test the involvement of the ChP for post-stroke cerebral T-cell invasion in human stroke patients. For this, we obtained autopsy samples of both lateral ventricles from five stroke patients dying of other cause than stroke in the subacute phase after stroke onset and six control patients without cerebral infarction (Suppl. Table 2). By histological analysis for T cells (CD3) and monocytes/macrophages (CD68) (Fig. 6a), we observed increased choroidal T-cell counts in stroke patients compared to control patients (Fig. 6b). Moreover, in accordance with the results obtained in the mouse stroke models, T cells were the main cell population in the ChP of stroke patients (Fig. 6b). We then analyzed the chemokine expression in human samples of the peri-infarct cortex and the contralateral homotypic control cortex from autopsy samples of six patients, which had died in the acute phase after stroke (Suppl. Table 3). We performed a NanoString analysis for quantitative transcriptional regulation of 561 inflammation-related human genes, revealing a distinct upregulation of 8 inflammatory genes in the peri-infarct cortex compared to the contralateral side

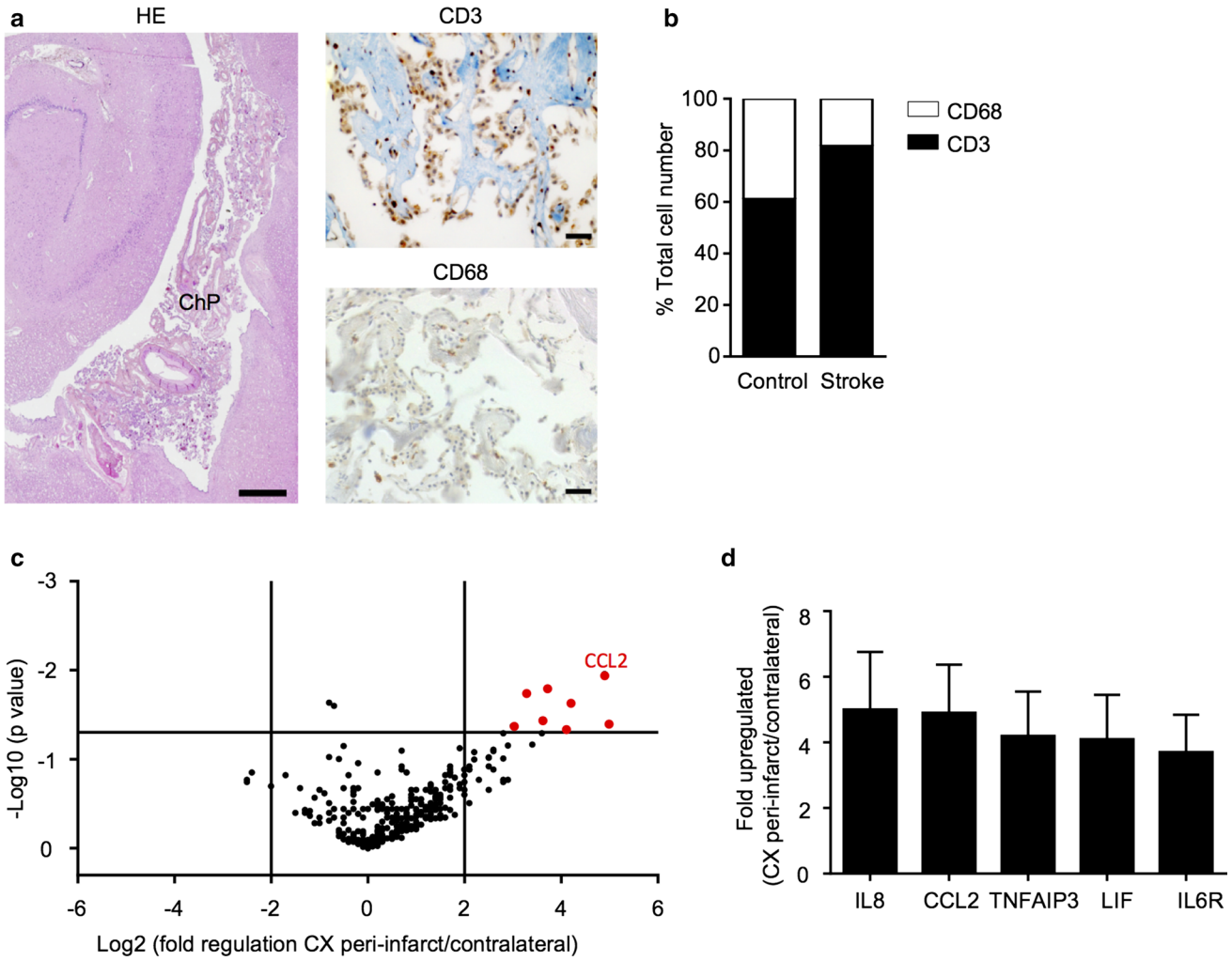

Fig. 6 Choroid plexus cellularity and cortical chemokines in human stroke patients. **a** Representative images of a hematoxylin–eosin-stained section of the human choroid plexus in the temporal horn of the lateral ventricle and surrounding brain tissue (*left, scale bar* 1 mm), CD3+ T cell and CD68+ monocytes/macrophage stainings (CD68) (*right*, *scale bars* 40 µm) used for subsequent analysis. **b** Quantitative analysis of the ratio between CD68 and CD3 positive cells in the ipsilateral ChP of control patients or stroke patients (n = 5–6 per group, see Suppl. Table 2). **c** Volcano plot depicting the regulation of gene expression assessed by Nanostring analysis between the ipsilateral peri-infarct tissue and homotypic contralateral side in patients in the acute phase after ischemic stroke (see Suppl. Table 3). *Red dots* indicate the significantly upregulated genes in the peri-infarct tissue. **d** *Bar graph* showing fold regulation of the top 5 significantly upregulated genes in the peri-infarct cortex compared to the contralateral hemisphere (n = 6 per group)

(Fig. 6c). Also in these human samples, CCL2 was one of the overall most highly upregulated genes, and together with IL-8 (CXCL8) the only significantly upregulated chemokine (Fig. 6d; Suppl. Table 6). These results demonstrate a remarkable similarity for the cellular infiltration pattern as well as cortical chemokine expression after human stroke compared to the murine stroke model, suggesting that a comparable intraparenchymal T-cell migration from the ChP to the ischemic lesion might also occur after human stroke.

Discussion

We describe in this study the ChP as a previously unrecognized critical invasion route for T cells into the ischemic brain after stroke. This finding of choroidal T-cell infiltration after stroke offers an explanation of previously elusive observations in the field of stroke immunology such as the specific clustering of T cells in the peri-infarct cortex, differences in T-cell invasion between stroke models and finally the ineffectiveness of blocking post-stroke T-cell invasion by targeting endothelial adhesion molecules in several previous reports.

Lymphocyte infiltration after stroke has become a main research area in experimental stroke research due to the implication of post-stroke neuroinflammation in secondary brain damage [4, 44]. However, preclinical research on post-stroke neuroinflammation has repetitively experienced irreproducibility of findings between laboratories using different stroke models and reported substantial differences in the extent of neuroinflammation between commonly used mouse models of acute brain ischemia [8, 47]. While models of permanent ischemia in the cerebral cortex (pMCAo, photothrombosis, thrombin-injection model) have reproducibly resulted in a pronounced cellular neuroinflammation, more extensive lesions induced by transient occlusion of the proximal MCA resulted in less cerebral leukocyte infiltration [6, 20, 47]. In the present study, we observed that only transient, proximal MCA occlusion induced cell death in the ipsilateral ChP, most likely by occlusion of the supplying anterior choroidal artery. Taking into account that based on our results approximately 60% of cerebral T cells invade via the ipsilateral ChP, it seems plausible that differential ChP damage in some stroke models accounts for a large part of inter-laboratory and -model differences observed in previous studies on post-stroke neuroinflammation.

In contrast to the endothelium of the BBB, the ChP endothelium is fenestrated, facilitating cellular migration into the ChP stroma. On the other side, the tight junctions of the ChP epithelium contribute to the BCSFB by limiting paracellular transport of small molecules and immune cell entry into the CSF [29, 35, 38]. These anatomical properties of the ChP implicate that circulating leukocytes can easily enter the ChP stroma but crossing the epithelial layer into the CSF would be far more energy demanding. Previous studies have proposed that ChP-resident T cells can be readily mobilized for cerebral invasion under inflammatory conditions. T cells in the ChP have in principle two routes to invade the brain parenchyma: crossing the epithelial layer into the CSF and invading the brain from the CSF at different sites or migrate from the ChP stroma directly into the brain parenchyma at the base of the ChP. The involvement of both invasion pathways for T cells from the ChP stroma have been barely investigated under physiological conditions or inflammatory brain disorders; nevertheless, the migration pathway via the CSF has been assumed in the majority of studies analyzing the ChP in autoimmune brain diseases [13, 33]. Yet, the migration of lymphocytes across the BCSFB remained questionable as the key adhesion molecules involved in this process—ICAM-1 and VCAM-1—are exclusively expressed on the apical side of ChP epithelial cells, thus, not accessible for stromal lymphocytes to enter the CSF [37, 46]. This means that key adhesion molecules which are expressed and critical for cell trafficking at the BBB are also expressed in the ChP but are not functional for T-cell invasion to the ChP because these molecules are not accessible for circulating leukocytes. This is of high clinical relevance, as the specific inhibition of endothelial or leukocyte adhesion molecules involved at the BBB failed so far to improve clinical outcome in stroke patients [12, 16] in contrast to numerous preclinical studies showing improved stroke outcome by depleting or reducing circulating lymphocytes. These discrepant findings might be attributable to the wrong assumption that cerebral T-cell invasion occurs along the vascular invasion routes, thereby targeting vascular adhesion molecules that play only a minor role at the ChP.

The results from our study unexpectedly suggest a rapid and directed T-cell migration from the ChP to the brain parenchyma. We have demonstrated the previously insufficiently investigated attachment of the ChP in the mouse lateral ventricle at the basomedial ventricle wall as a possible entry site for T cells into the CNS. Border structures such as tanycytes surrounding circumventricular organs or other cell types with tight intercellular junctions have to our knowledge not been described at the ChP base. The junction of the ChP to the brain parenchyma remains, therefore, a matter of debate and further neuroanatomical studies are urgently needed to clarify the anatomical basis for direct cell entry from the ChP stroma to the brain parenchyma. Here, we identified T cells after photoactivation in the ChP along the ChP–parenchyma junction, the corpus callosum and the peri-infarct cortex. Moreover, inhibition of CSF circulation did not affect cerebral T-cell invasion, strongly supporting a not yet considered migration from the ChP stroma into the brain parenchyma. Additional indirect indication for this novel migration pathway was the surprisingly

fast kinetics of T-cell translocation from the ventricle/ChP after photoactivation to the peri-infarct cortex within only few hours, which seems neither compatible with the passive transport of ventricular T cells along CSF flow nor the highly energy-demanding and tightly regulated migration across the BCSFB into the lateral ventricle and then across the ventricular ependymal cell layer directly into the forebrain parenchyma.

Results from our experiments in *CCR2*$^{-/-}$ mice support the concept of CCR2-dependent intraparenchymal migration of T cells after the parenchymal invasion from the ChP stroma. While potential mechanisms in ChP activation and recruitment of inflammatory cells into the ChP have previously been studied—and Type I Interferons been defined as key mediators—molecular cues for intraparenchymal T-cell migration have to our knowledge previously not been characterized. We have observed a distinct gradient for CCR2 ligands (i.e., CCL2, CCL7, CCL12) between the peri-infarct cortex and the ipsilateral ChP and have additionally defined innate immune cells in the peri-infarct cortex as their main source. However, we cannot exclude that the observed effects in the *CCR2*$^{-/-}$ model might be at least partially due to a generally ameliorated inflammatory milieu in the ischemic brain as we used in these experiments a global *CCR2*-knockout model. Particularly, studies in models of primary autoimmune neuroinflammation have shown a key role of CCR2 in recruiting monocytes and dendritic cells to the inflamed brain [7]. On the other side, a study by Chu et al. using a permanent MCA occlusion model as in our study revealed CCR2-independent recruitment of inflammatory monocytes to the ischemic brain [5] and resident microglial cells are sufficient to produce large amounts of T-cell-attractive CCL2 in response to brain injury [15, 40].

Based on the results from our study showing a predominant T-cell infiltration via the ChP route, it is conceivable that previous preclinical studies as well as current clinical trials testing specific blockage of T-cell migration across the BBB after acute brain ischemia might have been hampered by the alternative choroidal invasion route. Finally, further alternative invasion routes such as the meningeal entry site need to be further investigated [2]. Additional studies characterizing the distinct adhesion molecules involved at migration across the different brain barriers of the BBB, the BCSFB or alternative invasion sites such as the meninges are inevitable for the rationale design of clinical stroke trials targeting at cerebral T-cell invasion. Notably, results from previous studies analyzing both invasion routes into the brain under conditions of primary autoimmune neuroinflammation might be of only limited value due to the specific properties of stroke-induced inflammation such as the acute onset, pronounced glial activation and additional peripheral immunomodulation. Besides the complexity of various potential invasion routes of inflammatory leukocytes after acute brain, evasion pathways for lymphocytes from the post-ischemic brain to exit the brain and potentially re-enter the blood stream are unknown. Various routes have previously been described for lymphocytes to exit the brain parenchyma under inflammatory conditions including a recently described cerebral lymphatic system [22]. However, the contribution of potential evasion mechanisms for cerebral lymphocyte turnover rates after stroke is unknown. Therefore, the model in this study revealing rapid translocation from the ChP to the peri-infarct cortex in UBC-PA-GFP mice is limited by the assumption of a static system with no substantial T-cell turnover within 24 h after cell invasion.

Taken together, we observed an unexpected role of the ipsilateral ChP in the lateral ventricle as the major invasion route for T cells into the ischemic brain after stroke. We have defined the intracerebral migration route from the ChP into the peri-infarct cortex via a ChP–parenchyma junction, detected a potential chemokine gradient involved in the intraparenchymal migration and confirmed similar mechanisms in the human brain after acute stroke. These results question previously accepted concepts and therapeutic strategies in post-stroke neuroinflammation and are of direct clinical relevance for current and planned clinical trials testing therapies for inhibiting post-stroke cerebral leukocyte invasion.

Acknowledgements This work was funded by the excellence cluster of the German research foundation "Munich Cluster for Systems Neurology (SyNergy)" and the German Research foundation (DFG, LI-2534/1-1 and LI-2534/2-1) to A.L. The Swiss National Science Foundation (ProDoc Cell Migration - RM 1 and 3) to BE, the Swiss Heart Foundation to BE and GE. CCR2$^{RFP/RFP}$CX3CR1$^{GFP/+}$ were kindly donated by Israel F. Charo (University of California, San Francisco, USA) and Richard Ransohoff (Biogen Idec, Boston, USA). We thank the Human Brain and Spinal Fluid Resource Center, VA West Los Angeles Healthcare Center (Los Angeles, USA) for providing human brain samples. The authors would like to thank Kerstin Thuß-Silczakfor excellent technical assistance, Dr. Urban Deutsch for maintaining transgenic mouse colonies at the University of Bern, and Dr. Farida Hellal for advice on histological techniques.

Author contributions G.L., C.B., X.M., G.E., R.C., T.A., I.L., S.L., and L.M. performed experiments; G.L., C.B., A.G., T.A., R.M., A.E., N.P., B.E. and A.L. analyzed data; J.M. provided critical material and analyzed data; D.V., C.H., N.P., B.E. and G.L. contributed critical input to the manuscript; A.L. initiated the study, designed experiments and wrote the manuscript.

References

1. Becker K, Kindrick D, Relton J, Harlan J, Winn R (2001) Antibody to the alpha4 integrin decreases infarct size in transient focal cerebral ischemia in rats. Stroke 32:206–211

2. Benakis C, Brea D, Caballero S, Faraco G, Moore J, Murphy M, Sita G, Racchumi G, Ling L, Pamer EG et al (2016) Commensal microbiota affects ischemic stroke outcome by regulating intestinal gammadelta T cells. Nat Med 22:516–523. doi:10.1038/nm.4068
3. Canazza A, Minati L, Boffano C, Parati E, Binks S (2014) Experimental models of brain ischemia: a review of techniques, magnetic resonance imaging, and investigational cell-based therapies. Front Neurol 5:19. doi:10.3389/fneur.2014.00019
4. Chamorro A, Meisel A, Planas AM, Urra X, van de Beek D, Veltkamp R (2012) The immunology of acute stroke. Nat Rev Neurol 8:401–410. doi:10.1038/nrneurol.2012.98
5. Chu HX, Kim HA, Lee S, Broughton BR, Drummond GR, Sobey CG (2016) Evidence of CCR2-independent transmigration of Ly6C(hi) monocytes into the brain after permanent cerebral ischemia in mice. Brain Res 1637:118–127. doi:10.1016/j.brainres.2016.02.030
6. Chu HX, Kim HA, Lee S, Moore JP, Chan CT, Vinh A, Gelderblom M, Arumugam TV, Broughton BR, Drummond GR et al (2014) Immune cell infiltration in malignant middle cerebral artery infarction: comparison with transient cerebral ischemia. J Cereb Blood Flow Metab Off J Int Soc Cereb Blood Flow Metab 34:450–459. doi:10.1038/jcbfm.2013.217
7. Clarkson BD, Walker A, Harris MG, Rayasam A, Sandor M, Fabry Z (2015) CCR2-dependent dendritic cell accumulation in the central nervous system during early effector experimental autoimmune encephalomyelitis is essential for effector T cell restimulation in situ and disease progression. J Immunol 194:531–541. doi:10.4049/jimmunol.1401320
8. Dirnagl U (2006) Bench to bedside: the quest for quality in experimental stroke research. J Cereb Blood Flow Metab 26:1465–1478. doi:10.1038/sj.jcbfm.9600298
9. Dirnagl U (2014) Modeling immunity and inflammation in stroke: can mice be trusted? Stroke J Cereb Circ 45:e177–e178. doi:10.1161/STROKEAHA.114.005640
10. Donnan GA, Fisher M, Macleod M, Davis SM (2008) Stroke. Lancet 371:1612–1623. doi:10.1016/S0140-6736(08)60694-7
11. Dorr A, Sled JG, Kabani N (2007) Three-dimensional cerebral vasculature of the CBA mouse brain: a magnetic resonance imaging and micro computed tomography study. NeuroImage 35:1409–1423. doi:10.1016/j.neuroimage.2006.12.040
12. Elkins J (2016) Primary results of the ACTION trial of natalizumab in acute ischemic stroke (AIS). International stroke conference
13. Engelhardt B, Ransohoff RM (2012) Capture, crawl, cross: the T cell code to breach the blood-brain barriers. Trends Immunol 33:579–589. doi:10.1016/j.it.2012.07.004
14. Iadecola C, Anrather J (2011) The immunology of stroke: from mechanisms to translation. Nat Med 17:796–808. doi:10.1038/nm.2399
15. Inose Y, Kato Y, Kitagawa K, Uchiyama S, Shibata N (2015) Activated microglia in ischemic stroke penumbra upregulate MCP-1 and CCR2 expression in response to lysophosphatidylcholine derived from adjacent neurons and astrocytes. Neuropathology 35:209–223. doi:10.1111/neup.12182
16. Investigators EAST (2001) Use of anti-ICAM-1 therapy in ischemic stroke: results of the Enlimomab Acute Stroke Trial. Neurology 57:1428–1434
17. Kuscher K, Danelon G, Paoletti S, Stefano L, Schiraldi M, Petkovic V, Locati M, Gerber BO, Uguccioni M (2009) Synergy-inducing chemokines enhance CCR2 ligand activities on monocytes. Eur J Immunol 39:1118–1128. doi:10.1002/eji.200838906
18. Liesz A, Zhou W, Mracsko E, Karcher S, Bauer H, Schwarting S, Sun L, Bruder D, Stegemann S, Cerwenka A et al (2011) Inhibition of lymphocyte trafficking shields the brain against deleterious neuroinflammation after stroke. Brain J Neurol 134:704–720. doi:10.1093/brain/awr008
19. Lim JK, Obara CJ, Rivollier A, Pletnev AG, Kelsall BL, Murphy PM (2011) Chemokine receptor Ccr2 is critical for monocyte accumulation and survival in West Nile virus encephalitis. J Immunol 186:471–478. doi:10.4049/jimmunol.1003003
20. Llovera G, Hofmann K, Roth S, Salas-Perdomo A, Ferrer-Ferrer M, Perego C, Zanier ER, Mamrak U, Rex A, Party H et al (2015) Results of a preclinical randomized controlled multicenter trial (pRCT): anti-CD49d treatment for acute brain ischemia. Sci Transl Med 7:299ra121. doi:10.1126/scitranslmed.aaa9853
21. Llovera G, Roth S, Plesnila N, Veltkamp R, Liesz A (2014) Modeling stroke in mice: permanent coagulation of the distal middle cerebral artery. J Vis Exp JoVE:e51729. doi:10.3791/51729
22. Louveau A, Harris TH, Kipnis J (2015) Revisiting the mechanisms of CNS immune privilege. Trends Immunol 36:569–577. doi:10.1016/j.it.2015.08.006
23. Lun MP, Monuki ES, Lehtinen MK (2015) Development and functions of the choroid plexus-cerebrospinal fluid system. Nat Rev Neurosci 16:445–457. doi:10.1038/nrn3921
24. Macrez R, Ali C, Toutirais O, Le Mauff B, Defer G, Dirnagl U, Vivien D (2011) Stroke and the immune system: from pathophysiology to new therapeutic strategies. Lancet Neurol 10:471–480. doi:10.1016/S1474-4422(11)70066-7
25. Moskowitz MA, Lo EH, Iadecola C (2010) The science of stroke: mechanisms in search of treatments. Neuron 67:181–198. doi:10.1016/j.neuron.2010.07.002
26. Neumann J, Riek-Burchardt M, Herz J, Doeppner TR, Konig R, Hutten H, Etemire E, Mann L, Klingberg A, Fischer T et al (2015) Very-late-antigen-4 (VLA-4)-mediated brain invasion by neutrophils leads to interactions with microglia, increased ischemic injury and impaired behavior in experimental stroke. Acta Neuropathol 129:259–277. doi:10.1007/s00401-014-1355-2
27. Nibbs RJ, Graham GJ (2013) Immune regulation by atypical chemokine receptors. Nat Rev Immunol 13:815–829
28. Pan C, Cai R, Quacquarelli FP, Ghasemigharagoz A, Lourbopoulos A, Matryba P, Plesnila N, Dichgans M, Hellal F, Erturk A (2016) Shrinkage-mediated imaging of entire organs and organisms using uDISCO. Nat Methods 13:859–867. doi:10.1038/nmeth.3964
29. Ransohoff RM, Engelhardt B (2012) The anatomical and cellular basis of immune surveillance in the central nervous system. Nat Rev Immunol 12:623–635. doi:10.1038/nri3265
30. Ransohoff RM, Kivisakk P, Kidd G (2003) Three or more routes for leukocyte migration into the central nervous system. Nat Rev Immunol 3:569–581. doi:10.1038/nri1130
31. Relton JK, Sloan KE, Frew EM, Whalley ET, Adams SP, Lobb RR (2001) Inhibition of alpha4 integrin protects against transient focal cerebral ischemia in normotensive and hypertensive rats. Stroke 32:199–205
32. Saederup N, Cardona AE, Croft K, Mizutani M, Cotleur AC, Tsou CL, Ransohoff RM, Charo IF (2010) Selective chemokine receptor usage by central nervous system myeloid cells in CCR2-red fluorescent protein knock-in mice. PLoS One 5:e13693. doi:10.1371/journal.pone.0013693
33. Schwartz M, Baruch K (2014) The resolution of neuroinflammation in neurodegeneration: leukocyte recruitment via the choroid plexus. EMBO J 33(1):7–22. doi:10.1002/embj.201386609
34. Schwarzmaier SM, de Chaumont C, Balbi M, Terpolilli NA, Kleinschnitz C, Gruber A, Plesnila N (2016) The formation of microthrombi in parenchymal microvessels after traumatic brain injury is independent of coagulation factor XI. J Neurotrauma 33:1634–1644. doi:10.1089/neu.2015.4173
35. Shechter R, London A, Schwartz M (2013) Orchestrated leukocyte recruitment to immune-privileged sites: absolute barriers versus

educational gates. Nat Rev Immunol 13:206–218. doi:10.1038/nri3391
36. Shechter R, Miller O, Yovel G, Rosenzweig N, London A, Ruckh J, Kim KW, Klein E, Kalchenko V, Bendel P et al (2013) Recruitment of beneficial M2 macrophages to injured spinal cord is orchestrated by remote brain choroid plexus. Immunity 38:555–569. doi:10.1016/j.immuni.2013.02.012
37. Steffen BJ, Butcher EC, Engelhardt B (1994) Evidence for involvement of ICAM-1 and VCAM-1 in lymphocyte interaction with endothelium in experimental autoimmune encephalomyelitis in the central nervous system in the SJL/J mouse. Am J Pathol 145:189–201
38. Tietz S, Engelhardt B (2015) Brain barriers: crosstalk between complex tight junctions and adherens junctions. J Cell Biol 209:493–506. doi:10.1083/jcb.201412147
39. Tymianski M (2015) Neuroprotective therapies: preclinical reproducibility is only part of the problem. Sci Transl Med 7:299. doi:10.1126/scitranslmed.aac9412
40. Umekawa T, Osman AM, Han W, Ikeda T, Blomgren K (2015) Resident microglia, rather than blood-derived macrophages, contribute to the earlier and more pronounced inflammatory reaction in the immature compared with the adult hippocampus after hypoxia-ischemia. Glia 63:2220–2230. doi:10.1002/glia.22887
41. Urra X, Miro F, Chamorro A, Planas AM (2014) Antigen-specific immune reactions to ischemic stroke. Front Cell Neurosci 8:278. doi:10.3389/fncel.2014.00278
42. Victora GD, Schwickert TA, Fooksman DR, Kamphorst AO, Meyer-Hermann M, Dustin ML, Nussenzweig MC (2010) Germinal center dynamics revealed by multiphoton microscopy with a photoactivatable fluorescent reporter. Cell 143:592–605. doi:10.1016/j.cell.2010.10.032
43. Waggott D, Chu K, Yin S, Wouters BG, Liu FF, Boutros PC (2012) NanoStringNorm: an extensible R package for the preprocessing of NanoString mRNA and miRNA data. Bioinformatics 28:1546–1548. doi:10.1093/bioinformatics/bts188
44. Wang Q, Tang XN, Yenari MA (2007) The inflammatory response in stroke. J Neuroimmunol 184:53–68. doi:10.1016/j.jneuroim.2006.11.014
45. Wilson EH, Weninger W, Hunter CA (2010) Trafficking of immune cells in the central nervous system. J Clin Investig 120:1368–1379. doi:10.1172/JCI41911
46. Wolburg K, Gerhardt H, Schulz M, Wolburg H, Engelhardt B (1999) Ultrastructural localization of adhesion molecules in the healthy and inflamed choroid plexus of the mouse. Cell Tissue Res 296:259–269
47. Zhou W, Liesz A, Bauer H, Sommer C, Lahrmann B, Valous N, Grabe N, Veltkamp R (2013) Postischemic brain infiltration of leukocyte subpopulations differs among murine permanent and transient focal cerebral ischemia models. Brain Pathol 23:34–44. doi:10.1111/j.1750-3639.2012.00614.x

Supplementary figure 1

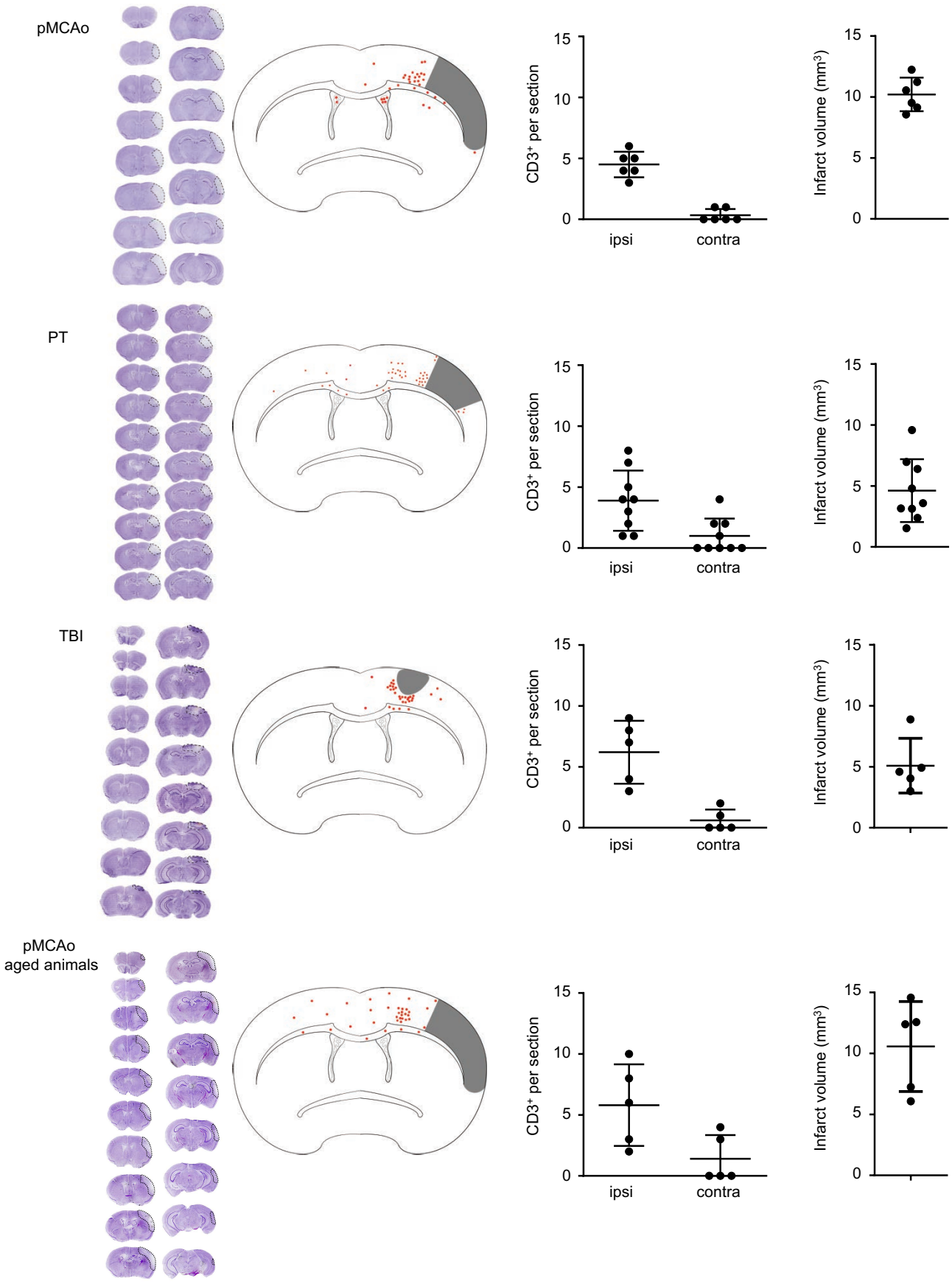

Supplementary figure 1. **(a)** Cresyl violet staining **(b)** accumulative topographic maps and **(c)** analysis of T cell quantification of each single $CD3^+T$ 5 days after permanent middle cerebral artery (pMCAo), phototrombosis (PT), traumatic brain injury (TBI) and pMCAo in aged animals. Cells were accumulated from one section at bregma level of 5-9 animals each. The infarct is depicted in grey. Comparative analysis are represented as mean±SD.

Supplementary figure 2

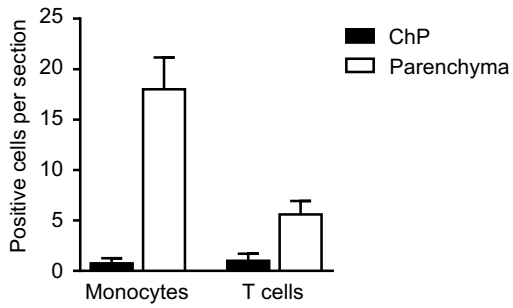

Supplementary figure 2. Monocyte and T cell quantification in the brain parenchyma and choroid plexus (ChP) 5 days after pMCAo from one section at bregma level. Comparative analysis are represented as mean±SD (n=5).

Supplementary figure 3

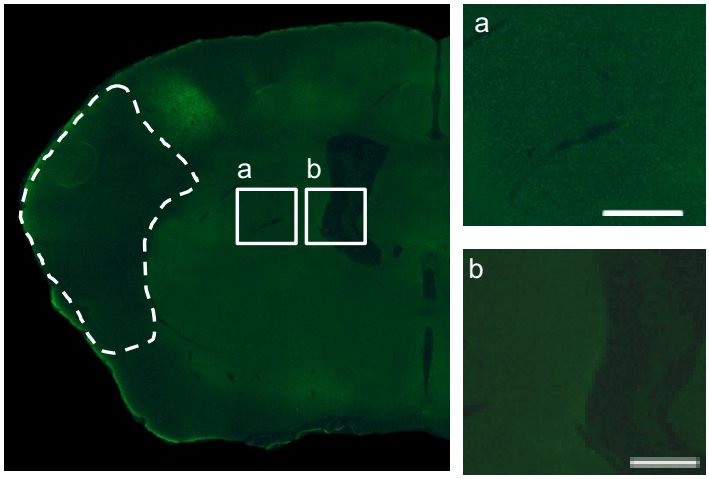

Supplementary figure 3. Coronal image from UBC-PA-GFP animal 24h after intraventricular/ChP optical labeling of T cells from an “in vivo pulse-chase” experiment. Dashed line indicates the border of the infarct core. Scale bar=500μm. Magnification pictures show no photoconverted cells in (a) brain parenchyma and (b) ventricle wall. Scale bar in a and b=250μm.

Supplementary figure 4

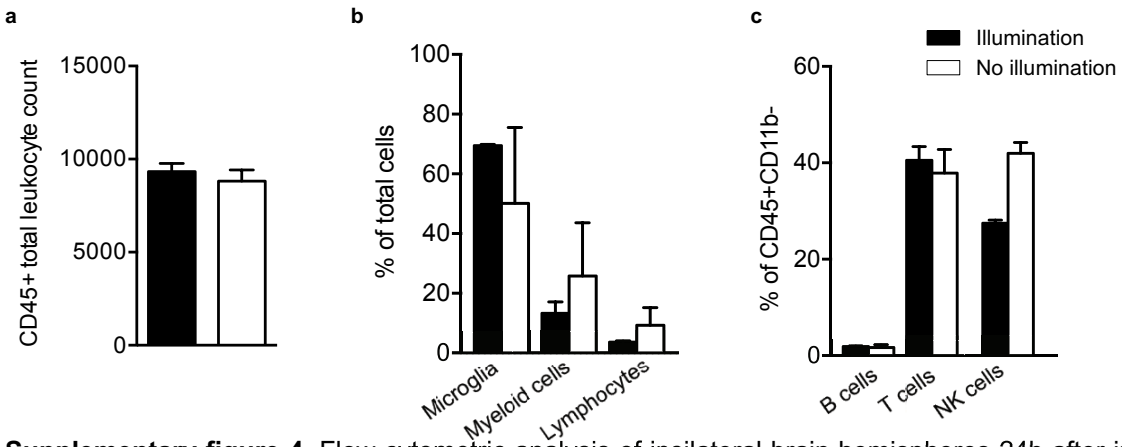

Supplementary figure 4. Flow cytometric analysis of ipsilateral brain hemispheres 24h after intraventricular/ChP optical illumination or no illumination reveled a similar (a) total leukocyte count, (b) distribution of leukocyte populations, and more specifically of (c) lymphocyte subpopulations (mean±SD). Mikroglia: $CD45^{int/dim}CD11b+$; Myeloid cells: $CD45^{high}CD11b+$; Lymphocytes: CD45+CD11b-.

Supplementary table 1. Number of excluded animals of the different experiments

Experiment	Total animals	Included animals	Excluded animals	Reason for exclusion
lysM-eGFP immunostaining	19	19	0	-
CD3 immunostaining	24	24	0	-
CD45 immunostaining	36	36	0	-
Brain FACS	10	10	0	-
ChP FACS	18	18	0	-
Phototrombosis	10	9	1	Death during surgery
Aged animals	5	5	0	
TBI	5	5	0	-
PA-GFP 5min illumination	15	15	0	-
PA-GFP 24h illumination	22	21	1	Death during cannula implantation
Matrigel experiment	12	6	6	Death during matrigel injection
tMCAo	4	4	0	-
pMCAo+PTCP	5	5	0	-
Chemokines and chemokines receptor experiment	6	6	0	-
CCL2-RFP	13	13	0	-
CCR2$^{-/-}$	13	13	0	-

Supplementary table 2. Characteristics of human patients for choroid plexus immunohistological analysis

Patient	Age (years)	Sex	Known comorbidities	Autolysis time (h)	Infarct location
Stroke 1	72	Male	COPD*	11.8	Right parietal lobe
Stroke 2	86	Male	Myocardial infarction	14.5	Right basal ganglia
Stroke 3	84	Male	-	14.0	Right frontal lobe
Stroke 4	77	Male	Congestive heart failure	12.3	Right thalamus
Stroke 5	70	Male	Pancreatic cancer#	18.2	Right parietal lobe
Stroke 6	79	Female	-	15.7	Right frontal lobe
Control 1	90	Male	COPD*	17.8	-
Control 2	84	Female	Alzheimer's disease	14.0	-
Control 3	84	Female	Alzheimer's disease, pneumonia	12.5	-
Control 4	88	Female	Atherosclerosis	14.0	-
Control 5	72	Female	Ovarian cancer#	14.0	-

*Chronic Obstructive Pulmonary Disease; #No cerebral metastasis; none of the patients received thrombolysis

Supplementary table 3. Characteristics of human patients for Nanostring analysis

Patient	Age (years)	Sex	Time from onset to death	Post-mortem interval	tPA treatment	Infarct location
N2	91	Female	70h	6h	No	Left hemisphere
N3	59	Male	75h	4h	No	Right hemisphere
N22	67	Male	62h	7h	Yes	Left hemisphere
N24	83	Female	100h	14.5h	Yes	Left hemisphere
N33	80	Male	101h	4.5h	No	Right hemisphere
N35	84	Male	40h	8h	No	Left hemisphere

Supplementary table 4. Fold upregulated genes in the cortex after pMCAo in mice

Gene	Fold up-regulation	p value	Gene	Fold up-regulation	p value
Ccl2	336.081	0.047	Il4	1.409	0.462
Ccl12	232.218	0.115	Ackr2	1.389	0.306
Ccl4	214.426	0.005	Il16	1.289	0.611
Cxcl10	160.267	0.013	Ccl19	1.284	0.388
Ccl7	95.847	0.031	Xcl1	1.275	0.621
Tnf	84.215	0.049	Ccl25	1.231	0.231
Ccl11	77.673	0.083	Ccr10	1.147	0.946
Cxcl1	41.672	0.041	Xcr1	1.142	0.843
Ccl3	41.480	0.035	Ccl17	1.123	0.726
Cxcl2	25.771	0.281	Itgam	1.110	0.939
C5ar1	18.713	0.082	Cxcr1	1.093	0.550
Cxcl3	16.905	0.316	Ccr6	1.078	0.443
Il6	15.591	0.154	Ccrl2	1.069	0.859
Ccr1	13.542	0.090	Darc	0.993	0.821
Ccl20	8.590	0.054	Cmtm2a	0.975	0.408
Ccl8	8.336	0.014	Cx3cr1	0.966	0.924
Cxcl16	7.941	0.032	Cxcr6	0.952	0.921
Cxcr2	7.010	0.279	Ccl22	0.940	0.572
Tlr2	5.615	0.004	Ccr8	0.930	0.707
Ccl9	5.500	0.038	Tymp	0.917	0.714
Cxcr4	4.804	0.076	Cmtm6	0.906	0.540
Ccl5	3.898	0.096	Hif1a	0.878	0.417
Cxcr5	3.826	0.167	Ccl24	0.876	0.337
Ccr2	3.591	0.266	Slit2	0.851	0.593
Ccr7	3.501	0.009	Ifng	0.840	0.371
Ccl6	3.370	0.068	Cxcl13	0.826	0.519
Il1b	3.229	0.299	Ackr3	0.792	0.407
Ccr4	2.957	0.269	Cxcl11	0.776	0.513
Ccr5	2.947	0.004	Cxcr3	0.760	0.902
Itgb2	2.867	0.093	Ackr4	0.751	0.404
Cxcl5	2.737	0.094	Cxcl15	0.698	0.356
Fpr1	2.690	0.046	Mapk1	0.694	0.346
Ccl28	2.510	0.159	Ccr9	0.681	0.525
Ppbp	2.481	0.164	Cxcl14	0.644	0.054
Ccr3	2.055	0.236	Cmtm4	0.644	0.070
Cmklr1	2.048	0.190	Mapk14	0.613	0.203
Tlr4	1.867	0.413	Ccr1l1	0.551	0.265
Cmtm3	1.736	0.001	Cmtm5	0.522	0.321
Cxcl9	1.720	0.196	Cx3cl1	0.475	0.049
Tgfb1	1.662	0.671	Ccl26	0.327	0.295
Ccl1	1.499	0.818	Gpr17	0.289	0.130
Pf4	1.453	0.567	Cxcl12	0.228	0.151

Supplementary table 5. Fold upregulated genes in the ChP after pMCAo in mice

Gene	Fold up-regulation	p value	Gene	Fold up-regulation	p value
Ccl12	11.424	0.022	Ccl9	1.326	0.297
Ccl2	9.409	0.019	Mapk1	1.325	0.185
Cxcl5	8.489	0.063	Ccl6	1.289	0.294
Cxcl1	8.392	0.063	Tgfb1	1.289	0.281
Ccl11	6.684	0.016	Ccr1	1.277	0.341
Cxcl9	5.614	0.108	Ccl19	1.265	0.219
Darc	4.944	0.029	Ccl25	1.259	0.402
Ccl7	4.072	0.013	Tlr2	1.245	0.327
Ccl20	3.848	0.052	Ccr10	1.222	0.491
Cxcr5	3.738	0.101	Il1b	1.193	0.203
Il6	3.400	0.089	Il16	1.164	0.451
Ccl8	3.389	0.202	Ccr9	1.161	0.609
Tnf	3.377	0.056	Gpr17	1.118	0.912
Ccl1	3.089	0.089	Cxcr6	1.100	0.595
Cxcl14	2.998	0.078	Mapk14	1.097	0.566
Il4	2.947	0.092	Tlr4	1.092	0.721
Cxcl10	2.775	0.132	Cmtm6	1.082	0.783
Ccl28	2.746	0.088	Cmtm2a	1.047	0.919
Ccl4	2.718	0.201	Hif1a	1.025	0.685
Itgam	2.565	0.018	Cmtm4	1.010	0.903
Ccl3	2.416	0.121	Cxcl3	1.010	0.676
Ccr4	2.393	0.180	Cxcl16	-1.025	0.731
Tymp	2.285	0.094	Ccr1l1	-1.035	0.871
Fpr1	2.197	0.012	Ccl5	-1.053	0.760
Ccr6	2.091	0.082	Slit2	-1.134	0.929
Ccl22	2.062	0.171	Cxcr2	-1.333	0.305
Ccl26	2.020	0.107	Ifng	-1.353	0.582
C5ar1	2.017	0.216	Cxcl12	-1.372	0.897
Ccl17	1.987	0.022	Cxcl2	-1.393	0.897
Cxcr4	1.987	0.289	Ackr2	-1.404	0.994
Itgb2	1.937	0.064	Cxcr3	-1.414	0.822
Cx3cr1	1.915	0.010	Ccrl2	-1.475	0.518
Cxcr1	1.781	0.233	Ackr4	-1.601	0.855
Cx3cl1	1.605	0.061	Ccr2	-1.603	0.432
Ccl24	1.575	0.355	Pf4	-1.673	0.792
Cmklr1	1.453	0.281	Cxcl15	-1.691	0.780
Ccr3	1.448	0.311	Ccr8	-1.829	0.427
Ccr7	1.441	0.708	Xcl1	-1.951	0.112
Cmtm5	1.392	0.240	Cxcl11	-2.079	0.262
Ccr5	1.371	0.109	Ppbp	-2.099	0.632
Ackr3	1.371	0.274	Cxcl13	-2.228	0.625
Cmtm3	1.328	0.163	Xcr1	-3.649	0.148

Supplementary table 6. Significantly upregulated genes in the peri-infarct cortex after stroke in humans (Nanostring)

Gene	Fold up-regulation	p value (<0.05)
IL8	5.0	0.040
CCL2	4.9	0.011
TNFAIP3	4.2	0.023
LIF	4.1	0.047
IL6R	3.7	0.016
CXCL1	3.6	0.036
ICAM1	3.6	0.051
IL6	3.4	0.068
NFKB2	3.3	0.018
TNFRSF1B	3.0	0.042
CXCL2	2.9	0.070
TGFBI	2.9	0.170
CD163	2.8	0.170
ITGAX	2.8	0.051
PLAUR	2.8	0.098
PTGS2	2.8	0.180
FCGR2A	2.6	0.130
MARCO	2.6	0.078
NFIL3	2.6	0.081
CLEC5A	2.5	0.120
CXCR4	2.5	0.096
IL18R1	2.5	0.095
SPP1	2.5	0.220
CFB	2.3	0.170
CTSC	2.2	0.100
IFI16	2.2	0.083
CXCL12	2.1	0.120
FCER1G	2.1	0.130
LCP2	2.1	0.130
SOCS3	2.1	0.310

5. Publication II

Results of a Preclinical Randomized Controlled (pRCT) Multicenter Trial: Anti-CD49d treatment for acute brain ischemia

Authors: Gemma Llovera[1,2], Kerstin Hofmann[1,2], Stefan Roth[1,2], Angelica Salas-Pérdomo[3,4], Maura Ferrer-Ferrer[3,4], Carlo Perego[5], Elisa R. Zanier[5], Uta Mamrak[1,2], Andre Rex[6], Hélène Party[7], Véronique Agin[7], Claudine Fauchon[8], Cyrille Orset[7,8], Benoît Haelewyn[7,8], Maria-Grazia De Simoni[5], Ulrich Dirnagl[6], Ulrike Grittner[9], Anna M. Planas[3,4], Nikolaus Plesnila[1,2], Denis Vivien[7,8], Arthur Liesz[1,2*]

Affiliations:

[1]Institute for Stroke and Dementia Research, Klinikum der Universität München, Feodor-Lynen-Str. 17, 81377 Munich, Germany

[2]Munich Cluster for Systems Neurology (SyNergy), Munich, Germany

[3]Department of Brain Ischemia and Neurodegeneration, Institutd'Investigacions Biomèdiques de Barcelona (IIBB), Consejo Superior de Investigaciones Científicas (CSIC), Barcelona, Spain

[4]Àrea de Neurociències, Institut d'Investigacions Biomèdiques August Pi i Sunyer (IDIBAPS), Barcelona, Spain

[5]Neuroscience Department, IRCCS-Istituto di Ricerche Farmacologiche Mario Negri, Milan, Italy

[6]Department of Experimental Neurology and Center for Stroke Research Berlin (CSB), Charité Universitäts medizin Berlin; German Center for Neurodegenerative Diseases (DZNE) and German Center for Cardiovascular Diseases (DZHK), Berlin sites; Excellence Cluster NeuroCure, Berlin, Germany

[7]INSERM, UMR-S U919, Institut National de la Santé Et de la Recherche Médicale (INSERM), University Caen Basse-Normandie, team Serine Proteases and Pathophysiology of the neurovascular Unit, GIP CYCERON, F-14074 Caen Cedex, France

[8]Experimental Stroke Research Platform (ESRP), IBiSA platform, Centre Universitaire de Ressources Biologiques (CURB), Université Caen Basse-Normandie, F-14074 Caen Cedex, France.

[9]Department of Biostatistics and Clinical Epidemiology, Charité-Universitäts medizin, Berlin, Germany

Author contributions:

A.L. initiated this trial; A.L., U.D., A.M.P., N.P., M-G.D.S. and D.V. designed the study protocol, supervised the study, and reviewed original data sets; G.L. performed the central analysis of all biological samples and data sets, V.A., C.F., M.F-F., B.H., K.H., G.L., U.M., C.O., H.P., C.P., A.R., S.R., A.S.-P., and E.R.Z. performed experiments; U.G. performed central statistical analysis; and U.D., A.L., G.L., A.M.P., N.P., M-G.D.S. and D.V wrote the manuscript

STROKE

Results of a preclinical randomized controlled multicenter trial (pRCT): Anti-CD49d treatment for acute brain ischemia

Gemma Llovera,[1,2] Kerstin Hofmann,[1,2] Stefan Roth,[1,2] Angelica Salas-Pérdomo,[3,4] Maura Ferrer-Ferrer,[3,4] Carlo Perego,[5] Elisa R. Zanier,[5] Uta Mamrak,[1,2] Andre Rex,[6] Hélène Party,[7] Véronique Agin,[7] Claudine Fauchon,[8] Cyrille Orset,[7,8] Benoît Haelewyn,[7,8] Maria-Grazia De Simoni,[5] Ulrich Dirnagl,[6] Ulrike Grittner,[9] Anna M. Planas,[3,4] Nikolaus Plesnila,[1,2] Denis Vivien,[7,8] Arthur Liesz[1,2]*

Numerous treatments have been reported to provide a beneficial outcome in experimental animal stroke models; however, these treatments (with the exception of tissue plasminogen activator) have failed in clinical trials. To improve the translation of treatment efficacy from bench to bedside, we have performed a preclinical randomized controlled multicenter trial (pRCT) to test a potential stroke therapy under circumstances closer to the design and rigor of a clinical randomized control trial. Anti-CD49d antibodies, which inhibit the migration of leukocytes into the brain, were previously investigated in experimental stroke models by individual laboratories. Despite the conflicting results from four positive and one inconclusive preclinical studies, a clinical trial was initiated. To confirm the preclinical results and to test the feasibility of conducting a pRCT, six independent European research centers investigated the efficacy of anti-CD49d antibodies in two distinct mouse models of stroke in a centrally coordinated, randomized, and blinded approach. The results pooled from all research centers revealed that treatment with CD49d-specific antibodies significantly reduced both leukocyte invasion and infarct volume after the permanent distal occlusion of the middle cerebral artery, which causes a small cortical infarction. In contrast, anti-CD49d treatment did not reduce lesion size or affect leukocyte invasion after transient proximal occlusion of the middle cerebral artery, which induces large lesions. These results suggest that the benefits of immune-targeted approaches may depend on infarct severity and localization. This study supports the feasibility of performing pRCTs.

INTRODUCTION

Ischemic stroke, a leading cause of death and disability worldwide (*1*), induces the rapid loss of specific brain functions, a result of insufficient blood flow to specific brain regions. Together with other downstream effects, stroke triggers an acute inflammatory response in the brain, which activates harmful signaling cascades that contribute to secondary brain damage (*2*). Although stroke places enormous medical and economic burdens on society, thrombolysis with tissue plasminogen activator (tPA) is currently the only clinically approved therapy for ischemic stroke. Safety considerations require, however, that tPA must be administered within a very narrow time window after the onset of symptoms, and tPA treatment has important contraindications such as hemorrhage or oral anticoagulation (*3*, *4*). Because of these constraints, tPA is only provided to a small percentage of all stroke patients in industrialized countries; the overall therapeutic impact of tPA is negligible when developing countries are also considered.

In recent decades, several experimental therapies have been developed and tested for their ability to mitigate stroke-related brain injury, which can include postischemic, excitotoxic neuronal damage, spreading depolarization, apoptosis, and/or inflammation (*5*, *6*). Unfortunately, none of the tested drugs that show promise in animal models of stroke have so far been translated into clinical use for stroke patients (*7*, *8*), and most major pharmaceutical companies have stopped research and development in this area. The cause of this failure in clinical trials is multifactorial and may include poorly designed preclinical and clinical studies, biased selection of substances for clinical testing, and underpowered clinical trials with overambitious and pathophysiologically irrelevant therapeutic windows (*5*, *9*). Indeed, academic and industrial researchers, as well as funding agencies and journals, now recognize the existence of a "reproducibility crisis": the results of preclinical studies in many research fields, including stroke, lack robustness, and only a small fraction of these studies can be replicated (*10*).

To overcome the current limitations of preclinical in vivo studies, strict operational and statistical guidelines have been developed for the data reporting, and suggestions have been implied for design and performance of preclinical studies (*11*). In addition, pRCTs have been proposed as a way to help bridge the gap between experimental laboratory research and clinical trials (*12*–*14*). Such studies would be primarily confirmatory, designed to test efficacy of previously defined therapeutic concepts in a study design with the highest standards for statistics, analysis, and reporting (*15*). Finally, such a study will have many of the

[1]Institute for Stroke and Dementia Research, Klinikum der Universität München, Feodor-Lynen-Straße 17, 81377 Munich, Germany. [2]Munich Cluster for Systems Neurology (SyNergy), 81377 Munich, Germany. [3]Department of Brain Ischemia and Neurodegeneration, Institut d'Investigacions Biomèdiques de Barcelona (IIBB), Consejo Superior de Investigaciones Científicas (CSIC), 08036 Barcelona, Spain. [4]Àrea de Neurociències, Institut d'Investigacions Biomèdiques August Pi i Sunyer (IDIBAPS), 08036 Barcelona, Spain. [5]Neuroscience Department, IRCCS-Istituto di Ricerche Farmacologiche Mario Negri, 20156 Milan, Italy. [6]Department of Experimental Neurology and Center for Stroke Research Berlin (CSB), Charité–Universitätsmedizin Berlin; German Center for Neurodegenerative Diseases (DZNE) and German Center for Cardiovascular Diseases (DZHK), Berlin sites; Excellence Cluster NeuroCure, 10117 Berlin, Germany. [7]INSERM, UMR-S U919, Université de Caen Basse-Normandie, team Serine Proteases and Pathophysiology of the neurovascular Unit, GIP Cyceron, F-14074 Caen Cedex, France. [8]Experimental Stroke Research Platform (ESRP), IBiSA platform, Centre Universitaire de Ressources Biologiques (CURB), Université de Caen Basse-Normandie, F-14074 Caen Cedex, France. [9]Department of Biostatistics and Clinical Epidemiology, Charité–Universitätsmedizin Berlin, 12203 Berlin, Germany.
*Corresponding author. E-mail: arthur.liesz@med.uni-muenchen.de

Downloaded from on August 5, 2015

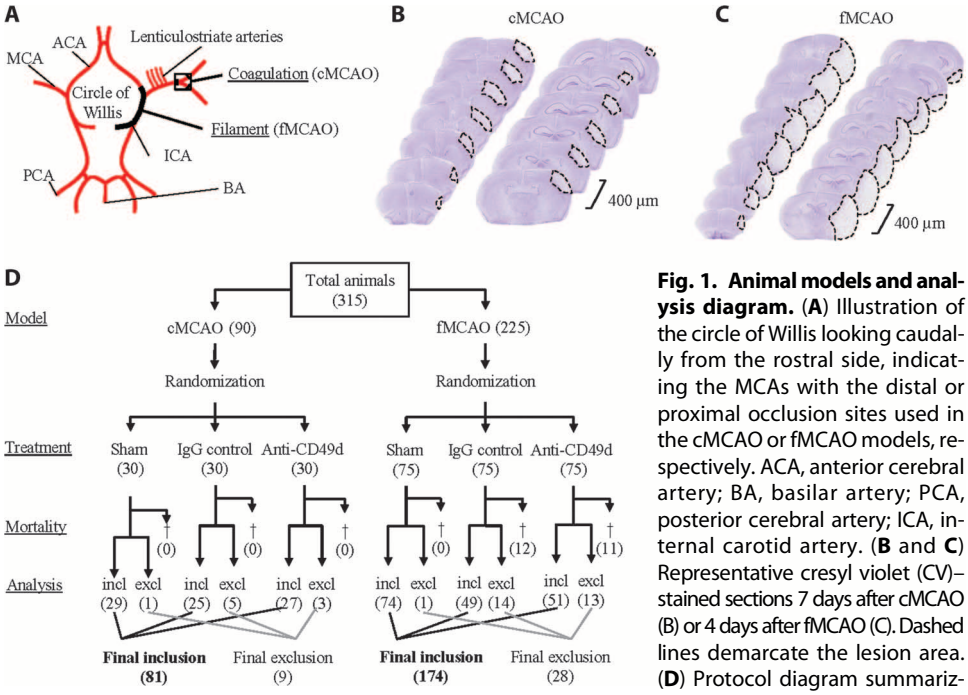

Fig. 1. Animal models and analysis diagram. (**A**) Illustration of the circle of Willis looking caudally from the rostral side, indicating the MCAs with the distal or proximal occlusion sites used in the cMCAO or fMCAO models, respectively. ACA, anterior cerebral artery; BA, basilar artery; PCA, posterior cerebral artery; ICA, internal carotid artery. (**B** and **C**) Representative cresyl violet (CV)–stained sections 7 days after cMCAO (B) or 4 days after fMCAO (C). Dashed lines demarcate the lesion area. (**D**) Protocol diagram summarizing the number of animals included (incl) (315 mice), with exclusion (excl) per group and included animal numbers for final analysis. Exclusion criteria were defined as described in Materials and Methods. "†" indicates dead animals.

characteristics of adequately powered clinical trials. Several international consortia have been established to perform such studies, and multicenter investigations have been reported, but no pRCT has been published to date. Therefore, our objective was to implement a preclinical multicenter trial by applying rigorous design, experimental, and analysis standards to test the efficacy of an anti-inflammatory therapeutic intervention (that is, blocking leukocyte migration with anti-CD49d antibodies) in two experimental models of stroke.

Brain leukocyte invasion is a key mechanism that mediates secondary neuronal injury after an acute brain lesion (*2*, *16*). Transendothelial migration is tightly regulated by adhesion molecules, specifically the interaction between the molecules VLA-4 (leukocyte very late antigen-4) and VCAM-1 (vascular cell adhesion molecule-1) (*17*, *18*). Antibodies against the α chain of VLA-4 (anti-CD49d antibodies) have shown efficacy in several models of autoimmune diseases, and the humanized antibody natalizumab is currently one of the most effective therapies for patients with multiple sclerosis (*19*). Four single-center studies reported that anti-CD49d antibodies confer cerebroprotective properties in mouse models of brain ischemia by blocking the postischemic invasion of leukocytes into the brain (*20*–*23*). However, one of these studies reported different efficacies between different stroke models (*20*). The neuroprotective potential of anti-CD49d treatment was challenged further by a subsequent study that reported no treatment effect (*24*). A phase 2 clinical trial is currently testing the effect of natalizumab in patients after acute ischemic stroke (ClinicalTrials.gov identifier: NCT01955707).

The availability of reliable preclinical data is essential for selecting the drug candidates with the highest clinical potential and for designing the most effective clinical study, thereby minimizing unnecessary, costly, and even harmful clinical trials. We therefore tested anti-CD49d treatment in a multicenter, randomized preclinical trial. The predetermined primary end point for the trial was infarct volume measured in two ischemic stroke models. The secondary end points were functional outcome and the invasion of leukocytes into the brain.

RESULTS

For this experimental trial, we used two different models of focal brain ischemia (Fig. 1, A to C) to address potential pathophysiological differences among commonly used stroke models (*25*, *26*). Small lesions confined to the cortex were induced by coagulation of the distal middle cerebral artery (cMCAO), whereas lesions in the cortex and subcortical structures were induced by transiently occluding the MCA at its origin for 60 min with an endovascular filament (fMCAO). A total of 315 male C57BL/6J mice from the following five independent European research centers were randomized in this trial by the author indicated by their initials [center 1: Caen (D.V.), center 2: Milan (M.-G.D.S.), center 3: Barcelona (A.M.P.), center 4: Munich (N.P.), and center 5: Berlin (U.D.)], whereas the sixth center centrally coordinated the study and analyzed the data (Munich, A.L.). A total of 81 and 174 mice were included in the final analyses of the cMCAO and fMCAO groups, respectively (Fig. 1D). The animals' physical features, mortality incidences, and reasons for exclusion are summarized in Table 1. The body temperature of the mice at center 3 differed significantly from the other centers, and the body weight of the mice at center 4 differed significantly from the other centers; however, all values were within their respective normal physiological range for mice.

Anti-CD49d treatment reduces infarct volume after cortical stroke

Previous studies performed in individual laboratories with relatively small sample sizes suggested that anti-CD49d antibodies might improve outcome after stroke (*20*–*23*); in contrast, another study reported no significant benefit of this treatment (*24*). We therefore examined the efficacy of anti-CD49d treatment in experimental ischemic stroke by performing a pRCT, using pooled infarct volume of all centers per each stroke model as the primary end points. The anti-CD49d antibody or a control immunoglobulin G (IgG) antibody (300 µg each) was administered intraperitoneally in a randomized and blinded fashion 3 hours after stroke induction. Analysis of the pooled data from all centers revealed that treatment with anti-CD49d antibodies resulted in 19% smaller infarct volume 7 days after cMCAO compared to administration of control IgG ($P < 0.05$) (Fig. 2A). In contrast, 4 days after inducing fMCAO, infarct volume did not differ between control IgG–treated and anti-CD49d–treated mice, regardless of whether the data were analyzed for each individual center or as a pooled data set (Fig. 2B). To additionally show the effect sizes (ESs, standardized mean difference) of

Downloaded from on August 5, 2015

Table 1. Animal characteristics.

Center	Stroke model	Time after lesion (days)	Total *n*	Mortality	Exclusion: No infarct	Exclusion: Other criteria*	Final *n*	Mean body temperature†	Mean body weight
1	Filament	4	45	1	9	1	34	37.43	25.02
2	Filament	4	45	9	6	—	30	37.88	23.13
3	Filament	4	45	6	3	—	36	38.77‡	23.35
4	Filament	4	45	—	—	—	45§	—	20.60‡
5	Filament	4	45	7	2	7	29	37.95	24.81
1	Coagulation	7	30	—	—	—	30	37.51	24.62
2	Coagulation	7	30	—	2	2	26	37.74	23.39
3	Coagulation	7	30	—	5	—	25	38.35‡	23.88

*Other exclusion criteria: Neuroscore <8 at 24 hours after fMCAO, overt mechanical damage, or disruption of the brain sample or sham animals with lesion. †Baseline values before anesthesia induction. ‡$P < 0.05$ [analysis of variance (ANOVA)]. §$P < 0.05$ (χ^2).

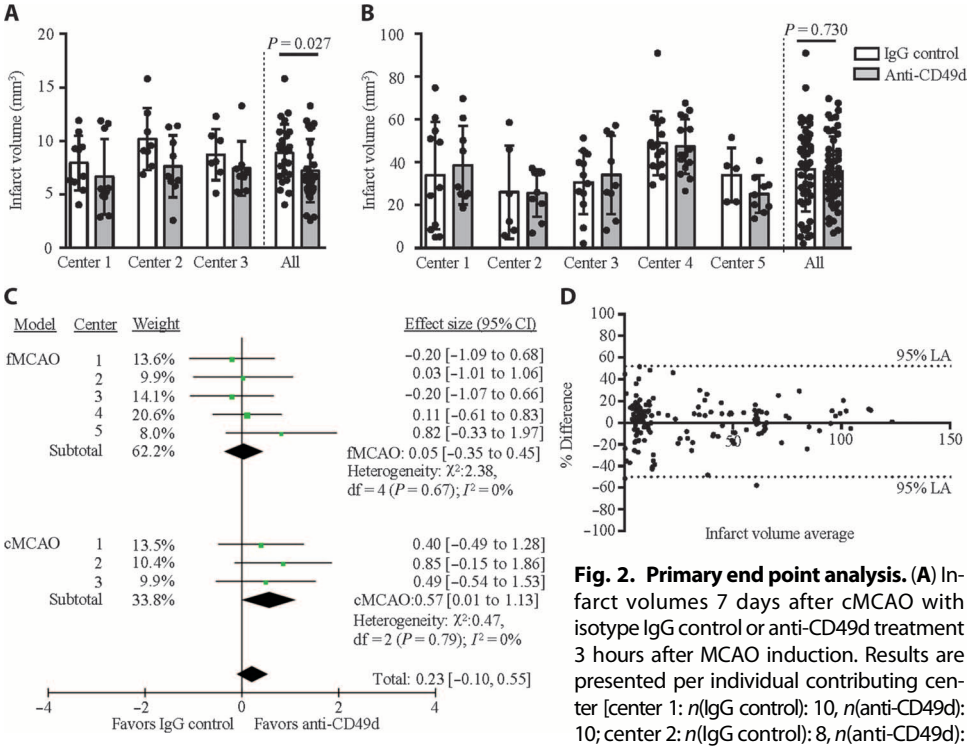

Fig. 2. Primary end point analysis. (**A**) Infarct volumes 7 days after cMCAO with isotype IgG control or anti-CD49d treatment 3 hours after MCAO induction. Results are presented per individual contributing center [center 1: *n*(IgG control): 10, *n*(anti-CD49d): 10; center 2: *n*(IgG control): 8, *n*(anti-CD49d): 9; and center 3: *n*(IgG control): 7, *n*(anti-CD49d): 8] and as pooled samples from all centers [*N*(IgG control): 25, *N*(anti-CD49d): 27]. Mixed model analysis revealed significantly (β = 1.8, SE = 0.8, *P* = 0.027) lower infarct volumes in the anti-CD49d treatment group. (**B**) Corresponding results for infarct volumes 4 days after fMCAO (β = −0.3, SE = 3.3, *P* = 0.947). Results are presented per individual contributing center [center 1: *n*(IgG control): 11, *n*(anti-CD49d): 9; center 2: *n*(IgG control): 6, *n*(anti-CD49d): 9; center 3: *n*(IgG control): 12, *n*(anti-CD49d): 9; center 4: *n*(IgG control): 15, *n*(anti-CD49d): 15; and center 5: *n*(IgG control): 5, *n*(anti-CD49d): 9] and as pooled samples from all centers [*N*(IgG control): 49, *N*(anti-CD49d): 51]. Center labels for contributing centers are consistent between the two stroke models. Data are presented as means ± SD. (**C**) Forest plot of ES estimation by the inverse-variance method in a random-effects model in individual centers and in all-center pooled data, corresponding to centers depicted in (A) and (B). (**D**) Bland-Altman plot for interrater concordance of infarct volume measurement for the two independent and blinded raters at the central study center. LA, limit of agreement.

antibody treatment in the two stroke models, we performed a meta-analysis using inverse-variance weighting (random-effects model) from all centers; these results are illustrated as a forest plot (Fig. 2C). Consistent with the results from the mixed model analysis used to test the primary end point (Fig. 2, A and B), the result from the cMCAO model showed no significant effect of treatment if analyzed separately for each center, whereas a subtotal analysis (pooled for cMCAO) revealed a significant treatment effect [ES, 0.57; 95% confidence interval (CI), 0.01 to 1.13]. As in the mixed model primary analysis, no significant effect was found in the analysis for pooled infarct volume after fMCAO. When the data were pooled from all treatment centers and both models, the ES no longer favored treatment (ES, 0.23; 95% CI, −0.1 to 0.55).

Next, we investigated the accuracy of our assessment of the primary end point. Infarct volume was independently measured by two researchers (G.L. and A.L.) at the central study center. These researchers were blinded with respect to the groups, and concordance of their results was confirmed using Bland-Altman analysis and calculation of intraclass correlation coefficient (ICC), which revealed excellent interrater reliability (ICC, 0.99; 95% CI, 0.990 to 0.994; Fig. 2D and fig. S1A). Moreover, each study center reevaluated the infarct volumes of the samples, confirming reliability between the central analysis and the analyses from each center (ICC range, 0.88 to 0.99; fig. S1B). Together, these results support the hypothesis that anti-CD49d treatment reduces infarct volume in cortical lesions after permanent MCA occlusion; moreover, our results suggest that treatment efficacy might depend on infarct type and severity, because anti-CD49d treatment was not effective after transient occlusion of the proximal MCA.

Downloaded from on August 5, 2015

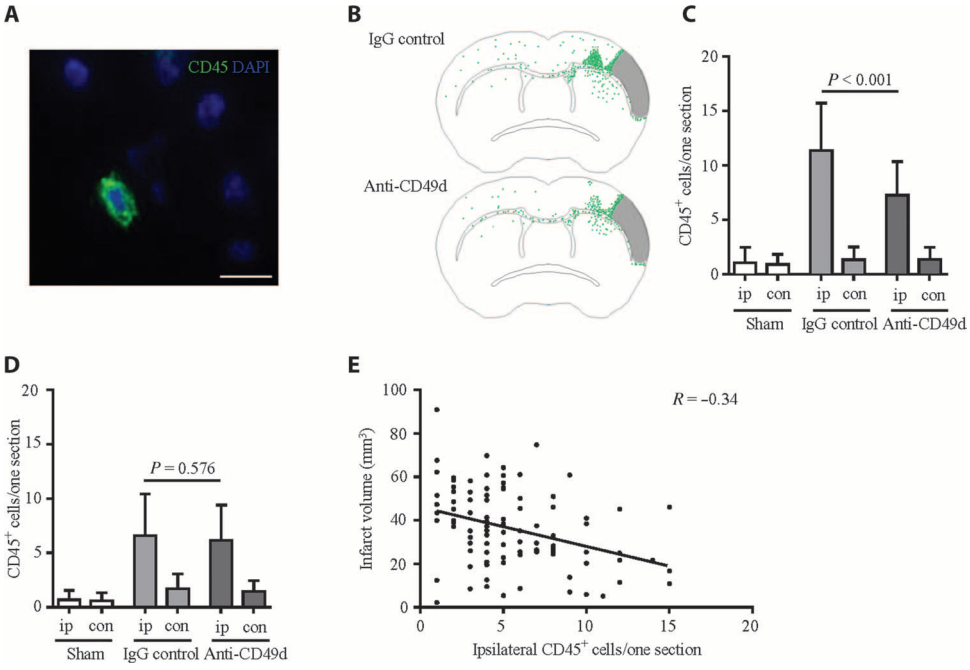

Fig. 3. Leukocyte brain infiltration after cMCAO and fMCAO. (**A**) Representative image of CD45 immunohistological staining in the peri-infarct area 7 days after cMCAO. Green, CD45–Alexa Fluor 488; blue, 4′,6-diamidino-2-phenylindole (DAPI). Scale bar, 10 μm. (**B**) Cumulative topographic representation of each single $CD45^+$ leukocyte detected on one coronal section per brain, excluding the infarct core area. Topographic maps for each section were superimposed for both treatment groups [*n*(IgG control): 25, *n*(anti-CD49d): 27]. Total $CD45^+$ count in ipsilateral hemispheres was 284 cells in the IgG group and 196 cells in the anti-CD49d group. (**C**) Quantitative analysis of $CD45^+$ cell count per one coronal section in ipsilateral (ip) and contralateral (con) hemispheres of sham-operated animals ($n = 30$) and anti-CD49d–treated ($n = 25$) or IgG control–treated ($n = 27$) mice 7 days after cMCAO. (**D**) Corresponding quantification of $CD45^+$ cells 4 days after fMCAO, sham-operated animals ($n = 74$), and anti-CD49d–treated ($n = 49$) or IgG control–treated ($n = 51$) mice. Data in (C) and (D) are presented as means ± SD. (**E**) Linear regression analysis of $CD45^+$ cell counts per ipsilateral hemisphere of both treatment groups (*x* axis) and infarct volume (*y* axis) 4 days after fMCAO. *r*, Pearson correlation coefficient.

Anti-CD49d treatment reduces the invasion of leukocytes into the brain after cortical stroke

Previous studies (*20*, *24*) suggested that anti-CD49d treatment exerts its primary therapeutic effect on brain ischemia by inhibiting leukocyte invasion of the brain. To investigate this process, we prepared brain sections from mice after MCAO or sham surgery; we then immunostained the sections with antibodies against CD45, a marker for leukocytes (Fig. 3A). The stained sections were analyzed by researchers who were blinded with respect to the surgical and treatment groups. Cumulative topographic maps of leukocyte invasion after cMCAO revealed that leukocytes infiltrated the region surrounding the infarct core, with predominant localization in the peri-infarct cortical area (Fig. 3B). Anti-CD49d treatment significantly ($P < 0.001$) reduced the number of leukocytes in the infarct area after cMCAO (Fig. 3, B and C), consistent with our finding of reduced lesion volume in anti-CD49d–treated mice after cMCAO. Mice that underwent fMCAO had significantly fewer cerebral leukocytes than those that underwent MCAOcMCAO [mean (SD), 5.4 (3.6) versus 11.4 (4.4) cells per section, respectively; $P < 0.001$], and anti-CD49d treatment did not affect the invasion of leukocytes after fMCAO (Fig. 3D). Because of the high variability in lesion size and location in the fMCAO model, we were unable to generate topographic maps; however, we measured a weak yet significant inverse correlation between infarct volume and cerebral leukocyte count in the fMCAO-induced group (Fig. 3E), suggesting a relationship between lesion size and cellular poststroke neuroinflammation.

Other secondary outcome parameters were not affected by anti-CD49d treatment

In addition to the infiltration of leukocytes into the brain, we also measured the following outcomes as predefined secondary end points: mortality, physiological parameters, and behavioral deficits. Our analysis revealed that none of these outcomes was significantly affected by anti-CD49d treatment. For the cMCAO model, we used the rotarod test and the adhesive removal test, two well-established functional tests for this stroke model. An analysis of functional outcome with the per-protocol analysis revealed that sensorimotor deficits in both tests (at three time points after stroke) did not differ significantly between the sham surgery group and either the control-treated or anti-CD49d–treated cMCAO groups. Hence, we were unable to discriminate between cMCAO and sham surgery, indicating that these commonly used tests lacked sufficient sensitivity to detect the limited neurological deficits in the cMCAO model (fig. S2, A to C and E). Additionally, the mean absolute values for both tests differed greatly between individual centers (fig. S2, A and B), indicating high intercenter variability in performing these tests, despite the use of harmonized procedures. To eliminate intercenter variability as a source for increased variability for this parameter, we performed a secondary analysis in which the poststroke deficits were normalized to their respective baseline values (fig. S2F). This analysis revealed a cMCAO-induced deficit in the adhesive removal test; however, treatment with the anti-CD49d antibody had no significant effect on this deficit. Because of the substantial behavioral deficits induced by fMCAO, the tests used for cMCAO could not be applied in this model. Therefore, we tested deficits in the fMCAO model by a composite Neuroscore, with no difference apparent between treatment groups (fig. S3A); this lack of treatment effect is consistent with the lack of treatment effect on infarct volume in this model. The composite Neuroscore test robustly detected significant deficits in the animals (compared to sham treatment) in all five research centers 4 days after stroke. A correlation analysis of this large cohort of animals ($n = 174$ fMCAO-induced mice) revealed moderate correlation between infarct volume and Neuroscore outcome ($r = 0.76$ and $r = 0.77$, 2 and 4 days after stroke, respectively; fig. S3B). Although cMCAO did not cause mortality (within 7 days after stroke), fMCAO resulted in similar mortality rates in the control IgG–treated (16.0%) and the anti-CD49d–treated (14.6%) groups (fig. S4). Similarly, the physiological parameters (body temperature and body weight) were affected by fMCAO but not by cMCAO (fig. S5). Specifically, fMCAO-induced brain

Downloaded from on August 5, 2015

damage led to pronounced hypothermia and weight loss, whereas sham surgery did not; however, these parameters were not affected by treatment with the anti-CD49d antibody.

DISCUSSION

Here, we report the results of an international multicenter, randomized, controlled, and blinded experiment for the preclinical testing of drug efficacy. The design of this study was modeled on phase 3 clinical randomized controlled trials, which are the current standard in clinical drug development and are required to license a new drug. Our study was performed in response to the "replication crisis" (*10*), the exceedingly low reproducibility, and lack of robustness of preclinical results in academic research (*27*–*29*). In addition, our approach may help to resolve the translational roadblock, in which promising preclinical approaches fail to be translated to clinically effective therapies (*30*–*32*). Thus, international research consortia—which provide larger sample sizes with sufficient statistical power and a study design that reduces the confounding effects of bias—have been proposed as a way to improve the robustness and translational predictability of preclinical research (*13*, *14*, *33*–*35*).

To improve the quality and reliability of preclinical research, several international research consortia have been established, including the European Union (EU)–funded Multi-PART (Multicentre Preclinical Animal Research Team) consortium for stroke research and the National Institutes of Health–funded CAESAR (Consortium for preclinicAl assESsment of cARdioprotective therapies) consortium for cardiovascular research. Systematic efforts by these consortia and others have revealed that inadequate reporting of data, statistical flaws, and missing cross-validation of data from independent study centers are major flaws in preclinical translational research (*5*, *13*, *33*, *36*, *37*). Virtually all preclinical studies performed by individual research groups are underpowered and often fail to adequately control for bias (for example, using randomization and blinding) (*38*). For example, the average group size in more than 2000 different experiments involving more than 35,000 rodents (in which hundreds of different treatments were tested in ischemic stroke models) is only 8.6 animals per group (median, 8; range, 1 to 54) (*39*). Ioannidis *et al.* (*34*) examined a random sample of in vivo animal studies published since 2006 and found that fewer than 30% of studies used randomization and fewer than 10% performed a blinded assessment of outcome; with respect to experimental stroke research, these percentages are even lower (*40*). A meta-analysis of 49 published preclinical meta-analyses (comprising 730 primary individual studies in the field of neuroscience) revealed that the median statistical power was only 21% (*41*). This means that of 100 studies that are conducted to investigate a genuine treatment effect, only 21 will actually be powered in such a way as to be able to demonstrate the effect, a result of small sample sizes. Until as recently as several decades ago, clinical trials were challenged by the same issues that face preclinical biomedical research today, including low internal validity, low statistical power, and a high rate of false positives. By developing and implementing rigorous standards for the design, execution, analysis, and reporting of studies, today's clinical trials can deliver robust and relevant results. Learning—and adopting key measures—from current clinical trial design (for example, randomization, blinding, and a priori power analysis), as in our pRCT, may help to overcome the current crisis of preclinical translational medicine. Such an approach has clear advantages over a meta-analysis, which pools results from studies with different methodological and statistical standards, potentially differing protocols, and lack of monitoring. In contrast, as explained in detail below, our pRCT approach aimed to harmonize protocols and warranted a prospective, blinded, and randomized study design, central monitoring of data quality, and centralized analysis and data deposition.

Here, we used the two most common experimental models of ischemic stroke to test a drug candidate that is already being tested in a phase 2 clinical trial after only a few, small-scale, single-center studies in mice. In all but one case (*8*), this approach in stroke research has led until now to costly failures and the exposure of patients to ineffective—or potentially harmful—drugs (*42*). Many other medical fields share this frustrating experience. The primary objective in the design of our study was to achieve maximum harmonization of the methods used by the various participating study centers. The basic protocol, as well as the primary and secondary end points, was predefined by coordination between the six laboratories. In clinical trials, patient care among various trial sites is relatively uniform and performed in accordance with national and international guidelines. In our study, achieving harmonization of the materials and standard operating procedures was a challenge in the initial phase of our study because the various laboratories generally use different strategies for testing drugs in the stroke models. We achieved the best possible harmonization of the surgical procedures and behavioral tests by using same-age and same-gender mice obtained from the same commercial breeder, centrally supplying all critical materials (for example, the filaments used to induce transient stroke), and defining the methods used for the surgical procedures, behavioral tests, and data acquisition. Several factors could not be harmonized fully, including the use of specific anesthetics and analgesics (a result of differences in local regulations regarding the conduct of animal experiments), the expertise of the surgeons, postsurgical care, body temperature maintenance, and monitoring of cerebral blood flow after vessel occlusion; all of these factors can potentially influence stroke outcome. Nevertheless, comparable differences in equipment, legal requirements, and the skills of the medical personnel also confound most clinical RCTs. Other variables included between-site differences in the use of sedation protocols, in postoperative anesthesia and analgesic drugs, and in mouse microbiota.

These remaining methodological differences might actually increase the robustness of our obtained results with respect to clinical translation. Indeed, we were able to demonstrate that drug efficacy could be demonstrated despite the above-mentioned procedural differences. Furthermore, increasing the sample size by pooling the efforts of multiple laboratories reduced statistical variability and increased sensitivity of outcome measures such as the infarct volume in the cMCAO model, cerebral leukocyte counts, and the Neuroscore.

Another aspect of the study that was handled individually by each study site was the approval of the animal experiments. Because of differing regulatory processes in Spain, France, Italy, and Germany, a uniform approval for all European partner sites was not achievable despite the European directive 2010/63/EU. However, future pRCTs could get approval more easily or via a single-point process for all partner sites if pRCTs showed more robust results than a single study and were regarded as a part of the preclinical evaluation of drug development.

Natalizumab, a humanized anti-CD49d antibody, is currently one of the most effective disease-modifying drugs for multiple sclerosis (*19*). With more than 7 years of clinical use, the efficacy and safety profiles for natalizumab are well established. The major risk associated with this

Downloaded from on August 5, 2015

treatment approach (the induction of progressive multifocal leukoencephalopathy) usually emerges after long-term treatment, but not after a single dose. Recently, several research groups established that lymphocyte invasion plays a role in stroke pathophysiology (*20*, *43*–*46*). For example, lymphocyte-deficient mice have substantially smaller lesion volumes compared to wild-type mice (*43*). Therefore, targeting the adaptive immune system is a promising therapeutic strategy for stroke. However, the contribution of secondary neuroinflammation to poststroke pathophysiology is far less explored, and the translatability of murine mechanisms to the human situation regarding stroke immunology is still under discussion (*47*, *48*). On the basis of previous experimental studies with anti-CD49d antibodies in stroke models (*20*–*22*) and the safety data on natalizumab use in patients with multiple sclerosis, a phase 2 clinical trial was initiated recently to test the effect of natalizumab in patients with acute ischemic stroke [ACTION (Effect of Natalizumab on Infarct Volume in Acute Ischemic Stroke) trial, ClinicalTrials.gov identifier: NCT01955707]. During the ACTION trial, an animal study was published that reported no effect of natalizumab on stroke (*24*), raising concerns about the efficacy of this approach (*24*, *49*). In contrast, in our multicenter study, consistent with previous results (*20*), we found that anti-CD49d treatment exerted a modest yet significant neuroprotective effect in the cMCAO model, but not in the fMCAO model of transient occlusion, which causes extensive damage. Notably, this protective effect was statistically significant when the cMCAO results were pooled from all centers but not when analyzed in each individual center. When we pooled results from both stroke models, no significant treatment effect was observed.

The difference in the neuroprotective efficacy of anti-CD49d treatment between the two models might be attributed to biological differences in the underlying pathophysiology and/or insufficient statistical power as a result of the unexpectedly high variability in the fMCAO model. In a head-to-head comparison of the fMCAO and cMCAO models, the authors found large differences in neuroinflammatory markers between the two models (*26*). Unexpectedly, moderate-sized cortical lesions, which appeared after permanent occlusion in the cMCAO model, induced higher levels of leukocyte brain invasion, microgliosis, and proinflammatory cytokine release than did the extensive hemispheric lesions of the transient ischemia model (*26*). Consistent with these results, we also found about twofold higher cerebral leukocyte counts after cMCAO than fMCAO. However, it should be noted that different time points (4 days after fMCAO versus 7 days after cMCAO) were used in the two models because of the high mortality rate in the fMCAO-treated mice after 4 to 5 days; moreover, the cMCAO model requires craniectomy and penetration of the dura. However, a recent study by Chu *et al.* reported twofold higher cerebral leukocyte cell counts after permanent occlusion by a filament in the fMCAO model compared to transient occlusion in the same stroke model, indicating that there may be pronounced leukocyte brain invasion in situations in which reperfusion is not established, regardless of the stroke model used (*50*). In our study, the cerebral leukocyte counts in the anti-CD49d–treated cMCAO group (the permanent occlusion model) were considerably higher than in the fMCAO group, and we found no treatment effect of anti-CD49d on the relatively low leukocyte numbers in the fMCAO model. Therefore, inhibition of the migration of leukocytes into the brain with anti-CD49d antibodies may be more effective in strokes that trigger a more robust inflammatory reaction. This possibility has been generally overlooked in preclinical testing of immunotherapeutics for stroke, and it has also not been considered in the design of clinical studies.

Because of its unique design (pooling results from five centers and the unprecedented large sample size in a single preclinical experiment), our study provides a critical view of commonly used methods in experimental stroke research. The variability of outcomes differed substantially between the two models; specifically, the overall SD in the control-treated cMCAO group was 30% [mean (SD), 8.9 (2.7); $n = 25$ mice], which is considerably lower than the surprisingly high SD in the control-treated fMCAO group [53%; mean (SD), 36.4 (19.9); $n = 49$]. Furthermore, our study also revealed an unexpectedly weak sensitivity of some of the most widely used behavioral tests, particularly in the cMCAO model, which induced only subtle neurological deficits. The rotarod and adhesive tape removal tests are two of the most common tests performed in experimental stroke research (*51*), and they have been successfully used by each laboratory in our study. Nevertheless, the rotarod test failed to detect poststroke deficits compared to sham surgery, even after the test results were normalized to baseline values, thus excluding intercenter differences. Moreover, the adhesive removal test results showed wide variability, even after normalization, and therefore lacked statistical power to detect treatment effects; nevertheless, this test was able to detect significant deficits after cMCAO. In addition, the Neuroscore, which was used to quantify deficits after fMCAO, also had high variability and revealed only a moderate correlation between test results and lesion volume. It was also apparent that the laboratory with previous experience using the Neuroscore (center 2) obtained more consistent results with this test than did laboratories that used this test for the first time (fig. S3). This finding might reflect a more general challenge with respect to harmonizing procedures, which was a necessary step in designing our pRCT. For example, deciding a priori to use mice of a specific age or deciding to centrally distribute the surgical material might necessitate changes in local standard operating procedures, which, in turn, could increase variability. Nevertheless, we reasoned that harmonizing the basic procedures and using similar materials were essential for achieving a multicenter, randomized, blinded pRCT, thereby minimizing intercenter effects and facilitating the analysis of pooled data based on group means.

On the basis of the previous considerations and new methodological insights gained in our study, we were able to define several points of potential improvement for future pRCTs: an obvious limitation for our analysis strategy was the constraint to a per-protocol analysis, lacking an additional intention-to-treat analysis. This is due to a substantial amount of missing data for the primary outcome measure (infarct volume) because of mortality or no infarct demarcation. This might be circumvented in future studies by using inclusion criteria similar to clinical trials such as imaging modalities for confirmation of an infarct, a defined neurological deficit range as an inclusion criterion, and use of a behavioral readout marker or mortality as primary end point. In analogy to clinical trials, which pool stroke patients with differing stroke etiology, future pRCTs might also consider pooling outcome of different models for testing drug efficacy.

One surprise in our study was the low performance of the behavioral tests, as well as exceedingly high variability of the fMCAO model. It would be desirable to evaluate such methodological characteristics in "pretrials" before future pRCTs, with the aim to validate the used methods and grade of harmonization in-between study centers before performing the actual pRCT. Such a pretrial would also give the opportunity to include a dose-escalation study for the investigated drug before defining the dose for the pRCT. Finally, central assessment of behavioral outcomes based on video recordings might reduce variability and improve test sensitivity, which should be evaluated in a pretrial for a future pRCT.

Downloaded from on August 5, 2015

Given the lack of funding for international collaborative confirmatory research, the apparent lack of incentives for individual researchers and laboratories, and the competitiveness associated with preclinical biomedicine, so-called pRCT studies—although deemed necessary—are often believed to be impossible to implement. Here, we report the feasibility of this approach, despite the existence of several obstacles, and we hope that this study will encourage researchers in all biomedical research fields to consider forming similar consortia to perform essential preclinical trials before advancing to clinical development; this approach is particularly relevant to biomedical research fields that have traditionally been hampered by lack of reproducibility and translational roadblock. We estimated the total full cost of our study at about €165,000 ($ 180,000), including more than €30,000 direct drug costs (table S1). Because the use of pRCTs may avoid unnecessary clinical trials and improve our ability to predict successful translation, these costs for a confirmatory study seem reasonable (*52*).

Our study demonstrates that poststroke treatment with anti-CD49d antibodies confers a neuroprotective benefit in a specific mouse model of stroke. We found differences between the results from two ischemic stroke models with respect to cerebral leukocyte invasion and the efficacy of anti-CD49d treatment; therefore, future clinical trials testing immunotherapeutic drugs for stroke will need to ensure that the included study population feature a substantial neuroinflammatory reaction to the brain injury, which may improve its potential to profit from such therapeutic approaches. Finally, the ability of a pRCT to advance translational research and increase the reliability of preclinical findings should be tested by comparing the results of clinical trials with the results of their preceding pRCTs.

MATERIALS AND METHODS

Study design

A key objective of this study was to implement and to test the feasibility of performing an international pRCT in experimental biomedicine. Another objective was to use this pRCT approach to robustly test the neuroprotective effect of CD49d-specific antibodies in two murine models of experimental stroke. This study was performed from June 2013 (initiation) through October 2014 (unblinding) by an international consortium consisting of six independent research groups. The infarct volume of the pooled samples from all centers and from each model was a predetermined primary end point of the study. The secondary end points were functional outcome and the migration of leukocytes into the brain. The Munich study center (A.L.) initiated the trial, coordinated the study design, and performed central data analysis, whereas the other five centers [Caen (D.V.), Milan (M.-G.D.S.), Barcelona (A.M.P.), Munich (N.P.), and Berlin (U.D. and A.R.)] contributed to study design, performed the experimental part of the study, and validated centrally determined infarct volumes. In total, 315 male C57BL/6J mice (8 to 10 weeks of age) were used [90 mice for cMCAOMCAO model (30 mice per treated group) and 225 mice for fMCAOMCAO (75 mice per treated group)]. Overall sample size per stroke model was determined a priori by performing a power calculation with G*Power (version 3.1) software using the two-tailed Wilcoxon-Mann-Whitney test for two groups. For both models, an α level of 0.05 and a power of 0.9 were required. For the cMCAOMCAO model, a Cohen's *d* ES of 0.9 was used [a conservative assumption based on our previous results demonstrating an ES *d* of 1.2 (*20*)]. In contrast, previous studies using the fMCAO model in mice did not detect a significant treatment effect that we could use to calculate ES. Therefore, we assumed an ES *d* of 0.6 to be biologically relevant, a highly conservative assumption based on our previous experience, which revealed greater variability of infarct volume after fMCAO compared to cMCAO. In addition, a 4-day mortality rate of 20% was assumed for the fMCAO group. This yielded a final sample size of 29 mice per treatment group for cMCAO and 63 mice per treatment group for fMCAO. Coded samples of anti-CD49d and control antibodies, as well as some additional items (for example, the filaments used to occlude the MCA and the behavioral test equipment), were distributed to each study center. The operational exclusion criteria were predefined (see below), and analytical exclusion criteria (see specifications below) were defined during data acquisition. The mice were allocated to the treatment and surgery groups using randomization lists generated with an online randomizer tool (www.randomizer.org) provided by the coordinating center. Treatment, surgery, analysis of infarct volume, and secondary outcome measures were performed by researchers who were blinded with respect to the treatment groups. Unblinding was performed after the statistical analyses were completed. Digital scans of the brain sections and all analysis files were stored on a central database that was accessible to all study contributors. The complete set of data is reported, including outliers. The full data set obtained from this study is publicly available at the figshare repository (http://dx.doi.org/10.6084/m9.figshare.1289824). The study protocol is available in the Supplementary Materials as fig. S6.

Animals

This study was conducted in accordance with the respective national guidelines regarding the use of experimental animals, and all procedures were approved by the respective government and institutional committees for the individual research groups [Munich: Regierungspräsidium Oberbayern; Barcelona: Ethics Committee (CEEA) of the University of Barcelona and the Departament d'Agricultura, Ramaderia, Pesca, Alimentació i Medi Natural de la Generalitat de Catalunya; Milan: Institutional guidelines and authorization by the Italian Ministry of Health; Berlin: Landesamt für Gesundheit und Soziales, Berlin; and Caen: Regional ethics committee of Lower Normandy]. Approval for the performed experiments was reached at each study site by different means, such as including the experiments in a 3-year laboratory program, as an addendum to an existing license, or applying for a new license as a "proof-of-principle" study. In total, 315 male C57BL/6J mice (8 to 10 weeks of age) were supplied to the research groups from Charles River Laboratories (stock #664). The animals were housed in a controlled temperature (22 ± 2°C) with a 12/12-hour light/dark cycle and access to pelleted food and water ad libitum. The number of mice per cage, the use of environmental enrichment, and food type were all determined individually by each research group in accordance with locally approved standard procedures. Where applicable, body weight (measured daily) and body temperature (measured on the surgery day and 1, 3, and 7 days after surgery) were measured for each mouse. All procedures regarding the study design, animal experiments, statistical analysis, and data reporting fulfill the criteria of the ARRIVE (Animal Research: Reporting of In Vivo Experiments) guidelines (see checklist in the Supplementary Materials as fig. S7).

Antibody treatment

Animals received an intraperitoneal injection of antibodies 3 hours after stroke was induced (by coagulation occlusion or filament insertion); 300 μg of monoclonal mouse anti-CD49d antibody (clone R1-2, eBioscience) or rat IgG2b isotype control antibody (clone LTF-2, Bio

Downloaded from on August 5, 2015

X Cell) was diluted to 1 mg/ml in phosphate-buffered saline (PBS) and prewarmed to 37°C before injection. The antibody concentration was chosen on the basis of information in two previous reports that used the same antibody clone in experimental stroke models (*20*, *24*).

Transient MCAO (fMCAO) model

Animals were anesthetized with isoflurane in a 30 to 70% mixture of O_2 and N_2O, and the temporal bone was exposed with an incision between the ear and the eye. A laser Doppler probe (at centers 1, 3, and 4) was affixed to the skull above the MCA territory. The animal was then placed in the supine position. Using a midline neck incision, the common carotid artery and the external carotid artery (right side, groups 1 to 3; left side, groups 4 and 5) were isolated and ligated; a 2-mm silicon-coated filament (#701912PK5Re, Doccol) was threaded into the internal carotid artery, and MCA occlusion was confirmed by a reduction in the corresponding laser Doppler flow. After 60 min of occlusion, the animals were reanesthetized, and the filament was removed. For the postsurgical survival period, the animals were housed in their home cages with access to water and food. Sham-operated control mice received the same surgical procedure, except the filament was not inserted. Body temperature was maintained during surgery using a feedback-controlled heating pad. Analgesia was provided during surgery and in the postoperative phase in accordance with each center's local regulations.

Surgical exclusion criteria: Centers 1, 3, and 4 used laser Doppler flow during the operation to confirm sufficient MCA occlusion (a reduction in blood flow to <20% of the baseline value). In addition, at all five contributing centers, mice that did not develop sufficient neurological deficits (that is, Neuroscore <8) 24 or 48 hours after MCAO were excluded. Mice that died during the observation period were excluded from all analyses, but differences in the mortality rate between the treatment groups during the observation period were determined.

Permanent MCAO (cMCAO) model

Centers 1, 2, and 3 performed the cMCAO procedure as described (*53*). In brief, the animals were anesthetized with isoflurane in a 30 to 70% mixture of O_2 and N_2O and placed in a lateral position. The skin was incised between the eye and the ear, the temporal muscle was removed, and the MCA was identified. A burr hole was drilled over the MCA, and the dura mater was removed carefully. The MCA was permanently occluded with either bipolar electrocoagulation forceps or an electrocauterizer. Permanent occlusion of the MCA was confirmed visually before closing the wound with sutures. During surgery, body temperature was maintained using a feedback-controlled heating pad. Sham-operated mice received the same surgical procedure without MCA coagulation.

Surgical exclusion criteria: Mice that developed a subarachnoid hemorrhage during surgery were excluded from the analysis. In addition, mice that died during the observation period were excluded from analysis.

Functional outcome tests

The rotarod and adhesive removal tests were performed 1, 3, and 7 days after cMCAO. These tests were chosen because they are the most commonly used tests for measuring the effect of cMCAO, which results in only minor behavioral deficits, and because these tests were used previously by all three centers that performed the cMCAO model.

The rotarod test was used to measure coordination and sensorimotor performance before and after cMCAO (*54*). Mice were trained daily for 3 days before MCAO or sham surgery, and baseline performance was recorded the day before cMCAO using the following strategy: the rod accelerated from 8 to 40 rpm over 240 s, with a mean of three consecutive trials per mouse and time points. The latency to fall off the rod was recorded, and postsurgical performance was calculated by dividing the postsurgical values by the individual animal's baseline performance.

The adhesive removal test was used to evaluate sensory and motor deficits (*55*). A round (4-mm-diameter) adhesive sticker was placed on the palmar side of the forepaw; the same pressure was applied for each adhesive application. The day before surgery (and at the indicated times after cMCAO or sham surgery), three trials per test were performed. The latency to contact the paw with the adhesive and the latency to remove the adhesive were recorded. Motor performance was expressed as the difference between the latency to contact the paw and the latency to remove the adhesive.

The Neuroscore was performed before surgery and 2 and 4 days after fMCAO or sham surgery; this test was used to evaluate the general status and focal neurologic dysfunction after fMCAO, which induces substantial deficits in contrast to the cMCAO model, and was performed as described (*56*). The score ranges from 0 (no deficits) to 56 (representing the poorest performance in all items) and is calculated as the sum of the general and focal deficits. The Neuroscore results were expressed as a composite neurological score, which included the following general deficits (scores): fur (0 to 2), ears (0 to 2), eyes (0 to 4), posture (0 to 4), spontaneous activity (0 to 4), and epileptic behavior (0 to 12); and the following focal deficits: body asymmetry (0 to 4), gait (0 to 4), climbing on a surface inclined at 45° (0 to 4), circling behavior (0 to 4), front-limb symmetry (0 to 4), circling behavior (0 to 4), and whisker response to light touch (0 to 4).

Tissue sampling and processing

Mice were deeply anesthetized 7 days after cMCAO, 4 days after fMCAO, and at the respective times for mice in the corresponding sham surgery groups. The brain was removed, frozen immediately on powdered dry ice, and stored at −20°C. All biological samples were shipped on dry ice to the central analysis center in Munich, where the samples were stored at −80°C until further analysis and for central archiving. All brains were cryosectioned by researchers who were blinded with respect to the surgery and treatment groups. Coronal brain sections (20 μm thick) were prepared at 400-μm intervals and used to analyze infarct volume. In addition, 12-μm-thick coronal sections were obtained at the level of the anterior commissure and were used for immunohistochemistry. Sections were mounted on Superfrost Plus slides (Thermo Scientific) and stored at −80°C.

Infarct volumetry

Infarct volume was measured in CV-stained sections as described (*53*). In brief, one series of serial (20-μm-thick) sections from each animal was air-dried at room temperature for 30 min. The slides were stained with a 0.1% CV solution at 60°C for 10 min and then rinsed twice in distilled water for 1 min. After washing and dehydration, the slides were covered with Roti-Histokit mounting medium (Roth). CV-stained sections were scanned at 600 dpi on a flatbed scanner (LiDE 210, Canon). For the cMCAO model, the direct infarct demarcation on CV-stained sections (unstained area) was measured after confirming the absence of edema at the investigated time point (7 days after cMCAO or sham surgery). For the fMCAO model, we corrected the infarct volume for edema with the following equation: (Ischemic area) = (Direct lesion volume) − [(Ipsilateral hemisphere) − (Contralateral hemisphere)]. In both models, total infarct volume was determined by integrating the measured areas and distances over the sections. To validate the sections in the MCAO mice with missing lesion demarcation on CV staining,

Downloaded from on August 5, 2015

neuronal loss was measured with the terminal deoxynucleotidyl transferase–mediated deoxyuridine triphosphate nick end labeling (TUNEL) method (TUNEL Apoptosis Detection Kit, Millipore). All sections were analyzed independently by two central investigators (G.L. and A.L.), both of whom were blinded with respect to the treatment groups; the mean of these two measurements was used for subsequent analyses. In addition, the original CV-stained slides were returned to the respective originating center for further validation. Interrater reliability between the two central investigators and the individual participating centers was measured and is shown in fig. S1.

Analytical exclusion criteria: The following criteria were used to exclude samples from the analysis: (i) missing biological samples due to the death of an animal before the study's end point (day 4 for fMCAO and day 7 for cMCAO; $n = 23$ mice excluded); (ii) overt mechanical damage or disruption when preparing the brain sections, rendering the sample unusable ($n = 2$ mice excluded); (iii) no ischemic brain lesion detectable in the MCAO group (detected as demarcation on CV staining or no neuronal apoptosis measured using TUNEL staining) ($n = 27$ mice excluded); (iv) demarcation of an ischemic lesion on CV-stained sections in sham-operated mice ($n = 2$ mice excluded); and (v) Neuroscore <8 points 24 hours after fMCAO ($n = 6$ mice excluded). The individual animals that were excluded on the basis of the aforementioned criteria were also excluded from the analysis of behavioral data sets and physiological parameters.

Immunofluorescence

We performed immunofluorescence staining for CD45 to identify leukocytes that had infiltrated the brain. Coronal sections (12 μm thick) were prepared at the level of the anterior commissure and dried at room temperature for 1 hour. After rinsing in PBS (pH 7.4), the slides were fixed with acetone at −20°C, rinsed in PBS, and incubated in blocking buffer (BB) containing 0.1% Triton, 0.05% Tween 20, 10% fetal calf serum, and 1% bovine serum albumin (w/v) in PBS at room temperature for 1 hour. The slides were then incubated overnight at 4°C in anti-CD45 antibody (1:100, clone 104-2, Abcam) in BB. The slides were then rinsed in PBS and incubated for 1 hour at room temperature in Alexa Fluor 488 goat anti-mouse IgG (H+L) (1:100, Invitrogen). Finally, the slides were rinsed in PBS, counterstained for 2 min with DAPI (1:4000, Invitrogen), and mounted using Fluoromount medium (Sigma). The slides were analyzed using an epifluorescence microscope (Axiovert 200M, Zeiss). CD45-positive cells were counted in one 12-μm section per brain at the position of the anterior commissure (about 0.1 mm rostral to bregma). The infarct core was identified with corresponding CV-stained sections, and this area was excluded from the localization analysis and quantification of CD45-positive cells. For the cMCAO model, the location of each CD45-positive cell was marked on a topographic map according to the mouse brain atlas, yielding a cumulative localization map of leukocyte invasion for each treatment group.

Statistical analysis

This study was designed as a prospective, multicenter, randomized controlled trial of experimental ischemic stroke induced in mice via two distinct models. The above-mentioned operational and analytical exclusion criteria were applied. If a mouse met one or more of the exclusion criteria, data and samples were excluded from all analyses. Sufficient normal distribution of all data sets was verified by checking histograms (unimodal distribution) and skewness ($|\text{skewness}| < 1$). Physiological parameters and cerebral leukocyte counts were analyzed by ANOVA followed by Tukey's multiple-comparison test (GraphPad Prism 6.0). The characteristics of the samples obtained from the individual centers (Table 1) were tested with Fisher's exact test, the χ^2 test, or ANOVA (where indicated), and mortality was analyzed by comparing the survival curves with the log-rank (that is, Mantel-Cox) test (GraphPad Prism 6.0). Infarct volume and behavioral deficits were tested using a linear mixed-effects model to account for heterogeneity between centers (SPSS version 22, IBM). We used random intercept models with treatment group as the independent variable and infarct volume as the dependent variable. ES estimates (standardized mean difference) were calculated using inverse-variance weighting in a random-effects model using RevMan version 5.3; RevMan 5.3 was also used to create the forest plot in Fig. 2C. Correlation analysis for infarct volume and behavioral deficits was performed using linear regression (GraphPad Prism). Concordance analysis for interrater reliability was done using the Bland-Altman method (GraphPad Prism) and calculation of ICCs (SPSS). A two-sided significance level of $\alpha = 0.05$ for both primary hypotheses was applied. *P* values for secondary hypotheses should be interpreted cautiously as exploratory analyses. No adjustment for duality of the two stroke models was applied. An overview of means and 95% CI is available for all primary and secondary end points in table S2.

SUPPLEMENTARY MATERIALS

www.sciencetranslationalmedicine.org/cgi/content/full/7/299/299ra121/DC1
Fig. S1. Analyses for interrater concordance.
Fig. S2. Behavioral tests before and after cMCAO.
Fig. S3. Composite Neuroscore for functional deficits after fMCAO.
Fig. S4. Mortality after cMCAO and fMCAO.
Fig. S5. Physiological parameter analysis after cMCAO and fMCAO.
Fig. S6. Study protocol.
Fig. S7. The ARRIVE guidelines checklist.
Table S1. Study costs (in euro).
Table S2. fMCAO and cMCAO means and CIs.

REFERENCES AND NOTES

1. G. A. Donnan, M. Fisher, M. Macleod, S. M. Davis, Stroke. *Lancet* **371**, 1612–1623 (2008).
2. Á. Chamorro, A. Meisel, A. M. Planas, X. Urra, D. van de Beek, R. Veltkamp, The immunology of acute stroke. *Nat. Rev. Neurol.* **8**, 401–410 (2012).
3. W. Hacke, M. Kaste, E. Bluhmki, M. Brozman, A. Dávalos, D. Guidetti, V. Larrue, K. R. Lees, Z. Medeghri, T. Machnig, D. Schneider, R. von Kummer, N. Wahlgren, D. Toni; ECASS Investigators, Thrombolysis with alteplase 3 to 4.5 hours after acute ischemic stroke. *N. Engl. J. Med.* **359**, 1317–1329 (2008).
4. E. C. Jauch, J. L. Saver, H. P. Adams Jr., A. Bruno, J. J. Connors, B. M. Demaerschalk, P. Khatri, P. W. McMullan Jr., A. I. Qureshi, K. Rosenfield, P. A. Scott, D. R. Summers, D. Z. Wang, M. Wintermark, H. Yonas; American Heart Association Stroke Council; Council on Cardiovascular Nursing; Council on Peripheral Vascular Disease, Council on Clinical Cardiology, Guidelines for the early management of patients with acute ischemic stroke: A guideline for healthcare professionals from the American Heart Association/American Stroke Association. *Stroke* **44**, 870–947 (2013).
5. V. E. O'Collins, M. R. Macleod, G. A. Donnan, L. L. Horky, B. H. van der Worp, D. W. Howells, 1,026 experimental treatments in acute stroke. *Ann. Neurol.* **59**, 467–477 (2006).
6. C. Iadecola, J. Anrather, Stroke research at a crossroad: Asking the brain for directions. *Nat. Neurosci.* **14**, 1363–1368 (2011).
7. M. A. Moskowitz, Brain protection: Maybe yes, maybe no. *Stroke* **41**, S85–S86 (2010).
8. J. A. Zivin, M. Fisher, U. DeGirolami, C. C. Hemenway, J. A. Stashak, Tissue plasminogen activator reduces neurological damage after cerebral embolism. *Science* **230**, 1289–1292 (1985).
9. K. A. Hossmann, The two pathophysiologies of focal brain ischemia: Implications for translational stroke research. *J. Cereb. Blood Flow Metab.* **32**, 1310–1316 (2012).
10. M. McNutt, Journals unite for reproducibility. *Science* **346**, 679 (2014).
11. C. Kilkenny, W. J. Browne, I. C. Cuthill, M. Emerson, D. G. Altman, Improving bioscience research reporting: The ARRIVE guidelines for reporting animal research. *PLOS Biol.* **8**, e1000412 (2010).
12. D. J. Lefer, R. Bolli, Development of an NIH consortium for preclinicAl AssESsment of CARdioprotective therapies (CAESAR): A paradigm shift in studies of infarct size limitation. *J. Cardiovasc. Pharmacol. Ther.* **16**, 332–339 (2011).

Downloaded from on August 5, 2015

13. U. Dirnagl, A. Hakim, M. Macleod, M. Fisher, D. Howells, S. M. Alan, G. Steinberg, A. Planas, J. Boltze, S. Savitz, C. Iadecola, S. Meairs, A concerted appeal for international cooperation in preclinical stroke research. *Stroke* **44**, 1754–1760 (2013).
14. P. M. Bath, M. R. Macleod, A. R. Green, Emulating multicentre clinical stroke trials: A new paradigm for studying novel interventions in experimental models of stroke. *Int. J. Stroke* **4**, 471–479 (2009).
15. J. Kimmelman, J. S. Mogil, U. Dirnagl, Distinguishing between exploratory and confirmatory preclinical research will improve translation. *PLOS Biol.* **12**, e1001863 (2014).
16. Q. Wang, X. N. Tang, M. A. Yenari, The inflammatory response in stroke. *J. Neuroimmunol.* **184**, 53–68 (2006).
17. B. Engelhardt, L. Sorokin, The blood–brain and the blood–cerebrospinal fluid barriers: Function and dysfunction. *Semin. Immunopathol.* **31**, 497–511 (2009).
18. B. Engelhardt, R. M. Ransohoff, The ins and outs of T-lymphocyte trafficking to the CNS: Anatomical sites and molecular mechanisms. *Trends Immunol.* **26**, 485–495 (2005).
19. R. Rudick, C. Polman, D. Clifford, D. Miller, L. Steinman, Natalizumab: Bench to bedside and beyond. *JAMA Neurol.* **70**, 172–182 (2013).
20. A. Liesz, W. Zhou, É. Mracskó, S. Karcher, H. Bauer, S. Schwarting, L. Sun, D. Bruder, S. Stegemann, A. Cerwenka, C. Sommer, A. H. Dalpke, R. Veltkamp, Inhibition of lymphocyte trafficking shields the brain against deleterious neuroinflammation after stroke. *Brain* **134**, 704–720 (2011).
21. K. Becker, D. Kindrick, J. Relton, J. Harlan, R. Winn, Antibody to the α4 integrin decreases infarct size in transient focal cerebral ischemia in rats. *Stroke* **32**, 206–211 (2001).
22. J. K. Relton, K. E. Sloan, E. M. Frew, E. T. Whalley, S. P. Adams, R. R. Lobb, Inhibition of α4 integrin protects against transient focal cerebral ischemia in normotensive and hypertensive rats. *Stroke* **32**, 199–205 (2001).
23. J. Neumann, M. Riek-Burchardt, J. Herz, T. R. Doeppner, R. König, H. Hütten, E. Etemire, L. Männ, A. Klingberg, T. Fischer, M. W. Görtler, H. J. Heinze, P. Reichardt, B. Schraven, D. M. Hermann, K. G. Reymann, M. Gunzer, Very-late-antigen-4 (VLA-4)-mediated brain invasion by neutrophils leads to interactions with microglia, increased ischemic injury and impaired behavior in experimental stroke. *Acta Neuropathol.* **129**, 259–277 (2015).
24. F. Langhauser, P. Kraft, E. Göb, J. Leinweber, M. K. Schuhmann, K. Lorenz, M. Gelderblom, S. Bittner, S. G. Meuth, H. Wiendl, T. Magnus, C. Kleinschnitz, Blocking of α4 integrin does not protect from acute ischemic stroke in mice. *Stroke* **45**, 1799–1806 (2014).
25. S. T. Carmichael, Rodent models of focal stroke: Size, mechanism, and purpose. *NeuroRx* **2**, 396–409 (2005).
26. W. Zhou, A. Liesz, H. Bauer, C. Sommer, B. Lahrmann, N. Valous, N. Grabe, R. Veltkamp, Postischemic brain infiltration of leukocyte subpopulations differs among murine permanent and transient focal cerebral ischemia models. *Brain Pathol.* **23**, 34–44 (2013).
27. F. Prinz, T. Schlange, K. Asadullah, Believe it or not: How much can we rely on published data on potential drug targets? *Nat. Rev. Drug Discov.* **10**, 712 (2011).
28. C. G. Begley, L. M. Ellis, Drug development: Raise standards for preclinical cancer research. *Nature* **483**, 531–533 (2012).
29. S. Perrin, Preclinical research: Make mouse studies work. *Nature* **507**, 423–425 (2014).
30. G. N. Duda, D. W. Grainger, M. L. Frisk, L. Bruckner-Tuderman, A. Carr, U. Dirnagl, K. M. Einhäupl, S. Gottschalk, E. Gruskin, C. Huber, C. H. June, D. J. Mooney, E. T. Rietschel, G. Schütte, W. Seeger, M. M. Stevens, R. Urban, A. Veldman, G. Wess, H. D. Volk, Changing the mindset in life sciences toward translation: A consensus. *Sci. Transl. Med.* **6**, 264cm12 (2014).
31. M. Endres, B. Engelhardt, J. Koistinaho, O. Lindvall, S. Meairs, J. P. Mohr, A. Planas, N. Rothwell, M. Schwaninger, M. E. Schwab, D. Vivien, T. Wieloch, U. Dirnagl, Improving outcome after stroke: Overcoming the translational roadblock. *Cerebrovasc. Dis.* **25**, 268–278 (2008).
32. S. R. Bornstein, J. Licinio, Improving the efficacy of translational medicine by optimally integrating health care, academia and industry. *Nat. Med.* **17**, 1567–1569 (2011).
33. U. Dirnagl, M. Fisher, International, multicenter randomized preclinical trials in translational stroke research: It's time to act. *J. Cereb. Blood Flow Metab.* **32**, 933–935 (2012).
34. J. P. Ioannidis, S. Greenland, M. A. Hlatky, M. J. Khoury, M. R. Macleod, D. Moher, K. F. Schulz, R. Tibshirani, Increasing value and reducing waste in research design, conduct, and analysis. *Lancet* **383**, 166–175 (2014).
35. J. P. Ioannidis, Why most published research findings are false. *PLOS Med.* **2**, e124 (2005).
36. N. A. Crossley, E. Sena, J. Goehler, J. Horn, B. van der Worp, P. M. Bath, M. Macleod, U. Dirnagl, Empirical evidence of bias in the design of experimental stroke studies: A metaepidemiologic approach. *Stroke* **39**, 929–934 (2008).
37. D. W. Howells, E. S. Sena, M. R. Macleod, Bringing rigour to translational medicine. *Nat. Rev. Neurol.* **10**, 37–43 (2014).
38. U. Dirnagl, Bench to bedside: The quest for quality in experimental stroke research. *J. Cereb. Blood Flow Metab.* **26**, 1465–1478 (2006).
39. CAMARADES (2014).
40. K. K. Tsilidis, O. A. Panagiotou, E. S. Sena, E. Aretouli, E. Evangelou, D. W. Howells, R. Al-Shahi Salman, M. R. Macleod, J. P. Ioannidis, Evaluation of excess significance bias in animal studies of neurological diseases. *PLOS Biol.* **11**, e1001609 (2013).
41. K. S. Button, J. P. Ioannidis, C. Mokrysz, B. A. Nosek, J. Flint, E. S. Robinson, M. R. Munafò, Power failure: Why small sample size undermines the reliability of neuroscience. *Nat. Rev. Neurosci.* **14**, 365–376 (2013).
42. Enlimomab Acute Stroke Trial Investigators, Use of anti-ICAM-1 therapy in ischemic stroke: Results of the Enlimomab Acute Stroke Trial. *Neurology* **57**, 1428–1434 (2001).
43. C. Kleinschnitz, N. Schwab, P. Kraft, I. Hagedorn, A. Dreykluft, T. Schwarz, M. Austinat, B. Nieswandt, H. Wiendl, G. Stoll, Early detrimental T-cell effects in experimental cerebral ischemia are neither related to adaptive immunity nor thrombus formation. *Blood* **115**, 3835–3842 (2010).
44. T. Shichita, Y. Sugiyama, H. Ooboshi, H. Sugimori, R. Nakagawa, I. Takada, T. Iwaki, Y. Okada, M. Iida, D. J. Cua, Y. Iwakura, A. Yoshimura, Pivotal role of cerebral interleukin-17–producing γδT cells in the delayed phase of ischemic brain injury. *Nat. Med.* **15**, 946–950 (2009).
45. A. E. Baird, The forgotten lymphocyte: Immunity and stroke. *Circulation* **113**, 2035–2036 (2006).
46. G. Yilmaz, T. V. Arumugam, K. Y. Stokes, D. N. Granger, Role of T lymphocytes and interferon-γ in ischemic stroke. *Circulation* **113**, 2105–2112 (2006).
47. J. Seok, H. S. Warren, A. G. Cuenca, M. N. Mindrinos, H. V. Baker, W. Xu, D. R. Richards, G. P. McDonald-Smith, H. Gao, L. Hennessy, C. C. Finnerty, C. M. López, S. Honari, E. E. Moore, J. P. Minei, J. Cuschieri, P. E. Bankey, J. L. Johnson, J. Sperry, A. B. Nathens, T. R. Billiar, M. A. West, M. G. Jeschke, M. B. Klein, R. L. Gamelli, N. S. Gibran, B. H. Brownstein, C. Miller-Graziano, S. E. Calvano, P. H. Mason, J. P. Cobb, L. G. Rahme, S. F. Lowry, R. V. Maier, L. L. Moldawer, D. N. Herndon, R. W. Davis, W. Xiao, R. G. Tompkins; Inflammation and Host Response to Injury, Large Scale Collaborative Research Program, Genomic responses in mouse models poorly mimic human inflammatory diseases. *Proc. Natl. Acad. Sci. U.S.A.* **110**, 3507–3512 (2013).
48. J. Mestas, C. C. Hughes, Of mice and not men: Differences between mouse and human immunology. *J. Immunol.* **172**, 2731–2738 (2004).
49. W. R. Schabitz, U. Dirnagl, Are we ready to translate T-cell transmigration in stroke? *Stroke* **45**, 1610–1611 (2014).
50. H. X. Chu, H. A. Kim, S. Lee, J. P. Moore, C. T. Chan, A. Vinh, M. Gelderblom, T. V. Arumugam, B. R. Broughton, G. R. Drummond, C. G. Sobey, Immune cell infiltration in malignant middle cerebral artery infarction: Comparison with transient cerebral ischemia. *J. Cereb. Blood Flow Metab.* **34**, 450–459 (2014).
51. M. Balkaya, J. M. Kröber, A. Rex, M. Endres, Assessing post-stroke behavior in mouse models of focal ischemia. *J. Cereb. Blood Flow Metab.* **33**, 330–338 (2013).
52. D. W. Howells, E. S. Sena, V. O'Collins, M. R. Macleod, Improving the efficiency of the development of drugs for stroke. *Int. J. Stroke* **7**, 371–377 (2012).
53. G. Llovera, S. Roth, N. Plesnila, R. Veltkamp, A. Liesz, Modeling stroke in mice: Permanent coagulation of the distal middle cerebral artery. *J. Vis. Exp.* e51729 (2014).
54. B. J. Jones, D. J. Roberts, The quantitative measurement of motor inco-ordination in naive mice using an accelerating rotarod. *J. Pharm. Pharmacol.* **20**, 302–304 (1968).
55. V. Bouet, M. Boulouard, J. Toutain, D. Divoux, M. Bernaudin, P. Schumann-Bard, T. Freret, The adhesive removal test: A sensitive method to assess sensorimotor deficits in mice. *Nat. Protoc.* **4**, 1560–1564 (2009).
56. F. Orsini, P. Villa, S. Parrella, R. Zangari, E. R. Zanier, R. Gesuete, M. Stravalaci, S. Fumagalli, R. Ottria, J. J. Reina, A. Paladini, E. Micotti, R. Ribeiro-Viana, J. Rojo, V. I. Pavlov, G. L. Stahl, A. Bernardi, M. Gobbi, M. G. De Simoni, Targeting mannose-binding lectin confers long-lasting protection with a surprisingly wide therapeutic window in cerebral ischemia. *Circulation* **126**, 1484–1494 (2012).

Acknowledgments: We thank F. Marchesi and D. Olivari for their skilled technical assistance. **Funding:** This work was supported by the excellence cluster of the German research foundation "Munich Cluster for Systems Neurology (SyNergy)" to A.L. and N.P. and the Daimler and Benz Foundation (32-05/12) to A.L.; grants from the Spanish Ministry of Economy (MINECO; SAF2011-30492 and SAF2014-56279) to A.M.P.; grants from the INSERM (French National Institute for Health and Medical Research), the University of Caen Basse-Normandie, and the GIS IBiSA to D.V.; the Italian Ministry of Health Young Investigators Award #GR-2008-1136044 to E.R.Z.; and grants from Bundesministerium für Bildung, Wissenschaft, Forschung und Technologie (BMBF) (01EO0801, Center for Stroke Research Berlin) and the Hermann and Lilly Schilling Foundation to U.D. **Author contributions:** A.L. initiated this trial; A.L., U.D., A.M.P., N.P., M.-G.D.S., and D.V. designed the study protocol, supervised the study, and reviewed original data sets; G.L. performed the central analysis of all biological samples and data sets; V.A., C.F., M.F.-F., B.H., K.H., G.L., U.M., C.O., H.P., C.P., A.R., S.R., A.S.-P., and E.R.Z. performed experiments; U.G. performed central statistical analysis; and U.D., A.L., G.L., A.M.P., N.P., M.-G.D.S., and D.V. wrote the manuscript. **Competing interests:** The authors declare that they have no competing interests. **Data and materials availability:** The full data set obtained from this study is publicly available at the figshare repository (http://dx.doi.org/10.6084/m9.figshare.1289824).

Submitted 24 February 2015
Accepted 23 June 2015
Published 5 August 2015
10.1126/scitranslmed.aaa9853

Citation: G. Llovera, K. Hofmann, S. Roth, A. Salas-Pérdomo, M. Ferrer-Ferrer, C. Perego, E. R. Zanier, U. Mamrak, A. Rex, H. Party, V. Agin, C. Fauchon, C. Orset, B. Haelewyn, M.-G. De Simoni, U. Dirnagl, U. Grittner, A. M. Planas, N. Plesnila, D. Vivien, A. Liesz, Results of a preclinical randomized controlled multicenter trial (pRCT): Anti-CD49d treatment for acute brain ischemia. *Sci. Transl. Med.* **7**, 299ra121 (2015).

Downloaded from on August 5, 2015

Science Translational Medicine
AAAS

Results of a preclinical randomized controlled multicenter trial (pRCT): Anti-CD49d treatment for acute brain ischemia

Gemma Llovera *et al.*

Sci Transl Med **7**, 299ra121 (2015);
DOI: 10.1126/scitranslmed.aaa9853

Editor's Summary

Tested, just like a human

Over the last few decades, clinical trial design and analysis have become increasingly stringent. These refinements—designed to ensure valid conclusions for formal drug approval—have improved clinical trial reliability. Now, Llovera *et al*. have applied the principles of the gold-standard randomized, controlled clinical trial to a preclinical investigation. They tested an antibody to CD49d, which inhibits leukocyte migration into the brain, in two mouse models of stroke. Data from their six-center, preclinical, randomized controlled trial in mice show that the antibody significantly reduced both leukocyte invasion and infarct volume after a small cortical stroke but that it did not have any effect in the other model, in which the animal suffered a larger injury. The authors outline the many lessons learned from their experience for further application of preclinical randomized controlled trials to translational research.

A complete electronic version of this article and other services, including high-resolution figures, can be found at:
/content/7/299/299ra121.full.html

Supplementary Material can be found in the online version of this article at:
/content/suppl/2015/08/03/7.299.299ra121.DC1.html

Related Resources for this article can be found online at:
http://stm.sciencemag.org/content/scitransmed/4/154/154ra133.full.html
http://stm.sciencemag.org/content/scitransmed/4/156/156ps20.full.html
http://stm.sciencemag.org/content/scitransmed/6/257/257re7.full.html

Information about obtaining **reprints** of this article or about obtaining **permission to reproduce this article** in whole or in part can be found at:
http://www.sciencemag.org/about/permissions.dtl

Downloaded from on August 5, 2015

Science Translational Medicine (print ISSN 1946-6234; online ISSN 1946-6242) is published weekly, except the last week in December, by the American Association for the Advancement of Science, 1200 New York Avenue NW, Washington, DC 20005. Copyright 2015 by the American Association for the Advancement of Science; all rights reserved. The title *Science Translational Medicine* is a registered trademark of AAAS.

www.sciencetranslationalmedicine.org/cgi/content/full/7/299/299ra121/DC1

Supplementary Materials for

Results of a preclinical randomized controlled multicenter trial (pRCT): Anti-CD49d treatment for acute brain ischemia

Gemma Llovera, Kerstin Hofmann, Stefan Roth, Angelica Salas-Pérdomo, Maura Ferrer-Ferrer, Carlo Perego, Elisa R. Zanier, Uta Mamrak, Andre Rex, Hélène Party, Véronique Agin, Claudine Fauchon, Cyrille Orset, Benoît Haelewyn, Maria-Grazia De Simoni, Ulrich Dirnagl, Ulrike Grittner, Anna M. Planas, Nikolaus Plesnila, Denis Vivien, Arthur Liesz*

*Corresponding author. E-mail: arthur.liesz@med.uni-muenchen.de

Published 5 August 2015, *Sci. Transl. Med.* **7**, 299ra121 (2015)
DOI: 10.1126/scitranslmed.aaa9853

The PDF file includes:

Fig. S1. Analyses for interrater concordance.
Fig. S2. Behavioral tests before and after cMCAO.
Fig. S3. Composite Neuroscore for functional deficits after fMCAO.
Fig. S4. Mortality after cMCAO and fMCAO.
Fig. S5. Physiological parameter analysis after cMCAO and fMCAO.
Fig. S6. Study protocol.
Fig. S7. The ARRIVE guidelines checklist.
Table S1. Study costs (in euro).
Table S2. fMCAO and cMCAO means and CIs.

Figure S1

A

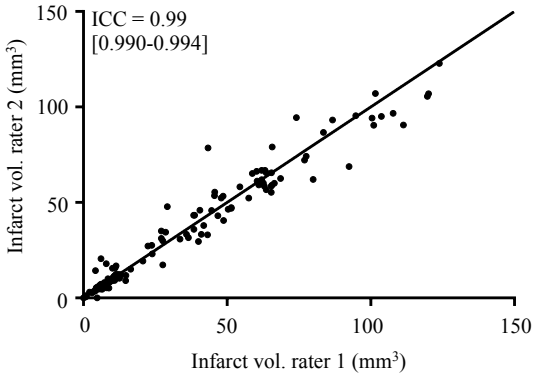

Fig. S1. Analyses for interrater concordance. (A) Concordance of infarct volume measurements was assessed in between the two independent raters at the central study center. Analyses confirmed excellent inter-rater concordance within the central study center. **(B)** Concordance was determined between the mean infarct volume (mm^3) of the central study center and the individual experimental centers. n(Center 1): 40; n(Center 2): 32; n(Center 3): 36; n(Center 4):30; n(Center 5): 16. Concordance was estimated by intra class correlation coefficient (ICC) and 95% confidence intervals [CI].

B

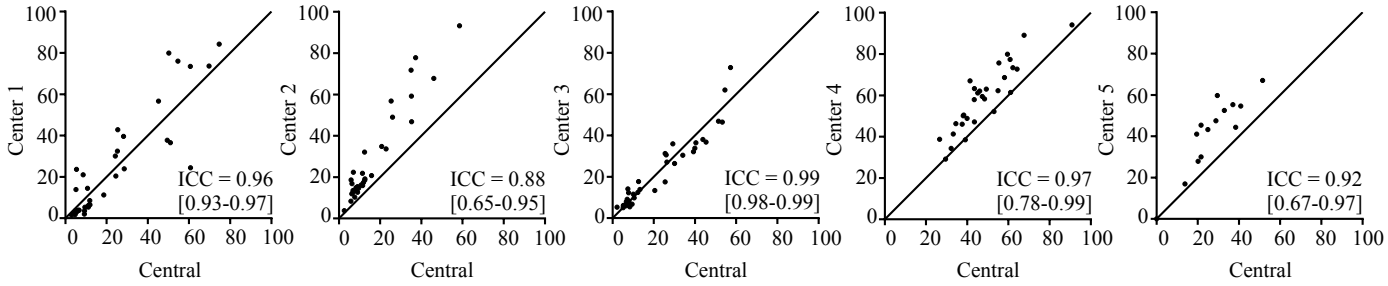

Figure S2

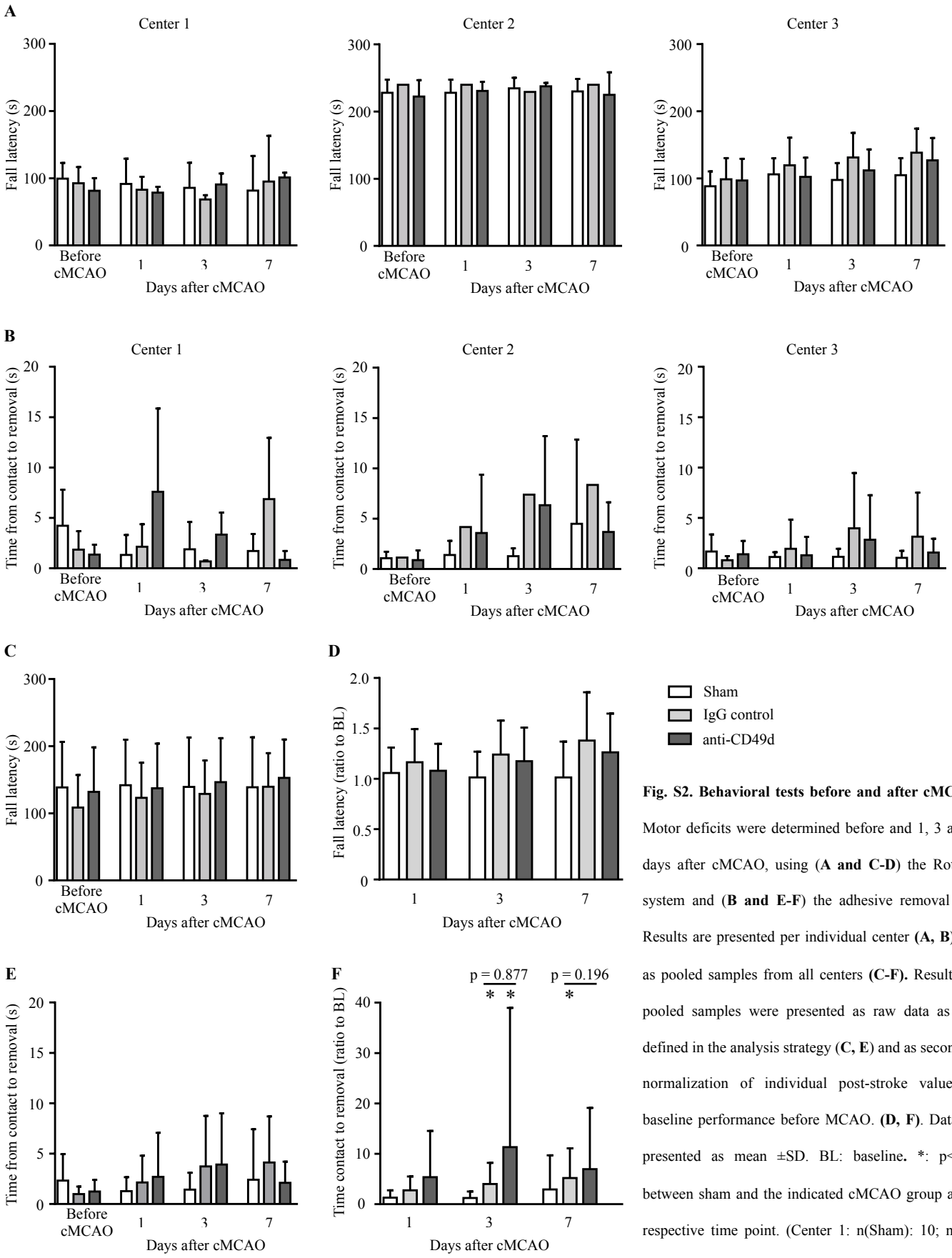

Fig. S2. Behavioral tests before and after cMCAO. Motor deficits were determined before and 1, 3 and 7 days after cMCAO, using (**A and C-D**) the Rotarod system and (**B and E-F**) the adhesive removal test. Results are presented per individual center **(A, B)** and as pooled samples from all centers **(C-F).** Results for pooled samples were presented as raw data as pre-defined in the analysis strategy (**C, E**) and as secondary normalization of individual post-stroke values to baseline performance before MCAO. **(D, F)**. Data are presented as mean ±SD. BL: baseline**.** *: $p<0.05$ between sham and the indicated cMCAO group at the respective time point. (Center 1: n(Sham): 10; n(IgG Control): 2; n(anti-CD49d): 2. Center 2: n(Sham): 9; n(IgG Control): 1; n(anti-CD49d): 5. Center 3: n(Sham): 10; n(IgG Control): 10; n(anti-CD49d): 10).

Figure S3

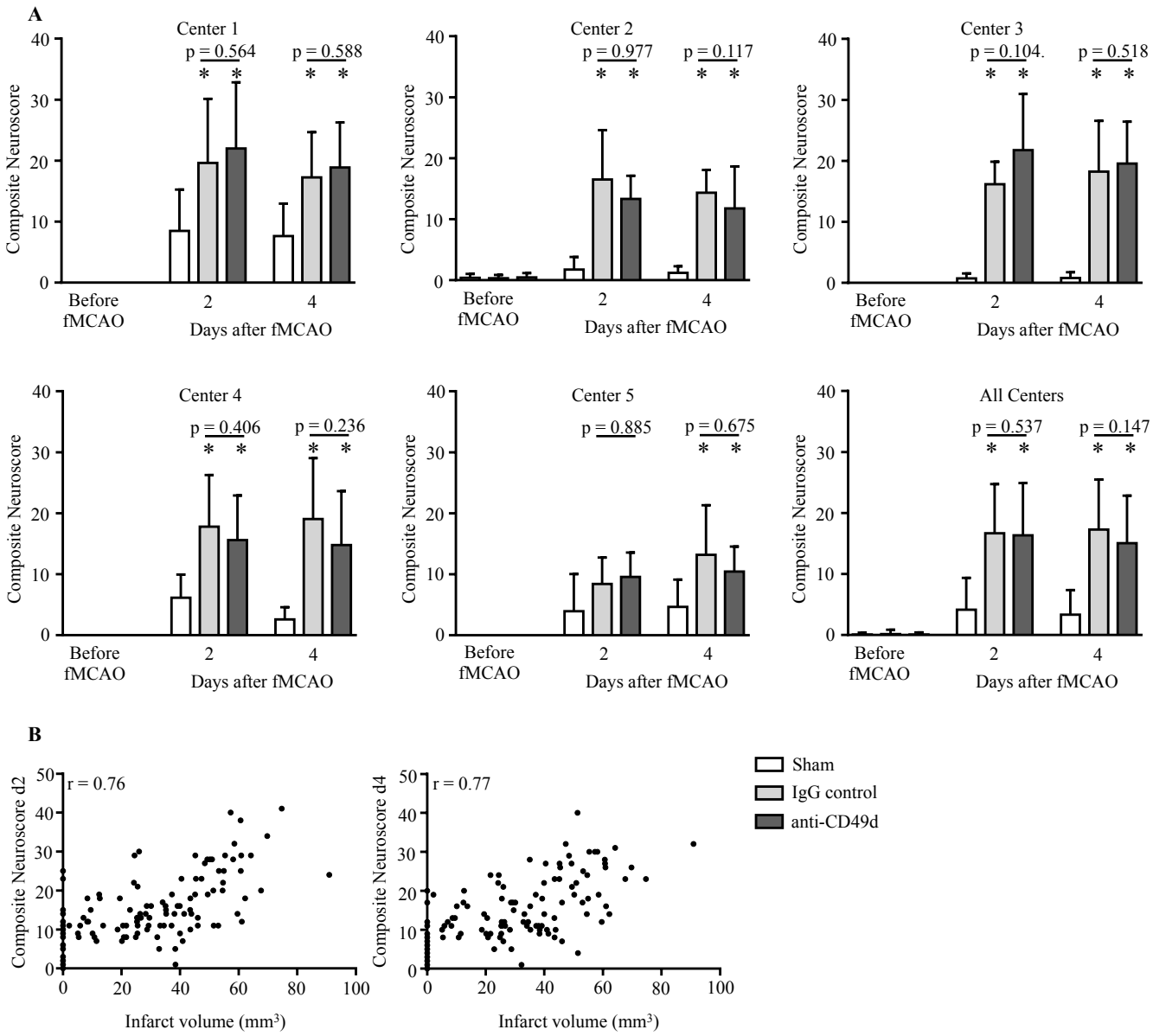

Fig. S3. Composite Neuroscore for functional deficits after fMCAO. (A) Each panel depicts results for the composite Neuroscore before fMCAO and 2 and 4 days after fMCAO per individual center and as pooled samples from all centers. * : $p<0.05$ between sham and the indicate cMCAO group at the respective time point. Data are presented as mean ±SD. (Center 1: n(Sham): 14; n(IgG Control): 11; n(anti-CD49d): 9. Center 2: n(Sham): 15; n(IgG Control): 6; n(anti-CD49d): 9. Center 3: n(Sham): 15; n(IgG Control): 12; n(anti-CD49d): 9. Center 4: n(Sham): 15; n(IgG Control): 15; n(anti-CD49d): 15. Center 5: n(Sham): 15; n(IgG Control): 5; n(anti-CD49d): 9). **(B)** Correlation of infarct volume and functional deficit as assessed by the composite Neuroscore was analyzed by linear regression for results at day 2 and 4 after fMCAO, respectively. n(Sham): 74; n(IgG Control): 49; n(anti-CD49d): 51. r=Pearson correlation coefficient.

Figure S4

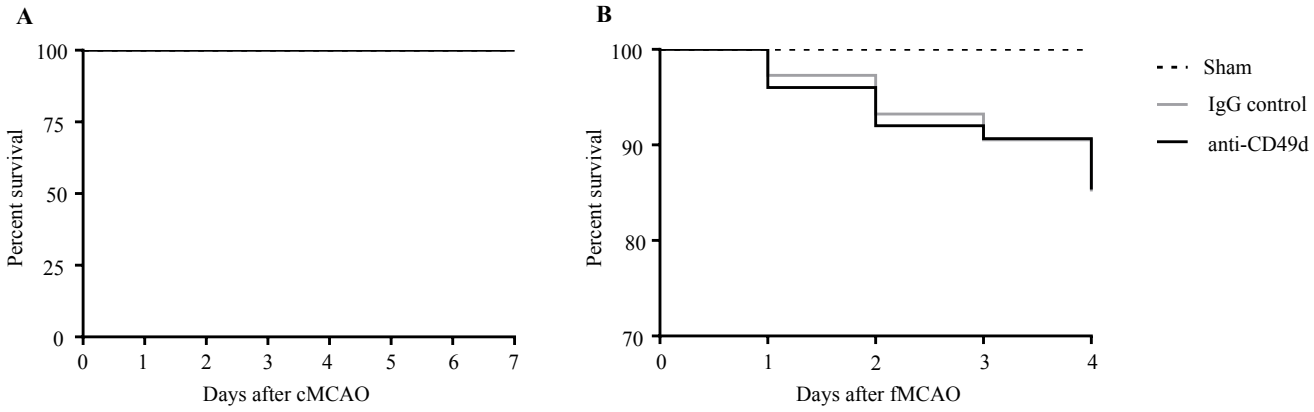

Fig. S4. Mortality after cMCAO and fMCAO. Mortality during the observation period is depicted as Kaplan-Meier curves. **(A)** We did not observe any post-operative mortality during the 7d observation period after cMCAO (control or anti-CD49d group) and the respective sham surgery. n(Sham): 30; n(IgG Control): 25; n(anti-CD49d): 27. **(B)** fMCAO induced a moderate mortality in both treatment groups without a significant difference between treatment during the 4d observation period. n(Sham): 74; n(IgG Control): 49; n(anti-CD49d): 51.

Figure S5

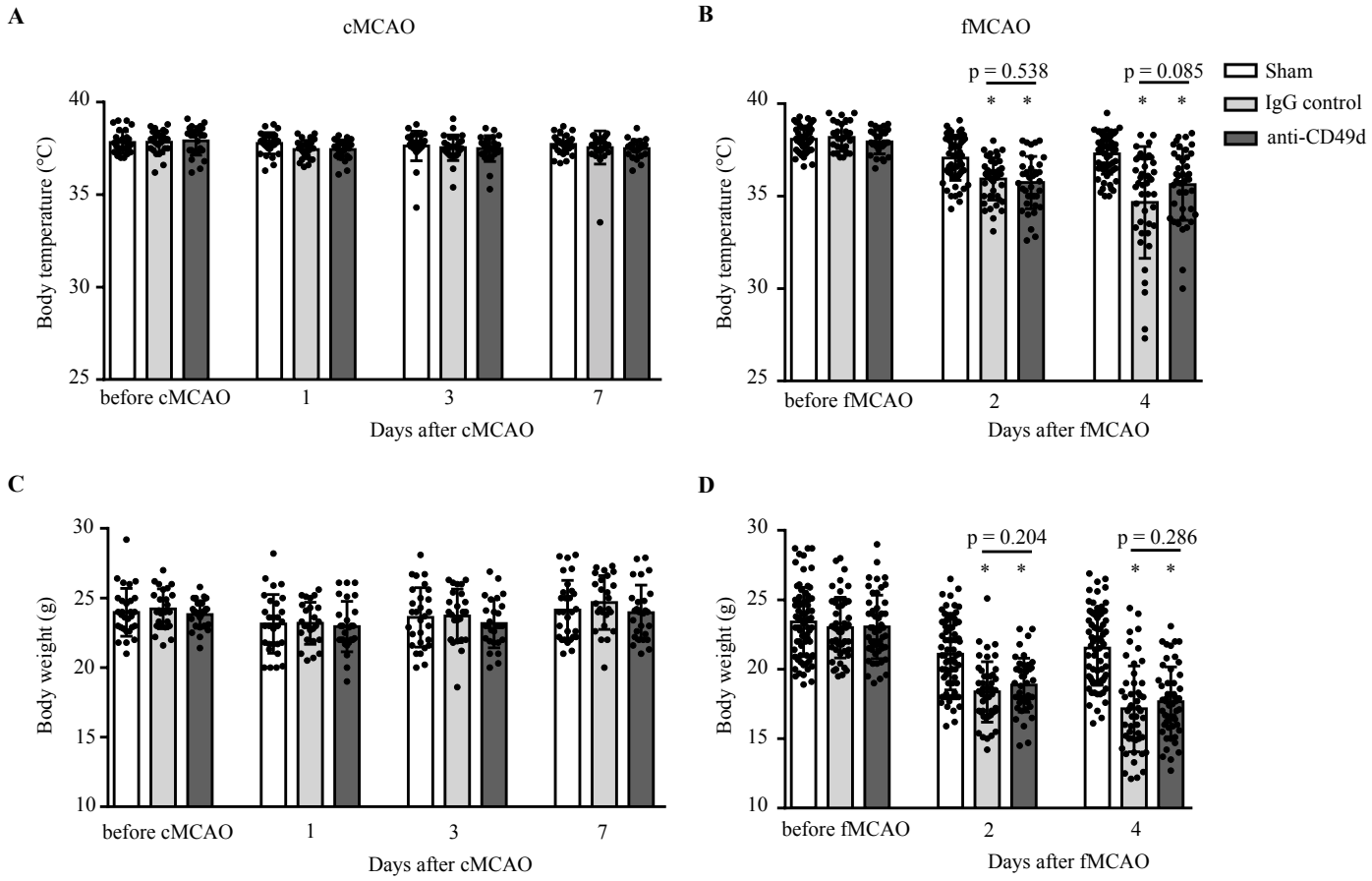

Fig. S5. Physiological parameter analysis after cMCAO and fMCAO. Body temperature and body weight were analyzed at the indicated time points before stroke induction and during the observation period. Body temperature was not affected by cMCAO (**A**), while a significant hypothermia was observed at 2d and 4d after fMCAO (**B**). Similarly, body weight was not altered after cMCAO (**C**) but mice had substantial body weight loss during the 4d observation period after fMCAO (**D**). However, no significant difference between treatment groups was detected for any of the two parameters. Data are presented as mean ±SD. BL: baseline. * : $p<0.05$ of the indicated MCAO group compared to the respective sham group. cMCAO: n(Sham): 30; n(IgG Control): 25; n(anti-CD49d): 27. fMCAO: n(Sham): 74; n(IgG Control): 49; n(anti-CD49d): 51.

Fig. S6. Study Protocol

Multicenter Anti-CD49d trial, FINAL v2
October, 16th 2013

Experimental groups: A. Planas, M.G. de Simoni, N. Plesnila, U. Dirnagl, D.Vivien
Facilitator and analysis centre: A. Liesz

Models:
1) 60min Filament-MCAO, mice awake during occlusion period, (15 mice per treatment groups + 15 Sham): all groups (total: 150 MCAO mice + 75 Sham)
2) Transcranial MCA-Coagulation model (10 per treatment groups + 10 Sham): Planas, de Simoni, Vivien (total: 60 MCAO mice + 30 Sham)

3 groups per model:
1) Sham-operation, no treatment
2) Verum: 300 µg Anti-Mouse CD49d (Clone R1-2)
3) Placebo: 300 µg Rat IgG2b isotype control (Clone: LTF-2)

PROTOCOL:

1) Antibody samples sent blinded (Vial A and B) to experimental groups
    - Antibody concentrations (verum and isotype) is set to 1mg/ml
    - Store at 4°C until use
    - → 300 µl i.p. injection per mouse

2) Doccol filaments sent to groups (10 filaments per group)

3) **Experimental protocol:**
    - 8-10 week old male C57Bl/6J mice (Charles River, stock # 664)
    - Random allocation list to treatment groups sent by the facilitator (e.g. ABBBAABA …)
    - i.p. injection of the antibody (after pre-warming to 37°C) 3h after MCAO-induction (i.e. after MCA coagulation or filament insertion)

    - Inclusion criteria:
        - Filament model: reduction in doppler flow to <20% after filament insertion compared to original values **OR** circling behavior during occlusion time and Bederson score ≥ 1 at 24h after MCAO
        - Coagulation model: visualized and controlled (after 1min) total occlusion of the MCA branch
    - Exclusion criteria (Surgical)
        - Both models: Bite wound before inclusion, exclusion due to excessive weight loss >35% compared to day -1 (→ sacrification)
        - Filament model: insufficient doppler flow reduction or missing functional deficit during occlusion time and at 24h after MCAO
        - Coagulation model: incomplete MCA branch occlusion, subarachnoid bleeding during operation
    - Exclusion criteria (Analytical)
        - Both models: major protocol violation (e.g. no drug applied, wrong occlusion time, etc.); death
        - Filament MCAO: Neuroscore at 24h below 8 Points; No cortical infarct demarcation (no infarct at all [incl. TUNEL neg.]
        - Coagulation MCAO: no infarct demarcation (no infarct at all [incl. TUNEL neg.]

    - General operational procedures: Filaments by Doccol will be provided (Cat.# 602123PK10), volatile anesthesia (induction: 4%, operation: 2% isoflurane, mixed in 70% 0_2 / 30 % N_20), feedback controlled heating during operation, mice awake during filament-occlusion time (60min), warming of mice during occlusion time (filament MCAO) and post-operation recovery for 2h, simplified access to water and food after Filament-

MCAO (e.g. in dish on cage bottom), mice placed back in same cages with same mates after MCAO as before, post-operation analgesia according to individual protocols

- **Survival:**
  - **Coagulation model: 7d** (= one week; e.g. Monday → Monday)
  - **60min Filament-MCAO: 4d** (= 96h; e.g. Monday → Friday)
- Daily measurement of: weight and mortality (please document time point of death!)
- Body temperature: Coagulation: d-1, d1, d3 and d7
  Filament: d-1, d2, d4
- Behavior tests (protocols below) :
  - Filament model: "Ischemia Neuroscore" (d-1, d2 and d4)
  - Coagulation model: Sticky label test and Rotarod (d-1, d1, d3, d7)
- Sacrifice 7d or 4d after MCAO, respectively:
  - Collecting plasma: cardial puncture and transfer blood to EDTA test tubes (will be provided); centrifuge for 15min at 2,000g; transfer plasma to Eppi
  - perfusion with saline (no fixation or sucrose rinse)
  - collecting spleens and brains
  - brains and spleens frozen on powdered dry ice

4) Frozen brains sent blinded (e.g. 1,2,3,…) on dry ice to A. Liesz, plasma and spleens remain preliminary with individual groups until further analysis
5) Central (blinded) sectioning (20µm each 400µm), staining (cresyl violet) and infarct volumetry of all brains by the same method
6) Additional sections (12µm) at the anterior commissure for later histological analyses (leukocytes and neuronal density)
7) Scanned brain slides uploaded to a shared online storage and original slides sent back to respective experimental group for counter-evaluation
8) Experimental groups unblinded for treatment → Unblinding of mouse allocation to treatment group (e.g. 1=A, 2=A, 3=B, …)

9) Final data analysis

- **Primary end points:** Infarct volume of pooled samples per model
- **Secondary end points:**
  - Mortality in the 60min F-MCAO model
  - Behavioral Tests between 3 groups: 2x treatment and Sham
  - Neuronal density between treatment groups per model
  - Brain leukocyte invasion between treatment groups per model
  - Systemic immune parameters (cytokine expression) between
    - a) 3 groups: 2x treatment and Sham
    - b) between models

BEHAVIORAL TESTS

Composite Neuroscore (for 60min fMCAO):

Scores range from 0 (healthy) to 56 (the worst performance in all categories) and represent the sum of the results of general and focal deficits (13 categories). Results are expressed as a composite neurological score.

These include general deficits: hair (0–2), ears (0–2), eyes (0–4), posture (0–4), spontaneous activity (0–4), and epileptic behavior (0–12), and focal deficits: body symmetry (0–4), gait (0–4), climbing on a surface held at 45°(0–4), circling behavior (0–4), front limb symmetry (0–4), compulsory circling(0–4), and whisker response to a light touch (0–4)

1. Hair (score 0-2)

Mouse on open bench top (OBT). Observation with no interference.
0- Hair neat and clean.
1- Localized piloerection and dirty hair in 2 body parts (typically nose and eyes).
2- Piloerection and dirty hair in more than 2 body parts.

2. Ears (score 0-2)

Mouse on OBT. Observation at the beginning with no interference, then stimulating by snapping fingers.
0- Normal. Ears are stretched laterally and behind. They react to noise.
1- Stretched laterally but not behind (one or both). They react to noise.
2- Same as 1 but they do not react to noise.

3. Eyes (score 0-4)
Mouse on OBT. Observation with no interference or stimulation.
0- Open, clean and quickly follow the surrounding environment.
1- Open and characterized by aqueous mucus. Slowly follow the surrounding environment.
2- Open and characterized by dark mucus.
3- Ellipsoidal shaped and characterized by dark mucus.
4- Closed.

4. Posture (score 0-4)
Place the mouse on the palm and swing gently.
0- The mouse stands in the upright position with the back parallel to the palm. During the swing, it stands rapidly.
1- The mouse stands humpbacked. During the swing, it flattens the body to gain stability.
2- The head or part of the trunk lies on the palm.
3- The mouse lies on one side, barely able to recover the upright position.
4- The mouse lies in a prone position, not able to recover the upright position.

5. Spontaneous activity (score 0-4)
Mouse on OBT. Observation with no interference or stimulation.
0- The mouse is alert and explores actively.
1- The mouse seems alert, but it is calm and sluggish.
2- The mouse explores intermittently and sluggishly.
3- The mouse is somnolent and numb, few movements on-the-spot.
4- No spontaneous movements.

6. Epileptic behavior (score 0-12)
Mouse on OBT. The worse epileptic behavior detected during the whole observational period should be recorded and reported according to the following score.
0- None.
3- The mouse is reluctant to handling, shows hyperactivity.
6- The mouse is aggressive, stressed and stares.
9- The mouse shows hyperexcitability, chaotic movements and presence of convulsion following handling.
12- Generalized seizures associated with wheezing and unconsciousness.

FOCAL DEFICITS (total score 0-28)

7. Body symmetry (score 0-4)
Mouse on OBT, observation of undisturbed resting behavior and description of the virtual nose-tail line
0- Normal.
   a. Body: normal posture, trunk elevated from the bench, with fore and hindlimbs leaning beneath the body
   b. Tail: straight
1- Slight asymmetry.
   a. Body: leans on one side with fore and hindlimbs leaning beneath the body
   b. Tail: slightly bent
2- Moderate asymmetry.
   a. Body: leans on one side with fore and hindlimbs stretched out
   b. Tail: slightly bent
3- Prominent asymmetry.
   a. Body: bent, on one side lies on the OBT
   b. Tail: bent
4- Extreme asymmetry.
   a. Body: highly bent, on one side constantly lies on the OBT
   b. Tail: highly bent

8. Gait (score 0-4)
Mouse on OBT. Observation of undisturbed movements.
0- Normal. Gait is flexible, symmetric and quick.
1- Stiff, inflexible. The mouse walks humpbacked, slower than normal mice.

2- Limping with asymmetric movements.
3- Trembling, drifting, falling.
4- Does not walk spontaneously. (In this case, stimulation will be performed gently pushing the mouse with a pen. When stimulated, the mouse walks no longer than three steps)

9. Climbing (score 0-4)
Mouse on a gripping surface 45° to OBT. Place the mouse in the centre of the gripping surface.
0- Normal. The mouse climbs quickly.
1- Climbs with strain, limb weakness present.
2- Holds onto slope, does not slip or climb.
3- Slides down slope, unsuccessful effort to prevent fail.
4- Slides immediately, no effort to prevent fail.

10. Circling behavior (score 0-4)
Mouse on OBT. Observation of the mouse walking undisturbed on the OBT.
0- Absent. The mouse equally turns left or right.
1- Predominantly one-sided turns.
2- Circles to one side, although not constantly.
3- Circles constantly to one side.
4- Pivoting, swaying, or no movement.

11. Forelimb symmetry (score 0-4)
Mouse suspended by the tail. Movements and position of forelimbs are observed.
0- Normal. Both forelimbs are extended towards the bench and move actively.
1- Light asymmetry. Contralateral forelimb does not extend entirely.
2- Marked asymmetry. Contralateral forelimb bends towards the trunk. The body slightly bends on the ipsilateral side.
3- Prominent asymmetry. Contralateral forelimb adheres to the trunk.
4- Slight asymmetry, no body/limb movement.

12. Compulsory circling (score 0-4)
Forelimbs on bench, hindlimbs suspended by the tail. This position reveals the presence of the contralateral limb palsy.
0- Absent. Normal extension of both forelimbs.
1- Tendency to turn to one side. The mouse extends both forelimbs, but starts to turn preferably to one side.
2- Circles to one side. The mouse turns towards one side with a slower movement compared to healthy mice.
3- Pivots to one side sluggishly. The mouse turns towards one side failing to perform a complete circle.
4- Does not advance. The front part of the trunk lies on the bench. Slow and brief movements.

13. Whisker response (score 0-4)
Mouse on the bench. Using a pen, touch gently the whiskers and the tip of the ears from behind, first one the lesioned and then on the contralateral side.
0- Normal symmetrical response. The mouse turns the head towards the stimulated side and withdraws from the stimulus.
1- Light asymmetry. The mouse withdraws slowly when stimulated on the ischemic side. Normal response on the contralateral side.
2- Prominent asymmetry. No response when stimulated on the ischemic side. Normal response on the contralateral side.
3- Absent response ipsilaterally, slow response when stimulated on the contralateral side.
4- Absent response bilaterally.

Rotarod (for cMCAO):

- Rotation protocol: 4min acceleration time (ramp time), 8-40rpm (min – max)
    - Start rotarod at 4rpm
    - Place all mice on rough rods
    - Start acceleration
    - Document latency to fall for each individual
    - If a mouse clings to the rod: stop the timer after 2 full passive rotations
- 3 runs per test, 15min pause interval between the runs
- Training of animals on 3 consecutive days before the operation is required
- Baseline measurement on day-1;
- Deficit analysis at 24h, 72h and on day 7 after MCAO.
- Report the raw data of latency to fall/passive rotation at baseline and at tests after MCAO for both runs

Template, which should be used for data acquisition:

Rotarod (latency in sec per run)

Mouse Nr.	Pre-MCAO				d1					d3					d7				
	1	2	3	**Mean**	1	2	3	**Mean**	**% Pre**	1	2	3	**Mean**	**% Pre**	1	2	3	**Mean**	**% Pre**
1																			
2																			
3																			
4																			
5																			
6																			
7																			
8																			
9																			
10																			
11																			
12																			
13																			
14																			
15																			
16																			
17																			
18																			
19																			
20																			
21																			
22																			
23																			
24																			
25																			
26																			
27																			
28																			
29																			
30																			

Sticky label test (for cMCAO):

Training: Do a few times 1 day before surgery

1. Place mouse in box for 2 mins for it to become accustomed to the new surroundings, and so that it looks around and loses its curiosity
2. Fix the mouse in your hand and place sticker on one palm (press tightly to make sure it is on properly)
3. Release the mouse from fixation and place carefully in the box. Start timer.
4. Count for a maximum of 2 minutes
5. Record when the mouse first shakes its paw (shake), when it first lifts its paw to its mouth (contact), and when it removes the sticker (remove).
6. Repeat 3 times and average (interchanging between left and right paw each time).
7. Clean box with a little bit of alcohol before placing the next mouse into the box.

Template, which should be used for data acquisition:

Training	

Test	

Test	

Date:

	L	**R**
Shake		
Contact		
Remove		
Shake		
Contact		
Remove		
Shake		
Contact		
Remove		

Date:

	L	**R**
Shake		
Contact		
Remove		
Shake		
Contact		
Remove		
Shake		
Contact		
Remove		

Date:

	L	**R**
Shake		
Contact		
Remove		
Shake		
Contact		
Remove		
Shake		
Contact		
Remove		

Test	

Test	

Date:

	L	**R**
Shake		
Contact		
Remove		
Shake		
Contact		
Remove		
Shake		
Contact		
Remove		

Date:

	L	**R**
Shake		
Contact		
Remove		
Shake		
Contact		
Remove		
Shake		
Contact		
Remove		

Supplementary Material S7

The ARRIVE Guidelines Checklist

Animal Research: Reporting In Vivo Experiments

Carol Kilkenny[1], William J Browne[2], Innes C Cuthill[3], Michael Emerson[4] and Douglas G Altman[5]

[1]The National Centre for the Replacement, Refinement and Reduction of Animals in Research, London, UK, [2]School of Veterinary Science, University of Bristol, Bristol, UK, [3]School of Biological Sciences, University of Bristol, Bristol, UK, [4]National Heart and Lung Institute, Imperial College London, UK, [5]Centre for Statistics in Medicine, University of Oxford, Oxford, UK.

	ITEM	RECOMMENDATION	Section/ Paragraph
Title	1	Provide as accurate and concise a description of the content of the article as possible.	Title (page 1)
Abstract	2	Provide an accurate summary of the background, research objectives, including details of the species or strain of animal used, key methods, principal findings and conclusions of the study.	Abstract (page 3)
INTRODUCTION			
Background	3	a. Include sufficient scientific background (including relevant references to previous work) to understand the motivation and context for the study, and explain the experimental approach and rationale. b. Explain how and why the animal species and model being used can address the scientific objectives and, where appropriate, the study's relevance to human biology.	Introduction: Paragraph 1,2,4 Introduction: Paragraph 3,5
Objectives	4	Clearly describe the primary and any secondary objectives of the study, or specific hypotheses being tested.	Introduction: Paragraph 5
METHODS			
Ethical statement	5	Indicate the nature of the ethical review permissions, relevant licences (e.g. Animal [Scientific Procedures] Act 1986), and national or institutional guidelines for the care and use of animals, that cover the research.	Methods: Animals (page20)
Study design	6	For each experiment, give brief details of the study design including: a. The number of experimental and control groups. b. Any steps taken to minimise the effects of subjective bias when allocating animals to treatment (e.g. randomisation procedure) and when assessing results (e.g. if done, describe who was blinded and when). c. The experimental unit (e.g. a single animal, group or cage of animals). A time-line diagram or flow chart can be useful to illustrate how complex study designs were carried out.	Methods: Study design (page 19-20)
Experimental procedures	7	For each experiment and each experimental group, including controls, provide precise details of all procedures carried out. For example: a. How (e.g. drug formulation and dose, site and route of administration, anaesthesia and analgesia used [including monitoring], surgical procedure, method of euthanasia). Provide details of any specialist equipment used, including supplier(s). b. When (e.g. time of day). c. Where (e.g. home cage, laboratory, water maze). d. Why (e.g. rationale for choice of specific anaesthetic, route of administration, drug dose used).	Methods: Antibody treatment (page 21) Tissue sampling (page 24) Animals (page 20) Antibody treatment (page 21)
Experimental animals	8	a. Provide details of the animals used, including species, strain, sex, developmental stage (e.g. mean or median age plus age range) and weight (e.g. mean or median weight plus weight range). b. Provide further relevant information such as the source of animals, international strain nomenclature, genetic modification status (e.g. knock-out or transgenic), genotype, health/immune status, drug or test naïve, previous procedures, etc.	Methods: Animals (page 20) Table1 Antibody treatment (page 21)

Supplementary Material S7

Housing and husbandry	9	Provide details of: a. Housing (type of facility e.g. specific pathogen free [SPF]; type of cage or housing; bedding material; number of cage companions; tank shape and material etc. for fish). b. Husbandry conditions (e.g. breeding programme, light/dark cycle, temperature, quality of water etc for fish, type of food, access to food and water, environmental enrichment). c. Welfare-related assessments and interventions that were carried out prior to, during, or after the experiment.	Methods: Animals (page 20)
Sample size	10	a. Specify the total number of animals used in each experiment, and the number of animals in each experimental group. b. Explain how the number of animals was arrived at. Provide details of any sample size calculation used. c. Indicate the number of independent replications of each experiment, if relevant.	Methods: Animals (page 20) Study design (page 19-20)
Allocating animals to experimental groups	11	a. Give full details of how animals were allocated to experimental groups, including randomisation or matching if done. b. Describe the order in which the animals in the different experimental groups were treated and assessed.	Study design (page 19-20) Antibody treatment (page 21) Animals (page 20)
Experimental outcomes	12	Clearly define the primary and secondary experimental outcomes assessed (e.g. cell death, molecular markers, behavioural changes).	Functional outcomes (page23) Inf.volume (page25)
Statistical methods	13	a. Provide details of the statistical methods used for each analysis. b. Specify the unit of analysis for each dataset (e.g. single animal, group of animals, single neuron). c. Describe any methods used to assess whether the data met the assumptions of the statistical approach.	Statistical Analysis (page 27)
RESULTS			
Baseline data	14	For each experimental group, report relevant characteristics and health status of animals (e.g. weight, microbiological status, and drug or test naïve) prior to treatment or testing. (This information can often be tabulated).	Table 1
Numbers analysed	15	a. Report the number of animals in each group included in each analysis. Report absolute numbers (e.g. 10/20, not 50%[2]). b. If any animals or data were not included in the analysis, explain why.	Fig 1D Table 1
Outcomes and estimation	16	Report the results for each analysis carried out, with a measure of precision (e.g. standard error or confidence interval).	Table 2 Table 3
Adverse events	17	a. Give details of all important adverse events in each experimental group. b. Describe any modifications to the experimental protocols made to reduce adverse events.	No important adverse events
DISCUSSION			
Interpretation/ scientific implications	18	a. Interpret the results, taking into account the study objectives and hypotheses, current theory and other relevant studies in the literature. b. Comment on the study limitations including any potential sources of bias, any limitations of the animal model, and the imprecision associated with the results[2]. c. Describe any implications of your experimental methods or findings for the replacement, refinement or reduction (the 3Rs) of the use of animals in research.	Discussion: Paragraph 4, 5, 6 Discussion: Paragraph 5 Discussion: Paragraph 6
Generalisability/ translation	19	Comment on whether, and how, the findings of this study are likely to translate to other species or systems, including any relevance to human biology.	Discussion: Paragraph 6
Funding	20	List all funding sources (including grant number) and the role of the funder(s) in the study.	Aknowledgements (page 34)

References:
1. Kilkenny C, Browne WJ, Cuthill IC, Emerson M, Altman DG (2010) Improving Bioscience Research Reporting: The ARRIVE Guidelines for Reporting Animal Research. *PLoS Biol* 8(6): e1000412. doi:10.1371/journal.pbio.1000412
2. Schulz KF, Altman DG, Moher D, the CONSORT Group (2010) CONSORT 2010 Statement: updated guidelines for reporting parallel group randomised trials. *BMJ* 340:c332.

Table S1. Study costs (in euro).

	Study center	Center 1	Center 2	Center 3	Center 4	Center 5	Total
Personnel	32,037	19,454	20,200	20,000	2,015	4,410	98,116
Animals	0	3,731	1,000	5,954	900	1,440	13,025
Antibodies and consumables	34,475	1,380	1,000	296	0	2,790	39,942
Shipping and others	2,685	1000	7,200	2,687	0	627	14,199
Total	**69,198**	**25,565**	**29,400**	**28,937**	**2,195**	**9,267**	**165,282**

Table S2. fMCAO and cMCAO means and CIs.

	fMCAO			cMCAO		
	Sham	**IgGControl**	**CD49d**	**Sham**	**IgGControl**	**CD49d**
Number of animals	74	49	51	30	25	27
Infarct volume	0	36.78 [31.17-42.39]	35.76 [31.19-40.34]	0	8.87 [7.76-9.98]	7.20 [6.03-8.38]
CD45+ cells ipsilateral hemisphere	1.54 [1.00-2.07]	5.38 [4.29-6.46]	5.53 [4.63-6.43]	1.034 [0.48-1.59]	11.36 [9.57-13.15]	7.26 [6.04-8.80]
Neuroscore d2	4.15 [2.94-5.36]	16.69 [14.38-19.01]	16.35 [13.94-18.76]	-	-	-
Neuroscore d4	3.32 [2.39-4.26]	17.29 [14.93-19.64]	15.06 [12.87-17.24]	-	-	-
Rotarod test BL	-	-	-	138.50 [113.2-163.8]	108.70 [79.42-138.0]	132.10 [98.00-166.1]
Rotarod test d1	-	-	-	142.90 [117.1-168.6]	123.1 [91.59-154.7]	137.30 [103.1-171.5]
Rotarod test d3	-	-	-	139.30 [111.8-166.9]	129.0 [99.05-159]	146.40 [112.7-180.2]
Rotarod test d7	-	-	-	138.90 [111.1-166.6]	139.50 [109.1-169.8]	152.70 [123.2-182.2]
Adhesive removal test BL	-	-	-	2.35 [1.34-3.30]	0.99 [0.53-1.44]	1.24 [0.64-1.84]
Adhesive removal test d1	-	-	-	1.28 [0.77-1.80]	2.15 [0.54-3.75]	2.70 [0.46-4.95]
Adhesive removal test d3	-	-	-	1.44 [0.81-2.06]	3.73 [0.69-6.77]	3.93 [13.20-6.53]
Adhesive removal test d7	-	-	-	2.42 [0.55-4.29]	4.12 [1.35-6.89]	2.11 [1.03-3.19]

References

Abbott, N.J., A.A. Patabendige, D.E. Dolman, S.R. Yusof, and D.J. Begley. 2010. Structure and function of the blood-brain barrier. *Neurobiology of disease* 37:13-25.

Bath, P.M., M.R. Macleod, and A.R. Green. 2009. Emulating multicentre clinical stroke trials: a new paradigm for studying novel interventions in experimental models of stroke. *International journal of stroke : official journal of the International Stroke Society* 4:471-479.

Bennett, J.L., A. Elhofy, M.C. Canto, M. Tani, R.M. Ransohoff, and W.J. Karpus. 2003. CCL2 transgene expression in the central nervous system directs diffuse infiltration of CD45(high)CD11b(+) monocytes and enhanced Theiler's murine encephalomyelitis virus-induced demyelinating disease. *Journal of neurovirology* 9:623-636.

Bhatia, R., M.D. Hill, N. Shobha, B. Menon, S. Bal, P. Kochar, T. Watson, M. Goyal, and A.M. Demchuk. 2010. Low rates of acute recanalization with intravenous recombinant tissue plasminogen activator in ischemic stroke: real-world experience and a call for action. *Stroke; a journal of cerebral circulation* 41:2254-2258.

Chamorro, A., A. Meisel, A.M. Planas, X. Urra, D. van de Beek, and R. Veltkamp. 2012. The immunology of acute stroke. *Nature reviews. Neurology* 8:401-410.

Choi, Y.K., and K.W. Kim. 2008. Blood-neural barrier: its diversity and coordinated cell-to-cell communication. *BMB Rep* 41:345-352.

Crossley, N.A., E. Sena, J. Goehler, J. Horn, B. van der Worp, P.M. Bath, M. Macleod, and U. Dirnagl. 2008. Empirical evidence of bias in the design of experimental stroke studies: a metaepidemiologic approach. *Stroke; a journal of cerebral circulation* 39:929-934.

Dargazanli, C., C. Arquizan, B. Gory, A. Consoli, J. Labreuche, H. Redjem, O. Eker, J.P. Decroix, A. Corlobe, I. Mourand, N. Gaillard, X. Ayrignac, M. Charif, A. Duhamel, P.E.

Labeyrie, C. Riquelme, G. Ciccio, S. Smajda, J.P. Desilles, G. Gascou, P.H. Lefevre, D. Mantilla-Garcia, F. Cagnazzo, O. Coskun, M. Mazighi, R. Riva, F. Bourdain, P. Labauge, G. Rodesch, M. Obadia, A. Bonafe, F. Turjman, V. Costalat, M. Piotin, R. Blanc, B. Lapergue, and E.R. Investigators. 2017. Mechanical Thrombectomy for Minor and Mild Stroke Patients Harboring Large Vessel Occlusion in the Anterior Circulation: A Multicenter Cohort Study. *Stroke; a journal of cerebral circulation* 48:3274-3281.

Deczkowska, A., K. Baruch, and M. Schwartz. 2016. Type I/II Interferon Balance in the Regulation of Brain Physiology and Pathology. *Trends in immunology* 37:181-192.

Dirnagl, U. 2004. Inflammation in stroke: the good, the bad, and the unknown. *Ernst Schering Research Foundation workshop* 87-99.

Dirnagl, U., and M. Fisher. 2012. International, multicenter randomized preclinical trials in translational stroke research: it's time to act. *Journal of cerebral blood flow and metabolism : official journal of the International Society of Cerebral Blood Flow and Metabolism* 32:933-935.

Dirnagl, U., A. Hakim, M. Macleod, M. Fisher, D. Howells, S.M. Alan, G. Steinberg, A. Planas, J. Boltze, S. Savitz, C. Iadecola, and S. Meairs. 2013. A concerted appeal for international cooperation in preclinical stroke research. *Stroke; a journal of cerebral circulation* 44:1754-1760.

Dirnagl, U., C. Iadecola, and M.A. Moskowitz. 1999. Pathobiology of ischaemic stroke: an integrated view. *Trends in neurosciences* 22:391-397.

Donnan, G.A., M. Fisher, M. Macleod, and S.M. Davis. 2008. Stroke. *Lancet* 371:1612-1623.

Editorial. 2013. Facilitating reproducibility. *Nature chemical biology* 9:345.

Elkins, J. 2016. Primary results of the ACTION trial of natalizumab in acute ischemic stroke (AIS). In International Stroke Conference. Los Angeles, California.

Engelhardt, B., and R.M. Ransohoff. 2005. The ins and outs of T-lymphocyte trafficking to the CNS: anatomical sites and molecular mechanisms. *Trends in immunology* 26:485-495.

Engelhardt, B., and L. Sorokin. 2009. The blood-brain and the blood-cerebrospinal fluid barriers: function and dysfunction. *Seminars in immunopathology* 31:497-511.

Enzmann, G., C. Mysiorek, R. Gorina, Y.J. Cheng, S. Ghavampour, M.J. Hannocks, V. Prinz, U. Dirnagl, M. Endres, M. Prinz, R. Beschorner, P.N. Harter, M. Mittelbronn, B. Engelhardt, and L. Sorokin. 2013. The neurovascular unit as a selective barrier to polymorphonuclear granulocyte (PMN) infiltration into the brain after ischemic injury. *Acta neuropathologica* 125:395-412.

Fu, Y., N. Zhang, L. Ren, Y. Yan, N. Sun, Y.J. Li, W. Han, R. Xue, Q. Liu, J. Hao, C. Yu, and F.D. Shi. 2014. Impact of an immune modulator fingolimod on acute ischemic stroke. *Proceedings of the National Academy of Sciences of the United States of America* 111:18315-18320.

Garijo, D., S. Kinnings, L. Xie, L. Xie, Y. Zhang, P.E. Bourne, and Y. Gil. 2013. Quantifying reproducibility in computational biology: the case of the tuberculosis drugome. *PloS one* 8:e80278.

Gelderblom, M., F. Leypoldt, K. Steinbach, D. Behrens, C.U. Choe, D.A. Siler, T.V. Arumugam, E. Orthey, C. Gerloff, E. Tolosa, and T. Magnus. 2009. Temporal and spatial dynamics of cerebral immune cell accumulation in stroke. *Stroke; a journal of cerebral circulation* 40:1849-1857.

Ghersi-Egea, J.F., N. Strazielle, M. Catala, V. Silva-Vargas, F. Doetsch, and B. Engelhardt. 2018. Molecular anatomy and functions of the choroidal blood-cerebrospinal fluid barrier in health and disease. *Acta neuropathologica*

Hacke, W., M. Kaste, E. Bluhmki, M. Brozman, A. Davalos, D. Guidetti, V. Larrue, K.R. Lees, Z. Medeghri, T. Machnig, D. Schneider, R. von Kummer, N. Wahlgren, D. Toni, and E. Investigators. 2008. Thrombolysis with alteplase 3 to 4.5 hours after acute ischemic stroke. *The New England journal of medicine* 359:1317-1329.

Hamidi, V., T. Wisloff, T. Ringerike, K.K. Linnestad, I. Harboe, and M. Klemp. 2010. Treatment of Patients with Acute Stroke in Stroke Units (with or without Early Supported Discharge). Oslo, Norway.

Howells, D.W., E.S. Sena, and M.R. Macleod. 2014. Bringing rigour to translational medicine. *Nature reviews. Neurology* 10:37-43.

Iadecola, C., and J. Anrather. 2011a. The immunology of stroke: from mechanisms to translation. *Nature medicine* 17:796-808.

Iadecola, C., and J. Anrather. 2011b. Stroke research at a crossroad: asking the brain for directions. *Nature neuroscience* 14:1363-1368.

Investigators, E.A.S.T. 2001. Use of anti-ICAM-1 therapy in ischemic stroke: results of the Enlimomab Acute Stroke Trial. *Neurology* 57:1428-1434.

Ioannidis, J.P. 2005. Why most published research findings are false. *PLoS medicine* 2:e124.

Ioannidis, J.P., S. Greenland, M.A. Hlatky, M.J. Khoury, M.R. Macleod, D. Moher, K.F. Schulz, and R. Tibshirani. 2014. Increasing value and reducing waste in research design, conduct, and analysis. *Lancet* 383:166-175.

Jauch, E.C., J.L. Saver, H.P. Adams, Jr., A. Bruno, J.J. Connors, B.M. Demaerschalk, P. Khatri, P.W. McMullan, Jr., A.I. Qureshi, K. Rosenfield, P.A. Scott, D.R. Summers, D.Z. Wang, M. Wintermark, H. Yonas, C. American Heart Association Stroke, N. Council on Cardiovascular, D. Council on Peripheral Vascular, and C. Council on Clinical. 2013. Guidelines for the early management of patients with acute ischemic stroke: a guideline

for healthcare professionals from the American Heart Association/American Stroke Association. *Stroke; a journal of cerebral circulation* 44:870-947.

Kimmelman, J., J.S. Mogil, and U. Dirnagl. 2014. Distinguishing between exploratory and confirmatory preclinical research will improve translation. *PLoS biology* 12:e1001863.

Kunis, G., K. Baruch, O. Miller, and M. Schwartz. 2015. Immunization with a Myelin-Derived Antigen Activates the Brain's Choroid Plexus for Recruitment of Immunoregulatory Cells to the CNS and Attenuates Disease Progression in a Mouse Model of ALS. *The Journal of neuroscience : the official journal of the Society for Neuroscience* 35:6381-6393.

Kunis, G., K. Baruch, N. Rosenzweig, A. Kertser, O. Miller, T. Berkutzki, and M. Schwartz. 2013. IFN-gamma-dependent activation of the brain's choroid plexus for CNS immune surveillance and repair. *Brain : a journal of neurology* 136:3427-3440.

Laschinger, M., and B. Engelhardt. 2000. Interaction of alpha4-integrin with VCAM-1 is involved in adhesion of encephalitogenic T cell blasts to brain endothelium but not in their transendothelial migration in vitro. *Journal of neuroimmunology* 102:32-43.

Lefer, D.J., and R. Bolli. 2011. Development of an NIH consortium for preclinicAl AssESsment of CARdioprotective therapies (CAESAR): a paradigm shift in studies of infarct size limitation. *Journal of cardiovascular pharmacology and therapeutics* 16:332-339.

Liesz, A., E. Suri-Payer, C. Veltkamp, H. Doerr, C. Sommer, S. Rivest, T. Giese, and R. Veltkamp. 2009. Regulatory T cells are key cerebroprotective immunomodulators in acute experimental stroke. *Nature medicine* 15:192-199.

Liesz, A., W. Zhou, E. Mracsko, S. Karcher, H. Bauer, S. Schwarting, L. Sun, D. Bruder, S. Stegemann, A. Cerwenka, C. Sommer, A.H. Dalpke, and R. Veltkamp. 2011. Inhibition of lymphocyte trafficking shields the brain against deleterious neuroinflammation after stroke. *Brain : a journal of neurology* 134:704-720.

Llovera, G., K. Hofmann, S. Roth, A. Salas-Perdomo, M. Ferrer-Ferrer, C. Perego, E.R. Zanier, U. Mamrak, A. Rex, H. Party, V. Agin, C. Fauchon, C. Orset, B. Haelewyn, M.G. De Simoni, U. Dirnagl, U. Grittner, A.M. Planas, N. Plesnila, D. Vivien, and A. Liesz. 2015. Results of a preclinical randomized controlled multicenter trial (pRCT): Anti-CD49d treatment for acute brain ischemia. *Science translational medicine* 7:299ra121.

Lopes Pinheiro, M.A., G. Kooij, M.R. Mizee, A. Kamermans, G. Enzmann, R. Lyck, M. Schwaninger, B. Engelhardt, and H.E. de Vries. 2016. Immune cell trafficking across the barriers of the central nervous system in multiple sclerosis and stroke. *Biochimica et biophysica acta* 1862:461-471.

Man, S., E.E. Ubogu, and R.M. Ransohoff. 2007. Inflammatory cell migration into the central nervous system: a few new twists on an old tale. *Brain pathology* 17:243-250.

McNutt, M. 2014. Journals unite for reproducibility. *Science* 346:679.

Meeker, R.B., K. Williams, D.A. Killebrew, and L.C. Hudson. 2012. Cell trafficking through the choroid plexus. *Cell adhesion & migration* 6:390-396.

Mony, J.T., R. Khorooshi, and T. Owens. 2014. Chemokine receptor expression by inflammatory T cells in EAE. *Frontiers in cellular neuroscience* 8:187.

Mortazavi, M.M., C.J. Griessenauer, N. Adeeb, A. Deep, R. Bavarsad Shahripour, M. Loukas, R.I. Tubbs, and R.S. Tubbs. 2014. The choroid plexus: a comprehensive review of its history, anatomy, function, histology, embryology, and surgical considerations. *Child's nervous system : ChNS : official journal of the International Society for Pediatric Neurosurgery* 30:205-214.

Moskowitz, M.A. 2010. Brain protection: maybe yes, maybe no. *Stroke; a journal of cerebral circulation* 41:S85-86.

O'Collins, V.E., M.R. Macleod, G.A. Donnan, L.L. Horky, B.H. van der Worp, and D.W. Howells. 2006. 1,026 experimental treatments in acute stroke. *Annals of neurology* 59:467-477.

Polman, C.H., P.W. O'Connor, E. Havrdova, M. Hutchinson, L. Kappos, D.H. Miller, J.T. Phillips, F.D. Lublin, G. Giovannoni, A. Wajgt, M. Toal, F. Lynn, M.A. Panzara, A.W. Sandrock, and A. Investigators. 2006. A randomized, placebo-controlled trial of natalizumab for relapsing multiple sclerosis. *The New England journal of medicine* 354:899-910.

Ransohoff, R.M., and B. Engelhardt. 2012. The anatomical and cellular basis of immune surveillance in the central nervous system. *Nature reviews. Immunology* 12:623-635.

Ransohoff, R.M., P. Kivisakk, and G. Kidd. 2003. Three or more routes for leukocyte migration into the central nervous system. *Nature reviews. Immunology* 3:569-581.

Redzic, Z. 2011. Molecular biology of the blood-brain and the blood-cerebrospinal fluid barriers: similarities and differences. *Fluids and barriers of the CNS* 8:3.

Rice, G.P., H.P. Hartung, and P.A. Calabresi. 2005. Anti-alpha4 integrin therapy for multiple sclerosis: mechanisms and rationale. *Neurology* 64:1336-1342.

Shechter, R., A. London, and M. Schwartz. 2013a. Orchestrated leukocyte recruitment to immune-privileged sites: absolute barriers versus educational gates. *Nature reviews. Immunology* 13:206-218.

Shechter, R., O. Miller, G. Yovel, N. Rosenzweig, A. London, J. Ruckh, K.W. Kim, E. Klein, V. Kalchenko, P. Bendel, S.A. Lira, S. Jung, and M. Schwartz. 2013b. Recruitment of beneficial M2 macrophages to injured spinal cord is orchestrated by remote brain choroid plexus. *Immunity* 38:555-569.

Stamatovic, S.M., R.F. Keep, and A.V. Andjelkovic. 2008. Brain endothelial cell-cell junctions: how to "open" the blood brain barrier. *Current neuropharmacology* 6:179-192.

Steffen, B.J., G. Breier, E.C. Butcher, M. Schulz, and B. Engelhardt. 1996. ICAM-1, VCAM-1, and MAdCAM-1 are expressed on choroid plexus epithelium but not endothelium and mediate binding of lymphocytes in vitro. *The American journal of pathology* 148:1819-1838.

Steinman, L. 2005. Blocking adhesion molecules as therapy for multiple sclerosis: natalizumab. *Nature reviews. Drug discovery* 4:510-518.

Strong, A.J., P.J. Anderson, H.R. Watts, D.J. Virley, A. Lloyd, E.A. Irving, T. Nagafuji, M. Ninomiya, H. Nakamura, A.K. Dunn, and R. Graf. 2007. Peri-infarct depolarizations lead to loss of perfusion in ischaemic gyrencephalic cerebral cortex. *Brain : a journal of neurology* 130:995-1008.

Szmydynger-Chodobska, J., N. Strazielle, J.R. Gandy, T.H. Keefe, B.J. Zink, J.F. Ghersi-Egea, and A. Chodobski. 2012. Posttraumatic invasion of monocytes across the blood-cerebrospinal fluid barrier. *Journal of cerebral blood flow and metabolism : official journal of the International Society of Cerebral Blood Flow and Metabolism* 32:93-104.

Takeshita, Y., and R.M. Ransohoff. 2012. Inflammatory cell trafficking across the blood-brain barrier: chemokine regulation and in vitro models. *Immunological reviews* 248:228-239.

Tymianski, M. 2015. Neuroprotective therapies: Preclinical reproducibility is only part of the problem. *Science translational medicine* 7:299fs232.

Ueno, M., Y. Chiba, R. Murakami, K. Matsumoto, M. Kawauchi, and R. Fujihara. 2016. Blood-brain barrier and blood-cerebrospinal fluid barrier in normal and pathological conditions. *Brain Tumor Pathol* 33:89-96.

Wang, Q., X.N. Tang, and M.A. Yenari. 2007. The inflammatory response in stroke. *Journal of neuroimmunology* 184:53-68.

Wilson, E.H., W. Weninger, and C.A. Hunter. 2010. Trafficking of immune cells in the central nervous system. *The Journal of clinical investigation* 120:1368-1379.

Wisloff, T., V. Hamidi, T. Ringerike, I. Harboe, and M. Klemp. 2010. Intravenous Thrombolytic Treatment After Acute Stroke and Secondary Antithrombotic Prevention Treatment (Antiplatelet and Anticoagulant Treatment) After Stroke. Oslo, Norway.

Yednock, T.A., C. Cannon, L.C. Fritz, F. Sanchez-Madrid, L. Steinman, and N. Karin. 1992. Prevention of experimental autoimmune encephalomyelitis by antibodies against alpha 4 beta 1 integrin. *Nature* 356:63-66.

Zhou, W., A. Liesz, H. Bauer, C. Sommer, B. Lahrmann, N. Valous, N. Grabe, and R. Veltkamp. 2013. Postischemic brain infiltration of leukocyte subpopulations differs among murine permanent and transient focal cerebral ischemia models. *Brain pathology* 23:34-44.

Zhu, Z., Y. Fu, D. Tian, N. Sun, W. Han, G. Chang, Y. Dong, X. Xu, Q. Liu, D. Huang, and F.D. Shi. 2015. Combination of the Immune Modulator Fingolimod With Alteplase in Acute Ischemic Stroke: A Pilot Trial. *Circulation* 132:1104-1112.

Zivin, J.A., M. Fisher, U. DeGirolami, C.C. Hemenway, and J.A. Stashak. 1985. Tissue plasminogen activator reduces neurological damage after cerebral embolism. *Science* 230:1289-1292.

Acknowledgments

First, I would like to thank my supervisor Dr. Arthur Liesz to give me the opportunity for being part of his fantastic team and projects. I am very beholden to his motivation and guidance during the last years. I indeed thank him for all the advice and support he gave me. I would also like to thank Dr. Christof Haffner for all the help and support he gave me. He always had an open door for discussions.

I would like to acknowledge our cooperation partners (Prof. Dr. Britta Engelhard, Dr. Gaby Enzmann, Dr. med. Thomas Arzberger, Dr. Joan Montaner, Prof. Denis Vivien, Prof. Dr. Nikolaus Plesnila, Prof. Anna M. Planas, Prof. Ulrich Dirnagl, Prof. Maria-Gracia De Simoni), for teaching me techniques, giving me the opportunity to work with their precious mouse lines or human samples and exchanging data.

I am also grateful to the animal facility of the ISD (Dr. Manuela Schneider, Dr. Anne von Thaden, Peggy Kunath, Stefanie Wurster, Tamara Voss) for helping me to manage the mouse lines.

I would like to express special thanks to Kerstin for all the technical support she gave me, without her, the immunological part of this thesis would not be possible. I also want to thank Farida and Thanassis for their motivation; they always had an open door for scientific discussion.

Thanks to all my colleagues, Stefan, Becky, Jun, Julia, Steffi, Vikram and Corinne for their scientific and non-scientific discussions which stimulated my work.

I am enormously thankful to my parents and my sister, for their motivation, support and love. I don't have words to express my gratefulness and love to my partner and friend Cesar for his support, patience, motivation and for taking care of our sons and me. Without him, this work would not have been possible.

Finally, I would like to thank all the proofreaders of the thesis.

Curriculum vitae

Personal information

Gemma Llovera Garcia

Born: 10.05.1984

Nationality: Spanish

Education

· since 2013 PhD Student at LMU Munich

PhD project title: "The choroid plexus in post-stroke neuroinflammation" in the laboratory of Dr. Arthur Liesz, Institute for Stroke and Dementia Research, Klinikum der Universität München, Germany.

Supervisor: Dr. Arthur Liesz

· 2009-2011 Master of Neuroscience degree at the Universitat Autonoma de Barcelona (UAB), Barcelona, Spain.

Master's project title: "pStat3 as a component of astroglial cell activation after neonatal hypoxia/ischemia in mice" in the Medical Histology Department of the Faculty of Medicine in the UAB, Barcelona.

Supervisor: Dr. Laia Acarin

· 2002-2009 Bachelor degree in Biology at the Universitat Autonoma de Barcelona (UAB), Barcelona, Spain.

· 2000-2002 High School of Science degree at the Escola Pia de Terrassa, Terrassa, Spain.

Awards

Master scholarship award by the Spanish ministry for science and innovation (2010).

Conferences

Oral presentation at 2nd European Stroke Organization Conference, Barcelona (Spain) in May 2016.

Oral presentation at 11th ESNI COURSE European School of Neuroimmunology, Glasgow (UK) in July 2011.

Poster presentation at 9th International Symposium on Neuroprotection and Neuroreepair, Leipzig (Germany) in April 2016. The choroid plexus post-stroke cerebral leukocyte invation. Llovera G, Hellal F, Arzberger T, Engelhardt B, Liesz A.

Poster presentation at XXVIIth International Symposium on Cerebral Blood Flow and Metabolism, Vancouver (Canada) in June 2015.The choroid plexus in brain lymphocyte invasion after stroke.Llovera G; Hellal F; Arzberger T; Engelhardt B; Liesz A.

Poster presentation at XI European Meeting on Glial Cells in Health and Disease, Berlin (Germany) in July 2013. Astrocyte-targeted production of IL-10 modifies glial phenotype. Llovera G, Almolda B, Barrera I, De Labra C, Ferrer B, Hofer MJ, Campbell IL, Hidalgo J, González Band Castellano B.

Poster presentation at 3rd Venusberg Meetion on Neuroinflammation, Bonn (Germany) in February 2013. The impact of astrocyte-targeted IL-10 production on microglia. Llovera G, Almolda B, Barrera I, De Labra C, Ferrer B, Hofer MJ, Campbell IL, Hidalgo J, Gonzalez B and Castellano B.

Poster presentation at XXVth International Symposium on Cerebral Blood Flow and Metabolism, Barcelona (Spain) in May 2011. pSTAT3 as a component of astroglial cell activation after neonatal hypoxia/ischemia in mice. Llovera G, Shrivastava K, Acarin, L.